FLUORESCENT DYE-DOPED SILICA NANOPARTICLES FOR BIOANALYSIS

By

LISA R. HILLIARD

A DISSERTATION PRESENTED TO THE GRADUATE SCHOOL
OF THE UNIVERSITY OF FLORIDA IN PARTIAL FULFILLMENT
OF THE REQUIREMENTS FOR THE DEGREE OF
DOCTOR OF PHILOSOPHY

UNIVERSITY OF FLORIDA

2005

To my parents,
from whom I have received unconditional love, guidance, and support.

To my big brother, Don,
my role model.

With love.

LRH

ACKNOWLEDGMENTS

I would like to thank my research advisor, Dr. Weihong Tan, for his guidance, support, and patience. I also thank the members of the Tan Research group for showing me what it means to be a "real scientist." I am greatly indebted to Dr. Julia Xiaojun Zhao for being a great mentor and a good friend. I thank Dr. Rahul Bagwe, Dr. Swadeshmukul Santra, Dr. Shelly John, Dr. Ruby Tapec-Dytioco, Dr. Monde Qhobosheane, Dr. Hong Wang, Dr. Jianwei Li, and Dr. Gang Yao for their support and advice in my research. I am also very thankful to Dr. Min Yang, Dr. Xiaohong Fang, Dr. Xiaojing Liu, Dr. Kensuke Arai, Dr. Hua (Jane) Lou, Dr. Zehui (Charles) Cao, Dr. Timothy J. Drake, Dr. Marie Vicens, Chaoyong (James) Yang, Alina Munteanu, Joshua E. Smith, Karen Martinez Diaz, Prabodhika Mallikaratchy, Lin Wang, Li Tan, Colin Medley, Dr. Charles Lofton, Dr. Steven Suljak, Dr. Dihua Shangguan, Dr. Zhiwen Tang, Hui Chen, Hui Lin, Kwame Sefah, Dosung Sohn, and Yanrong Wu for their friendship, encouragement, and help. I am especially grateful to Robert Ross and Douglas L. Schiavone for their research assistance.

I thank my University of Florida colleagues for their collaborative work: Dr. Samuel R. Farrah, Shannon McQuaig, and Johnny Davis of the Microbiology and Cell Science Department for their assistance in bacteria culture; Dr. Shouguang Jin and Dr. Yanping Wang of the Molecular Genetics and Microbiology Department for their assistance in bacteria growth and detection; Dr. Ben L. Koopman, Jue Zhao, Vijay Krishna of the Department of Environmental Engineering for their assistance in spore

growth and isolation; and Karen Kelley and Lynda Schneider of the ICBR and Gill Brubaker of the PERC for their assistance in sample characterization. I would also like thank my supervisory committee members – Dr. James D. Winefordner, Dr. Willard W. Harrison, Dr. Jon D. Stewart, and Dr. Ben L. Koopman – for their encouragement and assistance.

I am deeply indebted to my parents, Donnie and Barbara Hilliard, for their unconditional love, support, and guidance. I thank my brother, Don Hilliard, for his tough love and for being a great role model. I am grateful to my friends and extended family for their prayers and words of encouragement. I especially thank my grandmothers, Marie Davis and Hester Hilliard, for being my inspiration. I thank my church family at St. Augustine Catholic Church and Student Center for their words of wisdom and encouragement.

I sincerely thank all of the unnamed people who helped me to get this far in my journey, survive my UF graduate studies, and complete my dissertation project.

I am extremely grateful to God for His unconditional love, mercy, and grace. May I one day become the humble servant He intended me to be.

TABLE OF CONTENTS

LIST OF TABLES

LIST OF FIGURES

Abstract of Dissertation Presented to the Graduate School
of the University of Florida in Partial Fulfillment of the
Requirements for the Degree of Doctor of Philosophy

FLUORESCENT DYE-DOPED SILICA NANOPARTICLES FOR BIOANALYSIS

By

Lisa R. Hilliard

December 2005

Chair: Weihong Tan
Major Department: Chemistry

This research focuses on the use of dye-doped silica nanoparticles as highly fluorescent labeling probes for biological applications. Fluorescent dye-doped silica nanoparticles are uniform, core/shell, and spherical nanomaterials, consisting of a fluorescent dye core and a silica coating, and can serve as highly sensitive labeling probes due to high fluorescence signal amplification, photostability, and bioconjugation capabilities. To prepare and optimize the nanoparticles for bioanalysis, several different types of silica nanoparticles were synthesized and modified with biomolecules. DNA-conjugated nanoparticles were used for oligonucleotide hybridization studies and dye-doped silica nanoparticle-antibody conjugates were used in a simple immunoassay for the detection of harmful microorganisms.

Inorganic, organic, and pure dye-doped silica nanoparticles were synthesized using reverse or water-in-oil microemulsion and Stöber methods, resulting in particles ranging from 50-300 nm. Following synthesis, the desired surface functionality was introduced onto the particles in a post-coating step. Using this post-coating method, dye-doped silica

nanoparticles were well dispersed in solution and subsequently coupled to biomolecules more efficiently and less susceptible to aggregation and non-specific binding.

To demonstrate the utility of the nanoparticles for bioanalysis, DNA-conjugated nanoparticles for hybridization studies were obtained by immobilizing oligonucleotides to silica nanoparticles using a disulfide-coupling chemistry. Factors influencing the immobilization and hybridization processes were examined and optimized. The oligonucleotide-modified silica nanoparticles provided an efficient substrate for hybridization and can be used in the development of DNA biosensors.

For the detection and identification of pathogenic bacteria, dye-doped silica nanoparticles were used to develop a simple immunoassay. When conjugated to antibodies, the nanoparticles served as highly sensitive reporter antibodies for bacterial antigens because each antibody-antigen (Ab-Ag) binding event was linked with 100-10,000 dye molecules. The nanoparticle-antibody conjugates were capable of detecting 1 bacterial cell in solution. The immunological method based on these nanoparticle-antibody conjugates potentially can be useful in the testing of food, clinical, and environmental samples for pathogenic bacteria and endospores.

In summary, fluorescent dye-doped silica nanoparticles are viable fluorescent labels for biological applications when designed to meet the specific needs of the given application. Future efforts will include the further development of new types of dye-doped silica nanoparticles; surface modification and bioconjugation schemes to prevent nanoparticle aggregation, decrease fluorescence background signal and reduce non-specific binding to biological samples and substrates; and immunological detection

schemes using dye-doped silica nanoparticle-antibody conjugates for multiple bacteria detection.

CHAPTER 1
INTRODUCTION

Fluorescence-based techniques are some of the most widely used analytical methods for biological applications, such as clinical chemistry and disease diagnosis, DNA sequencing, biological imaging, and environmental monitoring. Fluorescence is an extremely sensitive, rapid, nontoxic, nondestructive, and comparatively inexpensive analytical technique that usually requires the use of a label. Consequently, there is a great demand for the continued development and optimization of fluorescent markers and probes that are geared toward bioanalysis and bioimaging. Fluorescent organic dyes are the most widely used class of labels for bioanalysis, due to their commercial availability, ready functionalization, high stability, solubility, and biocompatibility in aqueous buffer solutions. However, organic fluorophores have characteristics that can limit their effectiveness in such applications. Problems generally arise from poor photostability and brightness, especially for samples with high background fluorescence. In addition, the functionalization of the dyes can be costly and/or time consuming because different types of functional groups are required for conjugation of the dye to biomolecules. Therefore, the development and advancement of fluorescent probes that overcome these limitations and can be used in biochemical assays are highly desirable.

Nanotechnology is the understanding and control of matter at dimensions of roughly 1 to 100 nm (1 nm = 10^{-9} m), where unique phenomena can be used in novel applications. Encompassing nanoscale science, engineering and technology, nanotechnology involves generating, manipulating, imaging, measuring, modeling, and

employing materials at this scale. The physical, chemical, and biological properties of nanomaterials differ from the properties of individual atoms and molecules or bulk matter. Nanotechnology research focuses on understanding and creating improved materials, devices, and systems that exploit these new properties. In combination with biomedical and other biotechnological developments, nanotechnology is enabling major breakthroughs in bioanalysis. Numerous research has been published on the use of nanomaterials in bioanalysis, including DNA transfection,[1-5] drug delivery,[6,7] and immunoassays.[8-10] Of the nanomaterials used in biological applications, various types of nanoparticles have been employed to overcome some of the functional limitations encountered by fluorescent organic dyes.

Nanoparticles for Bioanalysis

In the last decade, semiconductor[11-17], metal[18,19], and dye-doped nanoparticles[20,21] have been developed and increasingly used as effective nanomaterials in biological applications. These particles have distinct advantages over organic dyes because of their unique optical properties, high signal amplification, photostability, and high surface to volume ratio.

Quantum dots (QDs) are semiconductor nanocrystals that show great promise for the simultaneous detection of multiple analytes. QDs have radii that are smaller than the bulk exciton Böhr radius, making them intermediate particles between molecular and bulk forms of matter.[11,22] Figure 1-1 shows the size of QDs and dye-doped nanoparticles and how they compare to the size of organic dyes and proteins. Due to quantum confinement, both the absorption and emission energies of quantum dots shift to higher values as the size of the nanoparticles decreases.[11,12,16,22] With a single excitation wavelength, a clear difference in emission peaks is observed with only a 1-2 nm

difference in QD size, as a result of their narrow emissions that are dependent on the size of the nanocrystals. Efforts have been made to improve the solubility of quantum dots in aqueous solution to use them in biological systems. The development of water-soluble quantum dots shows promise for the bioconjugation of QDs with biomolecules.[23-25] Quantum dots have been employed to label proteins and oligonucleotides for cell recognition, fluorescence anisotropy studies, and DNA detection.[26,27]

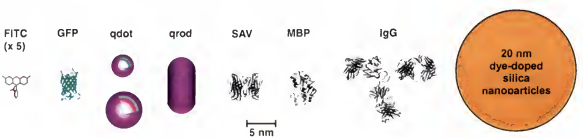

Figure 1-1. Size comparison of nanomaterials used in bioanalysis and proteins, which they may label. From left to right: fluorescein isothiocyanate (FITC), green fluorescent protein (GFP), CdSe/ZnS quantum dots and rods, streptavidin (SAV), maltose binding protein (MBP), immunoglobulin G (IgG), and dye-doped silica nanoparticles. Adapted from X. Michalet et al. *Science* **2005**, 307, 539.[23]

The unique QD advantage of multiple narrow emissions with a single wavelength excitation source offers new capabilities for high-throughput screening, multiplexed optical coding in gene expression studies, and medical diagnostics. The disadvantages associated with QDs include poor solubility in water of unmodified QDs, agglutination, blinking properties, moderate quantum yields, and highly toxic cadmium components.[28]

Gold nanoparticles are popular biomarkers due to the high affinity of the gold atom toward thiol-modified molecules. The striking ruby red color of colloidal gold makes it an ideal label for the colorimetric determination of molecular recognition processes.[29] Ultrasensitive analysis of oligonucleotides, proteins, and other biomolecules has been achieved using gold nanoparticles as labels.[30-36] In addition, many biological applications

have been demonstrated using gold nanoparticles as signaling probes,[37-49] especially in DNA analysis. The applications are based on the target biomolecules binding to probe molecules that are attached to gold nanoparticles and forming polymeric gold nanoparticle-biomolecule aggregates, which leads to a change in the color of the sample. Gold nanoparticles have also been used to detect biomolecules in a sandwich-based array format. A DNA-labeled gold nanoparticle can hybridize with a target sequence that has formed a duplex with a capture sequence immobilized to a solid support. Signal is obtained from the bound gold nanoparticle probe and further amplified by silver reduction of the gold nanoparticle probe. By utilizing different light scattering properties of target oligonucleotide-bound particles, a method has also been developed for multicolor labeling and imaging of DNA arrays, which shows an ability to distinguish between different DNA targets.

Dye-doped nanoparticles provide highly luminescent signals due to the high quantum yield of the hundreds to thousands of fluorescent dye molecules trapped inside of the particles. Various organic dye-doped polymer microspheres and nanoparticles have been developed.[50-53] Due to their hydrophobic properties, water insoluble organic dye molecules are easily incorporated inside polymer matrices to form luminescent polymer particles. Commonly used fluorophores, such as fluorescein isothiocyanate (FITC) and rhodamine isothocyanate (RITC), have been used to generate luminescent polymer particles. Polystyrene and poly (tert-butylacrylate) are the most frequently used to produce uniform polymer particles via a microemulsion method. The emulsion polymerization yields highly monodisperse particles, and sizes from approximately 20 nm to a few mm can be obtained by altering the reaction conditions (i.e. temperature,

monomer and initiator concentrations, and the ionic strength of the reaction solution). Fluorescent latex nanoparticles have been used to probe specific sequences on single DNA molecules.[54] However, polymer particles can be unsuitable for bioanalysis due to their hydrophobicity and bio-incompatibility. Large particle size, a tendency to agglomerate, swelling, and dye leakage also limit the use of dye-doped polymer particles as fluorescent biomarkers for ultrasensitive biochemical analysis.[28]

Dye-doped nanoparticles containing a silica shell are an alternative to polymer particles. The advantages of the dye-doped silica nanoparticles are the inherent hydrophilicity of the silica network (which avoids the precipitation problems of polymer particles) and the ease of bioconjugation.[21] In addition, the silica shell is not subject to microbial attack and there is no swelling or porosity change with a change in pH.[55] Consequently, fluorescent dye-doped silica nanoparticles that can be routinely synthesized and modified into biomarkers or labels suitable for fluorescence-based bioanalytical applications are of great interest.

Fluorescent Dye-doped Silica Nanoparticles

Fluorescent dye-doped silica nanoparticles are spherical, core/shell particles, consisting of thousands of dye molecules entrapped inside of a water soluble silica matrix. Due to the large number of dye molecules and high quantum yield, the dye-doped silica nanoparticles provide highly luminescent signals when used as probes. In addition, the silica matrix protects the dye molecules from environmental attack, making the dye-doped nanoparticles highly photostable. Moreover, silica is an excellent biocompatible and versatile substrate for the immobilization of biomolecules. To develop highly effective nano-luminescent probes, the synthesis, characterization, bioconjugation, and application of dye-doped silica nanoparticles have been investigated.

Nanoparticle Synthesis

There are two major silica nanoparticle synthesis methods, Stöber[58] and reverse microemulsion,[59-62] which provide a silica matrix by hydrolysis and polymerization of tetraethylorthosilicate (TEOS), as shown in Figure 1-2. The Stöber method is based on hydrolysis and polymerization of TEOS using either acid or base catalysis in a bulk alcohol, such as ethanol, solution. Using this method, different sizes of silica particles are obtained ranging from 100 nm to 1 μm in diameter. The size of the particles can be tuned by changing experimental parameters, such as temperature, polymerization time and silica precursor (TEOS) concentrations. The method requires a short synthesis time, usually 1-6 hours, but tends to result in relatively large, polydisperse nanoparticles. Thus, although this method is relatively simple and easy to carry out, it can be limited by the non-uniformity of the produced nanoparticles.

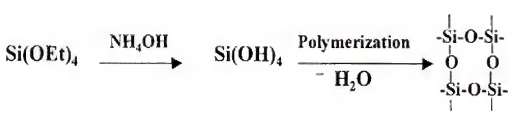

Figure 1-2. Silica nanoparticle synthesis via hydrolysis and polymerization of TEOS using either acid or base catalysis in a bulk ethanol solution.

In contrast, the reverse microemulsion method provides monodisperse and smaller sized silica nanoparticles. The reverse microemulsion method, also called a water-in-oil (W/O) microemulsion, is based on an isotropic and thermodynamically stable, single-phase system that consists of small amounts of water, a large volume of oil and a surfactant. The surfactant molecules lower the interfacial tension between water and oil, resulting in the formation of a transparent solution. Water nanodroplets or pools are

formed in the bulk oil phase and serve as nanoreactors for the synthesis of the nanoparticles from various materials, as shown in Figure 1-3. The size of the water pool influences the size of the nanoparticles. By changing the water to surfactant molar ratio (W_0 value), the size of the spherical nanoparticles can be controlled. In general, the higher the value of W_0, the larger the particle size will be. The excess base (usually NH_4OH) in the microemulsion initiates the polymerization reaction through hydrolysis of TEOS. The rate of the polymerization is much slower in the microemulsion in comparison to that in a bulk aqueous solution. Therefore, as the polymerization reaction proceeds, monodisperse silica nanoparticles are formed. Various nanoparticles have been prepared[56-59] using this method, showing its flexibility for the fabrication of different types and sizes of silica nanoparticles. This method has advantages in that it does not require extreme conditions of temperature and pressure and the particle size and shape can be simply controlled by varying microemulsion parameters.[57-60]

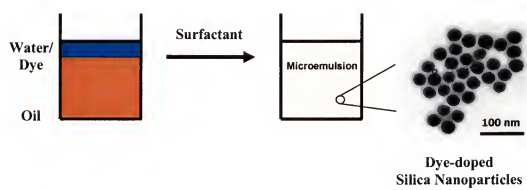

Figure 1-3. Reverse or water-in-oil (W/O) microemulsion system for silica nanoparticle synthesis.

One of the first types of dye-containing silica nanoparticles was synthesized using the W/O microemulsion method and contained the inorganic dye, tris (2,2'-bipyridyl) dichlororuthenium (II) (RuBpy).[61-66] The basic idea was to physically entrap a large

number of dye molecules inside a single nanoparticle so that each individual nanoparticle would emit strong fluorescent signal and thus serve as a highly fluorescent probe. The synthesis method was effective because of the electrostatic attraction between the positively charged metal ions in the inorganic dye molecules and the negatively charged silica matrix of the nanoparticles. Due to the hydrophilic property of inorganic dye molecules, they are easily dissolved in aqueous solution and retained in the water pool during the TEOS polymerization reaction. Thus, after the negatively charged silica matrix forms, the inorganic dye molecules are trapped inside of the matrix by electrostatic interactions, resulting in inorganic dye-doped silica nanoparticles.

Silica nanoparticles can also be doped with organic dyes. Given the higher quantum yield of organic dyes as compared to inorganic dyes, the doping of organic dyes inside silica nanoparticles is an attractive alternative. However, it is difficult to trap organic dye molecules inside of silica using either the W/O microemulsion or the Stöber method. Two factors hinder the retention of the organic dye molecules inside the silica matrix in the synthesis process of the silica nanoparticles. One is the hydrophobic property of the organic compounds. Some organic dye compounds can not dissolve in aqueous solution while others only partially dissolve in water. Thus, even if the organic dyes are first dissolved in the water pool of the W/O microemulsion system, they quickly transfer to the organic phase, resulting in only pure silica nanoparticles. The second factor is the lack of an attraction force between organic molecules and the silica matrix. Unlike RuBpy, most organic dye molecules have neutral charges, and thus, there is no electrostatic attraction to retain the dye molecules inside the silica matrix. Thus, water

solubility and positive charge are two essential requirements for obtaining dye-doped silica nanoparticles using the W/O microemulsion and Stöber methods.

To address the solubility problems for organic dyes, a Stöber-based synthesis approach was used to reduce the hydrophilicity of the silica matrix so that the highly hydrophobic rhodamine 6G (R6G) dye, a commonly used organic fluorescent dye, would be trapped inside the nanoparticle matrix.[67] TEOS was still used as a hydrophilic silica precursor in the system and a relatively hydrophobic silica compound, phenyltriethoxysilane (PTES), was also added to the system as a second precursor to aid in trapping the organic fluorophores. Since the matrix was changed to a mixed medium of hydrophilic and hydrophobic components, R6G was more retained in this matrix, resulting in R6G-doped silica nanoparticles. This method was previously used for the synthesis of hydrophobic-dye-doped microspheres.[68] Nanoparticles obtained through this approach exhibited high fluorescent intensity, excellent photostability, and minimal dye leakage after prolonged storage in aqueous solution.[67]

Another approach used the W/O microemulsion method to address the organic dye solubility problem to produce tetramethylrhodamine (TMR)-doped silica nanoparticles. Unlike the scheme of the synthesis of R6G-doped silica nanoparticles which altered the composition of the silica matrix, this synthesis method was designed to change the property of the water pool in the microemulsion system to make the TMR molecules more soluble in the nanoreactors for the synthesis of organic dye-doped silica nanoparticles.[69] Acetic acid was used to form the bulk of water pool; this compound has both organic and inorganic properties and acts as an aqueous solvent to dissolve and retain the TMR molecules inside of the water pool. Moreover, this compound also

provides enough protons to induce positive charges on the TMR molecules. Compared to inorganic dye-doped nanoparticles, the TMR -doped silica nanoparticles provided much higher fluorescent signals.

An alternative approach for the synthesis of TMR-doped silica nanoparticles was also developed using TMR-dextran.[69] By linking highly hydrophilic dextran molecules to TMR molecules, the TMR was trapped inside of the water pool in the microemulsion system. In addition, by adding hydrochloric acid to the water phase in the microemulsion system, the TMR molecules were firmly entrapped in the silica matrix, resulting in highly fluorescent TMR-doped silica nanoparticles.

Nanoparticle Surface Modification and Bioconjugation

Simple and reliable bioconjugation is very important for nanoparticle applications. The silica-based nanoparticles can be useful in bioanalysis only when they are conjugated to recognition biomolecules, which contain special components that selectively interact with target analytes. Silica surface chemistry has been well established for bioconjugation of various biomolecules when used as a solid support. Most of these surface modification methods are easily adapted to attach biomolecules to the silica nanoparticle surface. Using various biochemical binding approaches, the nanoparticle surface can be modified to contain functional groups that are useful for subsequent surface modification and biomolecule immobilization.[70-74]

The most frequently used biomolecule linking bridge, the avidin-biotin linkage, can also be used for bioconjugation of probe molecules onto silica nanoparticles.[75] The nanoparticles are usually modified with avidin and upon avidin-biotin binding, the recognition biomolecules remain on the nanoparticle surface for subsequent binding and identification of target biomolecules.

Another effective bioconjugation approach for the immobilization of proteins, such as enzymes and antibodies, onto the silica nanoparticles is to chemically link amine, carboxyl, or isothiocyanate groups on the nanoparticle surface. The advantage of this approach is a more stable, covalent binding between the silica nanoparticles and the biomolecule that can last until the biomolecule degrades or becomes inactive.[76-79] Following modification, the nanoparticles can be linked with biomolecules containing free carboxyl and amine groups, respectively.

The three major advantages of fluorescent dye-doped silica nanoparticles—high fluorescence intensity, excellent photostability, and ease of bioconjugation—make them ideal fluorescent labels for various types of biological applications. Table 1-1 shows a comparison of fluorescent dye-doped silica nanoparticles with organic dyes and quantum dots for use in bioanalysis and bioimaging.

Biological Applications using Fluorescent Dye-doped Silica Nanoparticles

Several significant biological applications have been demonstrated using dye-doped silica nanoparticles.[80-85] The following two applications using dye-doped silica nanoparticles highlight the impact that the particles have had to date in bioanalytical studies and biotechnology.

Nanoparticle-antibody conjugate labeling of cancer cells. Tris (2,2'-bipyridyl) dichlororuthenium(II) hexahydrate (Rubpy)-doped silica nanoparticles were used in nanoparticle-antibody conjugates to label and identify leukemia cells through fluorescence imaging.[21] A mouse anti-human CD10 antibody was used as the recognition element in the system, which was covalently immobilized onto the nanoparticle surface using isothiocyanate-treated nanoparticles. The leukemia cells were recognized as bright fluorescent areas in the fluorescence images and correlated well with

the optical images, as shown in Figure 1-4. Control experiments were done using unmodified RuBpy-doped silica nanoparticles and with cells that do not have a surface antigen on the cell membrane for CD10 antibody. The fluorescence images showed no fluorescence signal, indicating that the nanoparticles were able to selectively identify the cancer cells.

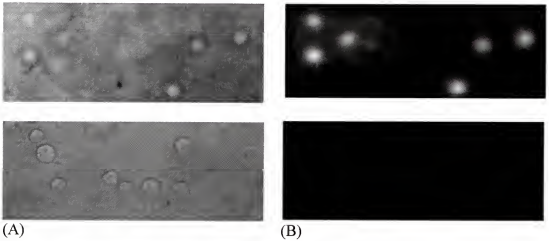

(A) (B)

Figure 1-4. Recognition of cancer cells using RuBpy-doped silica nanoparticle probes. (A) Optical images and (B) fluorescence images of cancer cells incubated with antibody-immobilized RuBpy-doped silica nanoparticles (top images) and unmodified RuBpy-doped silica nanoparticles as a control (bottom cells). Reprinted with permission from S. Santra et al. *Analytical Chemistry* **2001**, 73, 4992.[21]

Ultrasensitive DNA analysis. In conventional DNA analysis, a fluorophore labeled probe DNA sequence hybridizes to the target DNA and the fluorescence intensity is detected and reflects the amount of target DNA present. Each target DNA molecule is represented by only one dye molecule. In comparison, the dye-doped nanoparticle labeled assay can provide approximately 100-10,000 dye molecules for each target DNA sequence, which means that the signal is enhanced or amplified at least 100 times. Consequently, a single hybridization event is easily identified, making the detection of trace amounts of target DNA more feasible.

Table 1-1. Comparison of fluorescent labels for bioanalysis. Adapted from Zhao et al. *Encyclopedia of Nanoscience and Nanotechnology* **2004**, *1*, 256.[86]

	Dye-doped Silica NPs	Organic Dyes	Quantum Dots
Signal Amplification	Extremely high, up to 10,000x	Low	~20x signal of 1 dye molecule
Photostability	Excellent without photobleaching	Poor	Excellent with minimal photobleaching
Ability to Bioconjugate	Easy & universal	Easy, but non-universal	Good, under investigation
Aqueous Solubility	Excellent	Mostly excellent, but some low	Low, under investigation
Multiplex Analysis Capability	Possible & under investigation	Difficult	Excellent
Toxicity	Minimal	Some to severe	Some
Environmental Influence	None	Some to severe	Minor
Manufacturing & Reproducibility	Easy and batch production possible	-	Not easy
Compatibility with Existing Detection Systems	Excellent	Excellent	Excellent
Overall Feasibility for Biolabeling	Great potential, under investigation	Good	Great potential, under investigation

An ultrasensitive DNA analysis was developed using TMR-dextran-doped silica nanoparticle probes.[84] This DNA analysis assay was carried out using a typical sandwich method in which a capture DNA sequence was immobilized on a glass substrate,[48] a probe DNA sequence was attached to a dye-doped silica nanoparticle, and a target DNA sequence was complementary to both the capture and probe sequences, as shown in

Figure 1-5. In a two-step hybridization procedure wherein the target DNA hybridizes to the capture DNA and the probe DNA, the target DNA was recognized and signaled by the fluorescent nanoparticle probe. An imaging system was used to measure the fluorescence signal of the surface-bound nanoparticle-probes, and the number of fluorescent particle spots was proportional to the concentration of the target DNA. A detection limit of 5 fM was achieved using this nanoparticle-based assay.

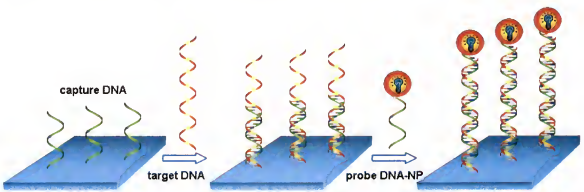

Figure 1-5. Schematic representation of a sandwich DNA assay using TMR-doped silica nanoparticles conjugated with probe DNA. Adapted from X.J. Zhao et al. *Journal of the American Chemical Society* **2003**, *125*, 11474.[84]

Dissertation Overview

Various fluorescent dye-doped silica nanoparticles have been synthesized, and adapted silica bioconjugation approaches have provided simple ways to modify the particles for biomolecule attachment. The three major advantages of the dye-doped silica nanoparticles — high fluorescence intensity, excellent photostability, and good biocompatibility — make the particles ideal fluorescent probes for use in many types of biological applications. However, for the fluorescent dye-doped silica nanoparticles to reach their full potential, a more fundamental understanding of the nanoparticles and how they interact with biomolecules and in complex biological systems is needed.

To further advance the use of fluorescent dye-doped silica nanoparticles for bioanalysis, novel types and methods for the synthesis of fluorescent dye-doped silica nanoparticles is still required. In addition, parameters for how to determine and manipulate the properties of the silica nanoparticle surface for a given biological application are needed. The research presented in this dissertation focuses on the further advancement of the synthesis, surface modification and bioconjugation, and use of dye-doped silica nanoparticles as highly fluorescent labels for biological applications.

In Chapter 2, modifications to the two main approaches for fluorescent dye-doped silica nanoparticle synthesis and a study of the microemulsion method are discussed. New approaches for the surface modification of dye-doped silica nanoparticles with various types of functional groups for subsequent conjugation with biomolecules are demonstrated in Chapter 3. (The microemulsion synthesis[87] and surface modification studies were done in collaboration with Rahul Bagwe.) Bioanalytical applications of fluorescent dye-doped silica nanoparticles (studies done in collaboration with Xiaojun J. Zhao) are documented in Chapters 4, 5, and 6. DNA-conjugated silica nanoparticles used for oligonucleotide hybridization studies[88] are described in Chapter 4. In Chapters 5 and 6, a dye-doped silica nanoparticle-antibody conjugate based immunoassay for the detection of *E. coli* O157:H7[89] and other harmful microorganisms are described. Conclusions and future work are discussed in chapter 7.

CHAPTER 2
SYNTHESIS AND CHARACTERIZATION OF FLUORESCENT ORGANIC AND INORGANIC DYE-DOPED SILICA NANOPARTICLES

Introduction

Fluorescent dye-doped silica nanoparticles have significant advantages over single-dye molecules in bioanalysis. They contain hundreds to thousands of organic or inorganic dye molecules doped inside a silica matrix. Incorporation of dye molecules inside the silica shell protects the fluorescent dye from the surrounding environment, increases photostability and provides signal enhancement.[21,66] These dye-doped silica nanoparticles are extensively used in biological applications,[21,66,90] as well as in photonics and non-linear optical materials. [91,92]

Although incorporation of dye into polymer nanoparticles has been well established, the doping of dye inside a silica matrix is a challenge. The hydrophilic environment of silica does not favor entrapment of hydrophobic dye molecules. To successfully entrap dye molecules inside of a silica matrix, polar dye molecules should be used to increase the electrostatic attraction of the dye with the negatively charged silica matrix, and the size of the dye molecules should be large enough to prevent dye leakage from the pores of the silica matrix. Consequently, dye doping and entrapment schemes have been developed for both Stöber and reverse microemulsion based synthesis of fluorescent dye-doped silica nanoparticles. For the Stöber method, organic dye molecules have been entrapped inside of a silica matrix by introducing a hydrophobic silica precursor during synthesis of the silica nanoparticles, as briefly discussed in

Chapter 1.[67] In addition to physical entrapment, organic dyes have been covalently attached to the silica precursor, via the conjugation of isothiocyanate-containing dyes with 3-aminopropyltriethoxysilane, prior to Stöber synthesis.[93,94] Alternatively, nanoparticles prepared using the water-in-oil microemulsion (W/O) method have been doped with organic dye molecules by attaching water soluble dextran molecules to the dye.[69]

In an attempt to develop alternative methods for the synthesis of highly fluorescent silica nanoparticles that are less than 100 nm in diameter and can be used in biological applications, modifications of either the Stöber or reverse microemulsion based synthesis methods were investigated by doping an organic dye, fluorescein, into silica nanoparticles. In addition, tris (2,2'-bipyridyl) dichlororuthenium (II) hexahydrate (RuBpy) dye-doped silica nanoparticle synthesis parameters were studied (Reproduced in part with permission from R.P. Bagwe, C. Yang, L.R. Hilliard, and W. Tan *Langmuir* **2004**, 20, 8336-8342. Copyright [2004] American Chemical Society)[87] to provide a solid foundation for the effective application of these nanoparticles in immunoassays and other bioassays.

Experimental Section

Materials. Triton X-100, sodium dodecyl sulfate (SDS), dioctyl sulfosuccinate (AOT), Igepal CO-520, and NP-5 (polyoxyethylene nonyl phenol ether), and tris (2,2'-bipyridyl) dichlororuthenium(II) hexahydrate (RuBpy) were purchased from Sigma-Aldrich and used in the W/O microemulsion system.. Aminopropyltriethoxysilane (APTS), tetraethylorthosilicate (TEOS), ethanol, heptane, cyclohexane, hexanol, and ammonium hydroxide (NH_4OH, 25-28 wt % ammonia), also purchased from Sigma-Aldrich, were used without further purification. Mouse IgG was purchased from

Biodesign International (Kennebunkport, ME), and bifunctional polyethylene glycol (PEG) was purchased from Nektar (Huntsville, AL). Fluorescein isothiocyanate (FITC) was purchased from Molecular Probes (Invitrogen, Eugene, OR).

Organic dye-precursor/substrate conjugation. The conjugation method for fluorescein isothiocyanate (FITC) and FITC-PEG-NHS to APTS and IgG was adapted from a protocol published by van Bladereen et al.[94] and based on the reaction of isothiocyanate (ITC) or *N*-hydroxysuccinimide (NHS) with primary amines, as shown in Figure 2-1. In a typical FITC-APTS conjugation, 3.4 mg FITC or FITC-PEG-NHS was reacted with 4 μL APTS in 620 μL absolute ethanol, at room temperature, under anhydrous conditions, for approximately 12-20 hours. For the FITC-IgG conjugate reaction, 0.2 μg IgG was reacted with 0.1 mg FITC in 250 μL, 0.1 M sodium bicarbonate buffer (pH 8.0) for 2-6 hours at room temperature. The resultant conjugates were then immediately used to synthesize nanoparticles using either the Stöber or reverse microemulsion synthesis method.

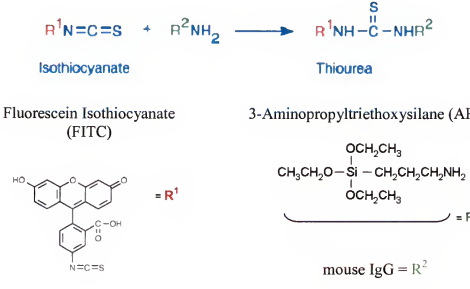

Figure 2-1. Reaction of fluorescein isothiocyanate (FITC) with APTS or IgG.

Nanoparticle synthesis. For the Stöber reactions, a beaker containing 5 mL, 95% ethanol and 5 mL NH_4OH (25-28% by weight) was suspended into an ultrasonicator and sonicated in an ice bath at 4°C. Immediately after starting the sonicator, 100-500 μL TEOS and an appropriate concentration of fluorescent dye was added to the beaker. After a reaction time of 1 hour, the particles were washed several times in ethanol, acetone, and water. The particles were allowed to air dry overnight or stored in ethanol at 4°C.

Microemulsion solutions were prepared by mixing adequate amounts of surfactant, organic solvent, dye, water, and ammonium hydroxide. In a typical microemulsion, 1.77 mL triton X-100, 7.5 mL cyclohexane, 1.88 mL n-hexanol, and 400 μL water was mixed, with magnetic stirring, until stable (~10 minutes), and then 80 μL of dye solution (0.1 M RuBpy dye in water or 0.01-0.1 M FITC dye precursor/conjugate in ethanol or sodium bicarbonate), 100 μL TEOS, and 60 μL NH_4OH was added. The reaction was then magnetically stirred for 24 hours at room temperature. Ethanol was added after 24 hours to break the microemulsion and release the silica nanoparticles. The particles were then washed 2-4 times in ethanol and stored in ethanol at 4°C. Structures of the inorganic dye, RuBpy, and the surfactants used are shown in Figure 2-2.

Nanoparticle characterization. The size and shape of the dye-doped silica nanoparticles synthesized were measured using a transmission electron microscope (TEM, Hitachi H-7000). Fluorescence measurements were performed on a Fluorolog Tau-3 spectrofluorometer (Jobin Yvon Spex Instruments, S.A. Inc.). The excitation/emission wavelengths for Fluorescein and RuBpy were 495/520 nm and 450/605 nm, respectively.

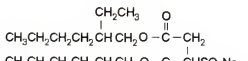

Dioctyl sulfosuccinate (AOT)

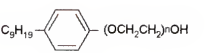

Igepal CO-520 (NP-5)

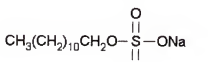

Sodium dodecyl sulfate (SDS)

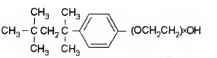

Triton X-100

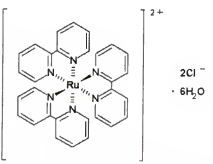

Tris (2,2'-bipyridine) dichlororuthenium (II) hexahydrate (RuBpy)

Figure 2-2. Structures of inorganic dye and surfactants used in fluorescent dye-doped silica nanoparticle synthesis using the reverse micromemulsion method.

Results and Discussion

Organic dye-doped silica nanoparticles using Stöber and reverse microemulsion synthesis methods. Fluorescein isothiocyanate (FITC) was doped into silica nanoparticles using various dye-precursor or substrate conjugation methods to facilitate either dye trapping or covalent attachment in Stöber or reverse microemulsion synthesis. The conjugation methods attempted include the following: (1) FITC-APTS, (2) FITC-IgG, (3) FITC-PEG, and (4) FITC-PEG-APTS.

Before doping the nanoparticles with dye, various modifications to the original Stöber method[95] and the method developed by van Blaaderen et al.[93,94] were investigated

in an attempt to produce particles 100 nm in diameter. Parameters considered include silane concentration, the time at which the silane is added to the reaction mixture, temperature, and reaction time. However, only 260± 26 nm particles were produced when 100 μL TEOS was quickly added to the reaction mixture. It should be noted that as the particle size increased, the particles became more uniform; the nanoparticles tended to be monodispersed at sizes larger than 500 nm. Figure 2-3 shows TEM images of particles synthesized using the Stöber and the reverse microemulsion method. Using the Stöber method, the smallest resultant nanoparticles were approximately 5 times larger than average particle produced using the microemulsion method.

FITC-APTS-silica nanoparticles. To determine the efficiency of the FITC-APTS conjugation method for dye-doped nanoparticle synthesis, 0.5-5 μmoles FITC with 0.8-10 μmoles APTS was reacted in anhydrous ethanol for approximately 12 hours. The FITC-APTS conjugate was then used to synthesize nanoparticles in the Stöber method. The FITC-APTS dye precursor facilitated the covalent attachment of the organic dye using APTS as the silane coupling agent. Previous studies have shown that the dye is homogeneously distributed in the silica nanoparticle.[94] Using this method, fluorescein doped silica nanoparticles, with a diameter of 396 ± 5 nm, were synthesized. To reduce the size of the nanoparticles, the ammonium hydroxide (catalyst) concentration was reduced. A reduction in catalyst concentration by ½ produced nanoparticles approximately 100 nm smaller, as shown in the TEM or SEM images for three synthesis trials in Figure 2-4 (A-C).

The fluorescence intensities of fluorescein-doped silica nanoparticles using various FITC-APTS conjugate concentrations (0.5-5 μmoles) in the Stöber method is shown in

Figure 2-5 for three different trials. Based on visual observation, the concentration of dye doped into the nanoparticles increased as the initial conjugate concentration increased. However, the fluorescence intensity measurements suggest that the fluorescence signal may be reduced when more than approximately 2.7 μmoles of FITC-APTS conjugate is used to synthesize the nanoparticles, probably due to self-quenching of the FITC, but more experiments are needed to confirm the trend.

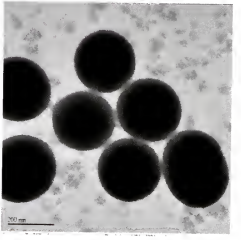

(A)

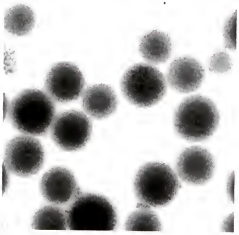

(B)

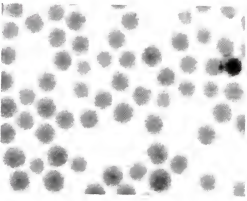

(C)

Figure 2-3. TEM images of silica nanoparticles synthesized using the Stöber and reverse microemulsion methods. (A) 260 ± 26 nm silica nanoparticles, synthesized using the Stöber method. (B & C) silica nanoparticles synthesized using the reverse microemulsion method; 45 ± 5 nm and 60 ± 6 nm, respectively.

FITC-APTS conjugates were also used in the reverse microemulsion method to covalently attach the FITC to the silica matrix. Microemulsions were prepared using 0.8

and 6.8 μmoles of conjugate; the dye concentration was comparable to that used in the synthesis of RuBpy-doped silica nanoparticles. The resultant 54 ± 6 nm, FITC-doped silica nanoparticles were highly fluorescent despite the fact that not much of the dye used in the synthesis was retained; most of the FITC-APTS remained in the supernatant when the nanoparticles were washed following synthesis. The particle size and fluorescence intensities of these nanoparticles are shown in Figure 2-4 (D) and Figure 2-5 (D), respectively. No significant difference was observed in the particle size for different trials/batches of nanoparticles synthesized using this method.

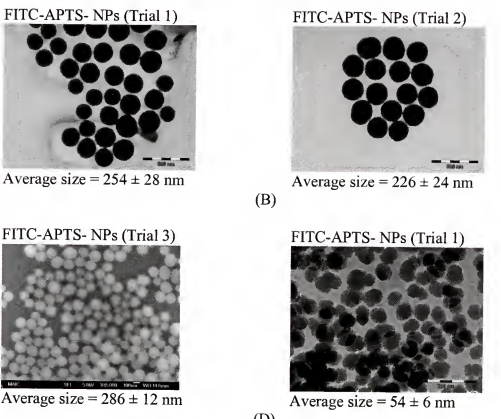

Figure 2-4. TEM and SEM images of FITC-APTS-silica nanoparticles synthesized using the (A-C) Stöber and (D) reverse microemulsion synthesis methods. (A, B, and D) TEM images of the nanoparticles. (C) A SEM image of the nanoparticles.

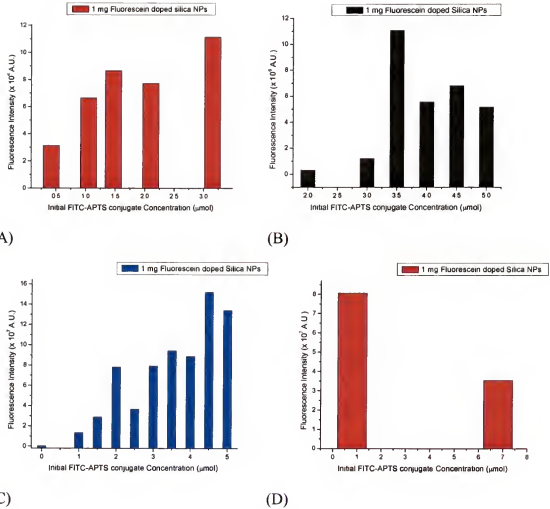

Figure 2-5. Fluorescence intensities of silica nanoparticle samples doped with various concentrations of FITC-APTS conjugates. FITC-APTS conjugates doped into silica nanoparticles using (A-C) the Stöber and (D) reverse microemulsion methods.

FITC-IgG-silica nanoparticles. In an attempt to trap the fluorescein dye inside the silica matrix, IgG (170 kD) was used as an alternative to dextran.[96] FITC-IgG, 0.02 μmol, 0.07 μmol, and 0.13 μmol, were added to reverse microemulsions, and the particle sizes and fluorescence intensities for the FITC-IgG silica nanoparticles are shown in Figure 2-6. Analysis of the effective dye concentration of these particles suggests that given the size of the IgG molecule (150-170 kD), as shown in the size comparison chart

in Figure 1-1, it may be too big for entrapment of large numbers of dye molecules in 60 nm nanoparticles.

FITC-IgG (0.02 μmol)

Average size = 73 ± 4 nm

(A)

FITC-IgG (0.07 μmol)

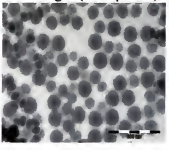

Average size = 54 ± 10 nm

(B)

FITC-IgG (0.13 μmol)

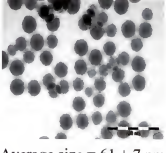

Average size = 61 ± 7 nm

(C)

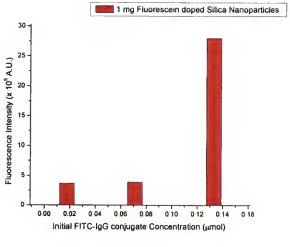

(D)

Figure 2-6. TEM images and fluorescence intensities of FITC-IgG-silica nanoparticles synthesized using the reverse microemulsion method.

FITC-PEG or FITC-PEG-APTS-silica nanoparticles. Various concentrations of two different sizes of PEG-FITC conjugates, made using PEG MW 3400 and PEG MW 5000, were used to facilitate the trapping of organic dye inside silica nanoparticles. No significant difference in particle fluorescence or size was observed for the two different molecular weights of PEGs. These two molecular weights were selected because they are close to the molecular weights of dextran molecules that have been previously shown to efficiently trap TMR into silica nanoparticles.[96] The particle sizes and fluorescence intensities of silica nanoparticles doped with FITC-PEG for dye entrapment or FITC-PEG-NHS for covalent attachment are shown in Figure 2-7.

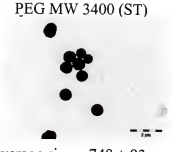

Average size = 748 ± 93 nm

(A)

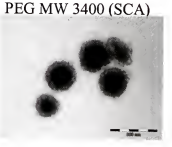

Average size = 343 ± 59 nm

(B)

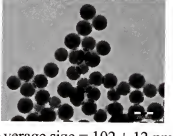

Average size = 102 ± 12 nm

(C)

Figure 2-7. TEM images and fluorescence intensities of FITC-PEG-silica nanoparticles synthesized using the (A, B, and E) Stöber method and (C and D) reverse microemulsion method with covalent attachment via FITC-PEG-NHS (Microemulsion based covalent attachment, MCA or Stöber based covalent attachment, SCA) or trapping of the dye via FITC-PEG (Microemulsion based trapping, MT or Stöber based trapping, ST).

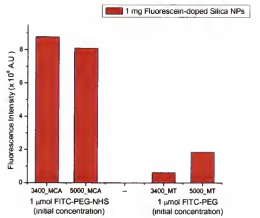

(D)

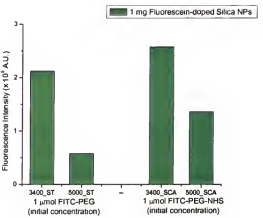

(E)

Figure 2-7. continued.

These various conjugation schemes were investigated in an attempt to develop additional synthesis methods for the doping of organic dyes (such as fluorescein, tetramethylrhodamine (TMR), and Texas Red) into silica nanoparticles, with minimal dye leakage. This brief study suggests that with further development, these synthesis schemes may be used to develop additional types of organic dye-doped silica nanoparticles. However, more work needs to be done to better control the nanoparticle size and fluorescence from batch to batch synthesis in order to produce nanoparticles that can be used as reliable fluorescent labels for bioanalysis.

RuBpy dye-doped silica nanoparticle synthesis. To gain a more fundamental understanding of silica nanoparticle synthesis and dye entrapment using the reverse microemulsion method, various synthesis parameters were investigated.[87] The effect of the nature of surfactant molecules, the concentrations of tetraethylorthosilicate (TEOS) and ammonium hydroxide (NH_4OH), the water to surfactant molar ratio (R) and cosurfactant to surfactant molar ratio (p) on the particle size and polydispersity of RuBpy dye-doped silica nanoparticles were investigated.

Effect of the nature of the surfactant. RuBpy dye-doped silica nanoparticles were prepared in microemulsions with different surfactants: AOT (anionic), NP-5 (non-ionic), and a mixture of AOT and NP-5. The particles were formed, in a ternary microemulsion of surfactant/heptane or cyclohexane/water, using the same reactant concentrations and water to surfactant molar ratio (R=10). The particles were spherical in shape, and the particle size was larger in microemulsions with NP-5 < AOT < AOT + NP-5. The average particle size in the AOT microemulsion was 30 nm and 14 nm in the NP-5 microemulsion, as shown in Figure 2-8 (A). The mixture of AOT and NP-5 resulted in the highest particle size of 130 nm. These variations in particle size are due to the structure of the microemulsion droplet as shown in Figure 2-9. AOT is a double tailed anionic surfactant and has wedge shaped geometry with a head group area smaller than the volume of the hydrocarbon tail. This geometry is suitable for the formation of reverse micelles having spherical droplet structure. A spherical geometry has been found in the entire single phase microemulsion zone of the phase diagram for this AOT-based microemulsion system, at different temperatures and with using various organic solvents.[97]

In the case of the microemulsion formed using NP-5 surfactant, at a water to surfactant molar ratio around 10 and higher, the microemulsion has a lamellar structure, wherein the water droplets tend to associate together and form inter-droplet water channels, as has been shown using electrical conductivity and light scattering studies.[98] Therefore, silica reacting species in NP-5 microemulsion are significantly less compartmentalized over droplets than those in AOT, leading to comparatively a faster nucleation rate and smaller sized nanoparticles in NP-5 microemulsion. With the double

tailed surfactant and wedge shape geometry, the AOT surfactant provides stronger steric film barriers to the interdroplet exchange of silica reacting species than those of NP-5. Consequently, fewer nuclei and larger particles are formed.

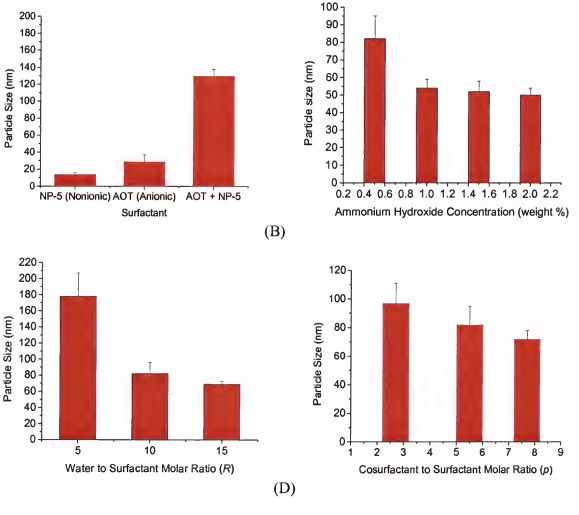

Figure 2-8. The effect of various reaction pararmeters on the size of RuBpy-doped silica nanoparticles. (A) effect of surfactant properties, (B) effect of ammonium hydroxide concentration, (C) effect of water to surfactant molar ratio, R, and (D) effect of cosurfactant to surfactant ratio, *p*. The water to surfactant molar ratio was ten unless otherwise stated.

Addition of NP-5 surfactant to the AOT microemulsion resulted in larger, monodisperse particles with a diameter of 130 nm. For particles prepared by the direct addition of a reactant (e.g. TEOS) to the microemulsion containing ammonium

hydroxide, in addition to the intermicellar exchange rate, the diffusion of the reactants inside the micellar core plays a very important role. NP-5 acts as a cosurfactant causing a decrease in interfacial rigidity, as a result of shielding of the negative charge between two anionic AOT surfactant molecules, and increases the hydrophobic interaction between the non-polar tails of AOT and NP-5, as shown in Figure 2-9 (C). This results in a decrease in microemulsion size,[99] thus leading to more compartmentalization of silica reacting species and a lower inter-micelle exchange rate. These conditions lead to formation of less nuclei and thus a larger particle size.

Effect of reactant concentrations (TEOS and NH_4OH). Formation of dye-doped silica nanoparticles inside W/O microemulsion takes place by hydrolysis of TEOS molecules using ammonium hydroxide as the catalyst. There are four main steps in particle formation: (1) association of TEOS with the W/O microemulsion, (2) TEOS hydrolysis and formation of monomers, (3) nucleation, and (4) particle growth. After addition of TEOS molecules to the W/O microemulsion, the TEOS molecules get partitioned between the W/O microemulsion and bulk organic medium by formation of a monomer having one silanol group (i.e. $Si(OR)_3OH$). Further, hydrolysis leads to the formation of silicic acid, with four silanol groups ($Si(OH)_4$). All of these species are associated with W/O microemulsion and contribute to the nucleation and growth. Since ammonium hydroxide is polar, it is present in the aqueous cores of reverse micelles. In order for hydrolysis to take place the TEOS molecules have to diffuse from the surrounding organic phase to the W/O microemulsion.[100-102]

The effect of the concentration of TEOS and ammonium hydroxide was studied in the quaternary microemulsion of Triton X-100/cyclohexane/hexanol/water using R=10

and p=5.5. As the TEOS concentration increased from 0.025 mM to 0.1 mM, with a constant concentration of ammonium hydroxide of 1.0 weight %, the particle size and polydispersity of silica nanoparticles did not change. The average particle size was found to be 82 ± 15 nm. This phenomenon is due to the fact that excess TEOS molecules remain in the unhydrolyzed state and are unable to partition into the microemulsion phase.

On the other hand, the concentration of ammonium hydroxide, which acts as a catalyst and providing OH^- ions necessary for hydrolysis of TEOS, does affect the nanoparticle size. The particle size decreases and the number density of particles increases, with an increase in the concentration of ammonium hydroxide. As shown in Figure 2-8 (B), the particle size and polydispersity decreased from 82 nm to 50 nm and 13 nm to 4 nm, respectively. The increase in OH^- ions causes an increase in the rate of hydrolysis of TEOS molecules, and hence a large number of monomers are produced. Intramicellar nucleation occurs when the number of monomers inside the microemulsion exceeds a critical number, typically 2.[103] Due to faster hydrolysis rate with an increase in OH^- ions, the ion/monomer occupancy number per micelle is greater than the critical nucleation number, resulting in a larger number of nuclei. Further, faster hydrolysis of TEOS produces increased amount of ethanol as a by-product. Ethanol acts as a cosurfactant, increasing the fluidity of the interface, thereby, increasing the intermicellar exchange rate. These conditions further enhance nuclei formation and lead to a smaller particle size. The resulting particle size is thus, smaller and particles are monodispersed, with increasing amount of ammonium hydroxide.

Effect of water to surfactant molar ratio. An increase in water to surfactant molar ratio of water in oil microemulsions changes three parameters. First, it increases the size of the water pool of the reverse micelles, thereby increasing the ratio of bulk water molecules to surfactant bound (hydrated) water molecules. Second, the increase in the size of the water pool increases the monomer-occupancy number or number of monomers per unit microemulsion droplet. Third, with an increase in R, the intermicellar exchange rate increases due to a decrease in the rigidity of the surfactant film.[101] Figure 2-8 (C) shows the effect of water to surfactant molar ratio on the particle size for RuBpy dye-doped silica nanoparticles prepared in a Triton X-100/cyclohexane/ water microemulsion. At R=5 the average particle size was 178 nm and decreased gradually to 69 nm at R= 15. At low R values the microemulsion droplet size is smaller and hence the number of TEOS molecules partitioned at the interface of the surfactant and water is less. As a result, there are a smaller number of monomers and nuclei formed. Further, conditions of bound water and rigid interface due to close packing of surfactant molecules make the mobility of these monomers less, decreasing the intermicellar exchange. These conditions make the environment conducive for less nuclei formation and a more enhanced growth rate. Hence the terminal particle size is larger. However, the number of monomers and oligomers available for growth are more, and hence the final particle size is larger. As the R value increases, the droplet size of the microemulsion increases and the amount of bulk water molecules also increases. As a result, more of the TEOS molecules are hydrolyzed at the interface. Also the polarity of droplet and the partition coefficient of TEOS increase with size of droplet. Under these conditions, the rate of intramicellar nucleation increases and the resultant particle size is smaller.

Furthermore, at R=15 in addition to an increasing the droplet size and increasing the bulk water molecule, the intermicellar exchange causes further enhancement in the nucleation rate, further decreasing particle size and increasing the monodispersity of dye-doped silica nanoparticles.

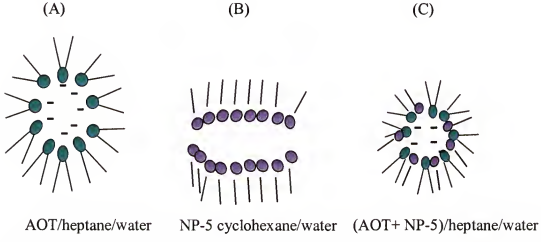

Figure 2-9. Structures of different microemulsion water pools. (A) AOT/heptane/water (B) NP-5/cyclohexane/water (C) (AOT + NP-5)/heptane/water. Reprinted with permission from R.P. Bagwe et al. *Langmuir* **2004**, 20, 8339.[87]

Effect of molar ratio of cosurfactant to surfactant. The molar ratio of cosurfactant to surfactant (*p*) was varied by changing the concentration of hexanol in microemulsion system of Triton X-100/cyclohexane/water. Addition of medium chained alcohol changes the microemulsion in two ways. First, an alcohol molecule adsorbs at the interfacial film of microemulsion droplets and thus alters the packing parameter of surfactant. This influences the radius of curvature of the droplet. Second, it decreases the interfacial rigidity causing more fluid interface and hence increase in intermicellar exchange.

With an increase in cosurfactant to surfactant molar ratio from 2.7 to 11, the particle size decreased as the concentration of cosurfactant increased, as shown in Figure 2-8 (D). These observations are due to the increase in the flexibility of the interfacial film

and increase in number of droplets with an increase in the concentration of cosurfactant. The increase in the number of droplets causes more TEOS molecules to be adsorbed at the oil-water interface than in the bulk. This adsorption leads to more partitioning of TEOS molecules, resulting in more nuclei formation inside the water-in-oil microemulsion droplets. Further, an increase in the fluidity of the interface causes more successful collisions between two droplets, thus favoring conditions for a large number of nuclei formation and decrease in growth rate of the nanoparticles.

Conclusions

Since the organic dye-doped silica nanoparticle experiments were conducted, more research has been done in the Tan laboratory to reproducibly produce 50-80 nm dye-doped silica nanoparticles using the Stöber method. Thus, the methods described here may be used as alternative methods for the synthesis of silica nanoparticles doped with organic or other hydrophobic dyes. However more work is needed to determine a protocol for reproducible organic dye-doped silica nanoparticle synthesis. In future work, more synthesis parameters can be investigated to produce 10-50 nm nanoparticles that are tailor-made for a given biological application with a maximum effective dye concentration, minimal dye leakage, and excellent photostability.

The reverse microemulsion study shows that the silica nanoparticle size is strongly affected by the nature of the surfactant used. The smallest and most monodispersed particles were obtained in the microemulsion system of NP-5/cyclohexane/water. In addition, an increase in the concentration of ammonium hydroxide increases the rate of nucleation, resulting in smaller nanoparticle size, monodisperse particles. The particle size was also found to be a function of water to surfactant molar ratio and cosurfactant to surfactant molar ratio, both showing particle size increase with an increase in their

respective ratios. This optimization study provides a solid foundation for the development and effective utilization of various sizes of RuBpy dye-doped silica nanoparticles that can be used in bioanalysis and biotechnological applications.

CHAPTER 3
SURFACE MODIFICATION AND BIOCONJUGATION OF FLUORESCENT DYE-DOPED SILICA NANOPARTICLES

Introduction

When conjugating biomolecules to fluorescent dye-doped silica nanoparticles, there are a number of strategies that may be used, including covalent coupling, adsorption, and affinity binding. Each has its benefits and drawbacks, which should be considered in the context of research objectives, reagent requirements and costs, and time requirements. Covalent coupling is often employed for the immobilization of biomolecules when a very active and stable nanoparticle probe is required.[104]

Using various biochemical binding approaches, the silica nanoparticle surface can be modified to contain functional groups that are useful for subsequent biomolecule immobilization. Some commonly used functional groups, as briefly mentioned in Chapter 1, include amines, carboxyls, isothiocyanates, thiols (to be described in more detail in Chapter 4), and avidin-biotin affinity based binding. These functional groups can be used to immobilize oligonucleotides, enzymes, antibodies, and other proteins.[86,104-106] Figure 3-1 shows a few examples of surface modification methods that can be used to covalently or physically (in avidin-biotin binding) attach biomolecules to the surface of silica nanoparticles.

An effective bioconjugation approach for the immobilization of proteins, such as antibodies and enzymes, onto the silica nanoparticles is to chemically link carboxyl groups on the nanoparticle surface. Then, the amine groups on the surface of the proteins

can react with activated carboxyl groups, leading to covalently bound proteins on the silica nanoparticles. To obtain the carboxyl-modified particles, the silica nanoparticles are silanized by immersion in 1% (v/v) solution of distilled, trimethoxysilylpropyl-diethylenetriamine (DETA) and 1 mM acetic acid for 30 minutes at room temperature. The DETA or amine-modified silica nanoparticles are thoroughly rinsed with deionized water to remove excess DETA. The silanized particles are then treated with 10% succinic anhydride in dimethylformamide (DMF) solution under an argon atmosphere and stirred for 6 hours. The resulting carboxyl- modified particles are washed with deionized water and then activated with a carbodimide hydrochloride (EDC) in conjunction with a water-soluble *N*-hydroxysuccinimide (NHS), allowing the subsequent coupling of proteins to the nanoparticles.

Streptavidin/Avidin Adsorption.

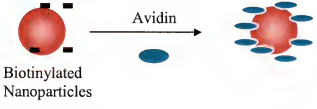

Amine-Glutaraldehyde Crosslinking.

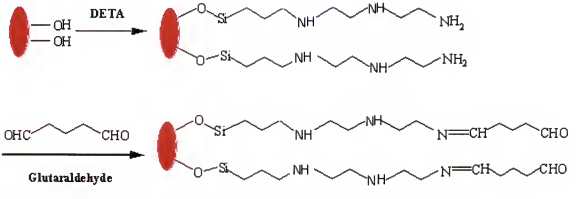

Figure 3-1. Commonly used methods for silica nanoparticle surface modification or functionalization.

Amine-Carboxyl Coupling.

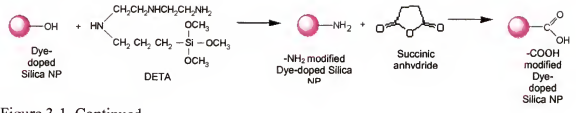

Figure 3-1. Continued.

Among fluorescent labels, dye-doped silica nanoparticles show distinct advantages due to their high quantum yield, photostability, hydrophilicity, and ease of surface modification with different functional groups for subsequent bioconjugation, due to well known silica chemistry. However, the high sensitivity provided by the fluorescence signal amplification, selectivity, and reproducibility of nanoparticle based bioassays can be limited by the tendency of the silica nanoparticles to aggregate irreversibly and cause non-specific binding. Following surface modification, an excess of active functional groups, which are capable of binding to or interacting with various other chemical and biological species, can lead to false positive and/or negative signals. Thus, the controlled addition of surface functional groups and subsequent bioconjugation is highly desirable. In this chapter, surface modification schemes are presented which improve the efficiency of biomolecule conjugation, specifically proteins, as well as reduces the degree of nanoparticle aggregation and nonspecific binding.

Experimental Section

Materials. Triton X-100 was purchased from Sigma-Aldrich (St. Lois, MO). Tetraethylorthosilicate (TEOS), trihydroxypropylmethylphosphonate (THPMP), 3-aminopropyltriethoxysilane (APTS), octadecyltriethoxysilane, n-heptane, cyclohexane, hexanol, ammonium hydroxide (NH_4OH), and tris(2,2'-bipyridine) dichlororuthenium (II) hexahydrate (RuBpy), were obtained from Aldrich Chemical (Milwaukee, WI).

Carboxyethylsilanetriol, sodium salt (CTES, 25 wt. % in water) was purchased from Gelest (Tullytown, PA). Unless otherwise noted, all reagent grade chemicals were used as received, and deionized, distilled water was used in the preparation of all aqueous solutions.

Synthesis and surface modification of fluorescent dye-doped silica nanoparticles. Silica nanoparticles were synthesized using a water-in-oil (W/O) or reverse microemulsion method. As described in Chapter 2, the microemulsion consisted of a mixture of 1.77 mL triton X-100, 1.6 mL n-hexanol, 7.5 mL cyclohexane, 80 μL, 0.1 M aqueous dye solution, 400 μL water, and 100 μL ammonium hydroxide that was stirred for 10-30 minutes at room temperature, and then 100 μL of TEOS was added. The mixture was allowed to stir for 24 hours, followed by the addition of appropriate ratios of TEOS and functionalized silanes for particle post-coating and surface modification. For post-coating, the mixture was further reacted for 24 hours and the silica particles were released from the microemulsion by the addition of ethanol. The particles were separated from the reaction mixture and washed four times with ethanol.

Characterization. RuBpy dye-doped silica nanoparticles were characterized with regard to particle size, degree of aggregation, overall surface charge and fluorescence properties. The samples were imaged using TEM or SEM. The effective size and degree of nanoparticle aggregation was also analyzed by dynamic light scattering (DLS), using a BI 90 Particle Sizer (Brookhaven Instruments Corp., Holtsville, NY). The zeta potential or overall surface charge of each nanoparticle sample in solution was determined using a Zeta Plus, zeta potential analyzer (Brookhaven Instruments Corp.

Holtsville, NY). Fluorescence measurements were conducted on a Fluorolog Tau-3 spectrofluorometer (Jobin Yvon Spex Instruments, S.A. Inc.).

Results and Discussion

Nanoparticle storage, handling, and aggregation. Nanoparticle aggregation is a disadvantage that can limit the use of the silica nanoparticles in biological applications. Thus, steps must be taken during and after the synthesis and conjugation steps to avoid aggregation as much as possible. Some special precautions which should be taken include the storage of the nanoparticle in an appropriate solution following synthesis because the drying of the silica nanoparticles facilitates nanoparticle aggregation. In addition, nanoparticle preparation and handling procedures should minimize the use of heat-generating agitation methods, which also facilitates nanoparticle aggregation. These methods include vortexing and sonication; particles should not be vortexed or sonicated any longer than necessary to facilitate nanoparticle dispersion.

Surface modification approaches. For microemulsion synthesized silica nanoparticle, the surface can be modified or functionalized either during or after synthesis. The post-coating method, as described in the Experimental Section above, is preferred whenever possible because it is less complicated and time-consuming and can control the number of functional groups added to the nanoparticle surface by the amount of functionalized silanizing agent used in the synthesis. In addition, this method can be used to change the overall surface charge of the nanoparticles while they are still isolated in the water pools of the microemulsion, thus, minimizing the interactions which tend to cause aggregation. For example, the addition of carboxyl groups to the surface of 60 nm silica nanoparticles results in a highly negative zeta potential (-35 mV) on the NP surface, causing the particle to be well dispersed in aqueous solutions and less prone to

aggregation, as shown the SEM image of nanoparticles modified during synthesis in Figure 3-2. Using the post-coating synthesis method, RuBpy dye-doped silica nanoparticles have been modified with different functional groups, including amine (NH_2), carboxyl (COOH), octadecyl (C-18), and polyethylene glycol (PEG) groups using functionalized silanes such as those shown in Figure 3-3, to prepare the surface for bioconjugation and/or to encourage dispersion in aqueous or non-aqueous solutions (via the nonpolar octadecyl group).

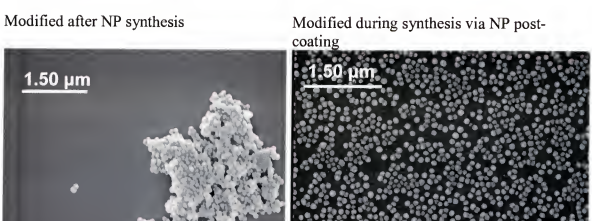

Figure 3.2 SEM images of carboxyl-modified silica nanoparticles.

Surface modification of fluorescent dye-doped silica nanoparticles. The introduction of desired functional groups on the surface of the dye-doped silica nanoparticles involves the condensation of tetraethylorthosilicate (TEOS) and organosilane reagents containing the active functional groups. In preliminary experiments, it was determined that the addition of TEOS along with the functionalized organosilane is necessary during the microemulsion post-coating step; the absence of tetraethylorthosilicate prevents surface modification. Further, the time interval between the addition of TEOS and the organosilane reagent(s) in the post-coating step needs to be

at least 20 to 30 minutes. This time interval is important because otherwise most of the active functional groups would be buried inside the particles, as the condensation reaction of the organosilane is faster than tetraethylorthosilicate. This observation was found to be in agreement with the work done by Deng et al.[107] who performed a systematic study of the effect of the addition of organosilanes at different stages on silica particle growth in microemulsions.

For Amine functionality

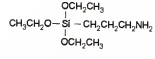

(3-Aminopropyl)triethoxysilane (APTS)

For Carboxylate functionality

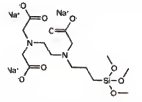

N-(Trimethoxysilylpropyl)ethylene-diamine, triacetic acid, (CMS)

For Phosphonate functionality

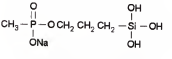

(3-Trihydroxysilyl)propyl methylphosphonate (THPMP)

For Dodecyl (C-12) functionality

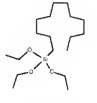

Dodecyl triethoxysilane (DDTES)

Figure 3-3. Silane coupling agents used for introducing various functional groups to silica nanoparticle surface during synthesis.

Aggregation studies on fluorescent dye-doped silica nanoparticles. Amine functionality is highly desirable for bioconjugation. However, when amine groups are added to the surface of the silica nanoparticles, the particles tend to aggregate, as shown in Table 3-1. To reduce the degree of nanoparticle aggregation, the effect of varying the volume ratio of amine (3-aminopropyltrimethoxysilane) to phosphonate group (3-trihydroxypropylmethylphosphonate) from 0-100:1on the particle size and zeta potential

value was studied. When high concentrations of amine groups were added to the surface, nanoparticle agglomeration as measured by the hydrodynamic particle size was very high (2500 nm) and the zeta potential value was very low (-5 mV). The presence of amine groups on the surface was confirmed using the fluorescamine test[108] for particles prepared under same condition but without dye molecules. The results showed a strong fluorescence peak at 455 nm in all cases. As the amount of inert functional group, methyl phosphonate, was added to the surface, the zeta potential value became more highly negative (-35 mV), and the particle size decreased due to strong electrostatic repulsion forces between nanoparticles (100 nm).

The nanoparticles prepared under these conditions were found to be stable for more than eight months in aqueous solution. This observation can be explained by considering the pKa values of amine, phosphonate, and silica groups on the surface of nanoparticles dispersed in water, which are 9.0, 2.0 and 7.0 respectively. At physiological pH 7.4, the amine groups have a positive charge and the methylphosphonate and silica groups have negative charges. The amine-modified silica nanoparticles can form back-bonding to surface silanol groups, as shown in Figure 3-4(A). Hence, the overall charge on the surface is very low, as shown by the low zeta potential value, and the particles tend to aggregate because there is no driving force on the surface of the nanoparticles to keep them apart. As methylphosphonate groups are introduced on the surface, most of the amine groups on the silica surface interact with methylphosphonate groups as shown in Figure 3-4 (B), preventing back-bonding. Consequently, the nanoparticles were highly dispersed as indicated by the high zeta potential value (-35 mV) and hydrodynamic

particle size (115 nm) more representative of the actual size of the nanoparticles. The silica nanoparticles were 80-100 nm in diameter, as determined by TEM.

Table 3-1. Particle size and zeta potential of unmodified and amine-modified RuBpy-doped silica nanoparticles.

	Hydrodynamic Particle Size	Zeta Potential
RuBpy Nanoparticles (TEOS only)	203 nm	2.23 mV
30% APTS[a] Post Coating	1529 nm	28.20
50% APTS[a]	1521 nm	30.10
1% APTS Activation[b]	729 nm	-0.19
10% APTS Activation[b]	729 nm	-2.84

[a] The RuBpy-doped silica nanoparticles were modified with amine groups during the nanoparticle synthesis.
[b] Amine-containing silane (APTS) reacted with the nanoparticle following synthesis.

Effects of BSA blocking on RuBpy-doped silica nanoparticle-antibody conjugation. During the conjugation of antibody to RuBpy-doped silica nanoparticles, the carboxyl-modified nanoparticles formed large aggregates that negatively affected the usage of the fluorescent nanoparticles as reporter antibodies in immunoassays. To reduce the aggregation of the nanoparticles, the reporter antibodies were briefly sonicated, vortexed, and reacted with 1% bovine serum albumin (BSA) and 40 mM primary amine. The BSA interacted with any unreacted functional groups on the nanoparticle surface and prevented any nonspecific binding of the reporter antibodies with themselves or the bacteria samples.

Conclusions

A reverse microemulsion based surface modification method was used to successfully prepare uniform fluorescent dye-doped silica nanoparticles of desired size

and surface functionality at room temperature. Colloid stability studies, based on particle sizing and zeta potential, indicate that the addition of appropriate ratios of inert functional groups (methylphosphonate) and active functional groups (carboxyl groups) to the surface of silica nanoparticles results in a highly negative zeta potential, which is necessary to keep the silica particles well dispersed and at the same time enable carboxyl-based bioconjugation. Using this surface modification scheme and similar strategies, fluorescent dye-doped silica nanoparticles can be more readily conjugated with biomolecules and used as highly fluorescent, sensitive, and reproducible labels in DNA applications, immunological assays, and various other types of bioanalytical applications.

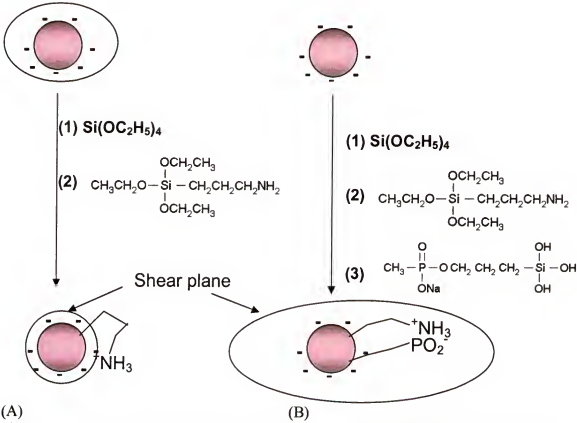

Figure 3-4. Schematic diagram showing the mechanism by which the back-bonding of amine-modified silica nanoparticles is reduced. (A) Back-bonding of NH_2 functional groups to silanols on the particle surface. (B) Elimination of back-bonding due to interactions between the amine and phosphonate groups on the particle surface, thus, increasing the shear plane and electrostatic repulsion of the particles.

CHAPTER 4
DNA-CONJUGATED SILICA NANOPARTICLES

Introduction

Deoxyribonucleic acid (DNA) and ribonucleic acid (RNA) form the most basic units of information storage within cells. Despite the complexity of the genetic code, nucleic acids are the only type of biological molecule in which binding properties can be fully anticipated due to the Watson-Crick base-pairing process, which causes one oligonucleotide to bind to its complementary sequence. By targeting segments of this genetic data with synthetic segments of labeled or unlabeled DNA probes, specific regions of target DNA can be detected, localized, or quantified, even in environments containing many other non-complementary sequences. As the genetic code is deciphered by scientific efforts, such as the Human Genome Project, there is a great demand for additional techniques for genetic mutational scanning, molecular bar coding, and gene expression monitoring, and DNA sequencing that may lead to diagnostic tests able to identify genetic markers associated with certain disease states.

A short DNA segment can be synthetically designed and used to probe and hybridize to a target DNA strand. Usually, complementary oligonucleotide probes are used that possess conjugated fluorophores, radiolabels, enzymes, haptens, or other groups that can be used to detect hybridization signal.[104] These oligonucleotide conjugates can be used to detect target sequences in Southern blots, electrophoresis gels, tissues, or cells, after amplification by PCR techniques, or in solution. The immobilization of labeled or unlabeled oligonucleotide probes onto solid supports or substrates is also a commonly

used technique for the isolation, identification and genetic analysis of specific DNA sequences. A major factor in the development of assays for DNA hybridization is the ability to modify a nucleic acid while not affecting base-pairing. Thus, in addition to the actual base composition of the oligonucleotide probe, the attachment of the nucleic acid to a detectable component or a solid support forms the basis for constructing a sensitive hybridization reagent.

Hybridization to immobilized oligonucleotides is increasingly used in clinical diagnostics, genetic analysis, and research on hybridization. Early methods for the immobilization of pre-synthesized oligonucleotides to a substrate involved adsorption to surfaces, such as nitrocellulose[109] or nylon membrane filters. These noncovalent methods suffered from poorly defined oligonucleotide strand orientation, packing density, mobility, and attachment, which prohibited efficient hybridization. Early covalent attachment methods relied on chemical modifications of the DNA via phosphodiester linkages, cyanogen bromide activation, and carbodiimides for immobilization to agarose, cellulose, Sephadex, and Sephacryl.[110-112] However, rates of DNA hybridization when using immobilization methods were reported to be at least ten-fold slower when compared to solution phase kinetics.[113]

Of the many established methods used for the covalent immobilization of pre-synthesized oligonucleotides to a substrate,[114-122] the utilization of disulfide-coupling chemistry has proven to be one of the simplest and most efficient methods.[115] Disulfide-coupling chemistry has been used in the ligation of peptide to peptide, DNA to DNA, peptide to DNA, DNA to haptens, DNA to paramagnetic beads, and DNA to controlled porosity glass (CPG).[123-126] Unlike most of the other covalent attachment processes

involving disulfide bonds, the thiol/disulfide exchange method does not require the reduction of the disulfide groups to generate more reactive, but unstable, thiol species prior to immobilization. The disulfide-modified oligonucleotides are directly coupled to the silane-activated silica surface without any pretreatment. Potential side reactions are minimized due to the specificity of the reaction.[115]

As highlighted in Chapters 1 and 3, silica nanoparticles have been conjugated with a variety of biomolecules (including proteins, enzymes, peptides, and DNA) and used as fluorescent biomarkers to monitor biological events or detect biological targets.[13,16,76,127] In an effort to expand upon the potential bioanalytical applications of silica-based nanoparticles, covalently linked silica nanoparticles and oligonucleotide probes were prepared to produce DNA-conjugated silica nanoparticles for DNA/RNA hybridization using the thiol/disulfide exchange method (Reproduced with permission from L.R. Hilliard and X.J. Zhao *Analytica Chimica Acta* **2002**, *470*, 51-56. Copyright [2002] Elsevier).[88] This covalent immobilization method is an alternative to other methods currently used to modify silica nanoparticles, especially when the use of disulfide functionality is required. The oligonucleotide or DNA-conjugated silica nanoparticles produced using this method proved to be an effective substrate for hybridization and are potentially useful in DNA/mRNA analysis.

Experimental Section

Synthesis and silanization of nanoparticles. Silica nanoparticles were synthesized using a standard water-in-oil microemulsion method with a water to surfactant molar ratio, $W_0 = 10$, as previously described in Chapter 2. Characterization of the silica nanoparticles was done using a transmission electron microscope (TEM, Hitachi model H7000). As shown in Figure 4-1, uniform silica nanoparticles were

produced. The TEM image shows that the nanoparticles used in our DNA immobilization experiments were 60 ± 5 nm in diameter. Before DNA immobilization, the newly synthesized silica nanoparticles were silanized with 1% 3-mercaptopropyl-trimethoxysilane (MPTS) in 95% ethanol and 16 mM acetic acid (pH 4.5) for 30 minutes at room temperature and rinsed once with 95% ethanol and 16 mM acetic acid (pH 4.5) before being cured for approximately two hours in a vacuum oven at 150°C.

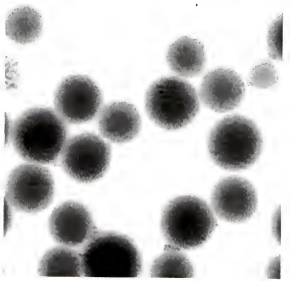

Figure 4-1. TEM image of silica nanoparticles. The silica nanoparticles, synthesized using the microemulsion method, were uniform in size, 60 ± 5 nm.

Oligonucleotide immobilization. The attachment of 5' disulfide-modified oligonucleotides (presynthesized, by IDT DNA Technologies) to silica nanoparticles was performed via a thiol/disulfide exchange reaction. The 5'-disulfide oligonucleotides were diluted to a concentration of 1-5 μM in 500 mM, $NaHCO_3/NaCO_3$ buffer (pH 9.0). The silica nanoparticles (8 μg/μL) were added to the oligonucleotide solution and allowed to incubate in a humid chamber for 20 hours at room temperature. The particles were then washed three times in TNTw buffer (10 mM Tris-HCl, 150 mM NaCl, and 0.05% Tween 20, pH 7.5) with 0.5-2 minute sonication and 5 minute centrifugation at 4000 rpm after

each wash. The DNA-conjugated silica nanoparticles were then dispersed in a buffer of 20 mM Tris-HCl, 37.5 mM $MgCl_2$ (pH 8.0) for subsequent hybridization.

DNA hybridization and measurement. A 2-6 fold excess of 3' FAM-labeled target oligonucleotides was added to unlabeled oligonucleotide-conjugated silica nanoparticles and allowed to incubate for 30 minutes in a hybridization buffer of 20 mM Tris-HCl, 37.5 mM $MgCl_2$ (pH 8.0). The nanoparticles were then washed three times in the hybridization buffer with 5 minute centrifugation at 4000 rpm after each wash. DNA hybridization between the immobilized DNA probes on the nanoparticle surfaces and the target DNA in the solution was detected via fluorescence measurements using a spectrofluorometer (F-112A, SPEX Industries). The samples, 50 μL aliquots, were excited at 488 nm using a xenon lamp with slit widths of 2.5 nm and an integration time of 0.1 seconds. Fluorescence signal was observed at an emission wavelength of 520 nm, and calibration data was used to determine the efficiency of hybridization.

Results and Discussion

The reliability and integrity of hybridization reactions on the DNA-conjugated silica nanoparticle probes is dependent upon the stability, accessibility, and specificity of the oligonucleotides on the silica nanoparticle surface, and thus, greatly dependent upon the properties and degree of covalent attachment. The immobilization efficiency should be high and provide a stable linkage to the silica particle surface. The immobilized nucleic acid molecules must be readily available for hybridization to complementary sequences and exist in a sufficiently fluid environment for reaction kinetics to approach those for solution phase experiments. This accessibility has been found to depend more on the method of immobilization than on the type of support used.[128] Reports have shown that DNA can become totally inaccessible when as little as 3% of the bases are

involved in the covalent linkage.[128] The use of a spacer arm or linker to attach oligonucleotides to the silica particles via the strand terminus should improve the hybridization kinetics and efficiencies by increasing the degrees of freedom of the oligonucleotides and availability of the bases. It has been demonstrated that the use of a linker of at least 28Å in length between the support and the oligonucleotide is the minimum requirement in order to provide hybridization efficiencies which approach those of solution phase reactions, and are at least four times greater than if no linker is used.[129] Based on these requirements for oligonucleotide stability, accessibility, and specificity, silica nanoparticles and oligonucleotide probes with a C_6-chain linker were covalently linked using the thiol/disulfide exchange method to produce functional nanoparticles for hybridization.

1) Silica Nanoparticle Silanization

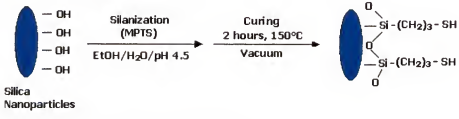

2) Oligonucleotide Probe Immobilization

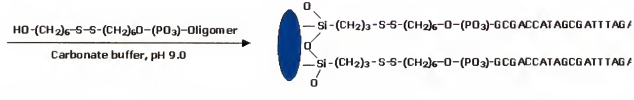

3) Oligonucleotide-conjugated Silica Nanoparticle Hybridization with Target Oligonucleotides

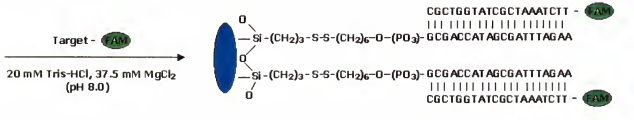

Figure 4-2. The immobilization of DNA onto silica nanoparticles and DNA hybridization.

The attachment of disulfide-modified oligonucleotides to silica nanoparticles was performed via a stable thiol/disulfide exchange reaction, in which the disulfide on the 5'-end of the 20 base-pair oligonucleotide probe reacted with the thiol functional group of the MPTS layer on the silica nanoparticles. Under basic conditions, the alcohol-based leaving group [R = $HS-(CH_2)_6OH$] facilitates the thiol to disulfide exchange. To promote high hybridization efficiency, a C_6 chain linker was added to the oligonucleotide probe. The three major steps involved in the covalent immobilization of oligonucleotides onto silica nanoparticles via disulfide bonds and subsequent use as a substrate for nucleic acid hybridization are illustrated in Figure 4-2.

DNA immobilization efficiency. To determine the efficiency of the immobilization method, various concentrations of oligonucleotide probes, functionalized with disulfide groups on the 5'-end and labeled with carboxyfluorescein (FAM) dye molecules on the 3'-end (S-S-Oligomer-FAM, See Figure 4-2, Step 2 for the probe sequence. In the Figure 4-2, the probe is not dye labeled.), were immobilized using the thiol/disulfide exchange reaction. First, the effect of silica nanoparticle concentration on the immobilization of oligonucleotide probes onto nanoparticles was investigated. S-S-Oligomer-FAM, 2 μM, was immobilized onto 0.5-16 μg/μL of nanoparticles for approximately 15 hours. The attachment density was calculated based on measurements of variable nanoparticle concentration as a function of constant probe concentration. A linear immobilization correlation with optimal attachment density (i.e. the amount of oligonucleotide probes covalently attached to the nanoparticles) was achieved with a nanoparticle concentration of 8 μg/μL, as shown in Figure 4-3. Analysis of the washing solutions of DNA nanoparticle samples that were reacted with higher concentrations of

DNA showed that more DNA was immobilized onto the particle surface as the initial DNA concentration increased, suggesting that the high density of DNA on the silica nanoparticles contributes to self-quenching of the FAM dye molecules and may inhibit hybridization.

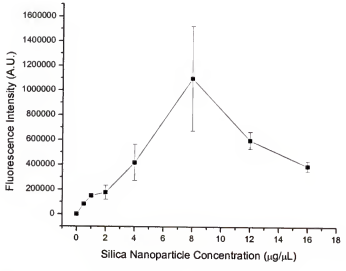

Figure 4-3. Effect of silica nanoparticle concentration on DNA immobilization efficiency. Various concentrations of silica nanoparticles were conjugated with 2 μM oligonucleotide probes.

Using 8 μg/μL silica nanoparticles, the maximum, immobilized oligonucleotide probe concentration was determined by varying the probe concentration between 40 nM and 20 μM. Thorough washing of the DNA nanoparticle samples, three or more times in 20 mM Tris–HCl, 37.5 mM $MgCl_2$ (pH 8.0) using original sample volume, removed physically absorbed DNA probes and ensured that the fluorescence signal measured was indicative of the oligonucleotide concentration immobilized and not that physically adsorbed to the silica surface or in solution, as shown in Figure 4-4. As probe concentration increased, the relative fluorescence signal increased until it reached a plateau at an actual oligonucleotide concentration of approximately 2 μM, when the

initial probe concentration in solution was 10 μM, as shown in Figure 4-5. The quantification of the actual amount of oligonucleotides immobilized was determined by detecting the concentration of probe left in the supernant and washing solutions of the given samples. Calibration data was then used to calculate the probe concentration left in solution versus that covalently immobilized to the silica surface.

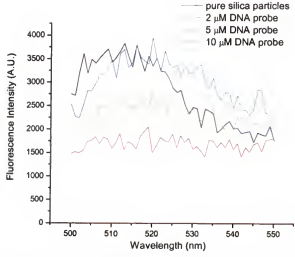

Figure 4-4. Non-specific binding of DNA probe to silica nanoparticles. Pure-silica nanoparticles (no silanization) were reacted with S-S-Oligomer-FAM for 1 hour and washed three times in TNTw buffer. The fluorescence intensity measurements show that no DNA was physically adsorbed to the nanoparticle surface.

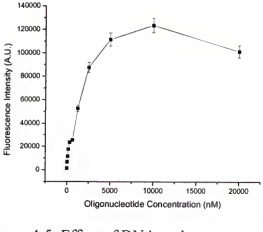

Figure 4-5. Effect of DNA probe concentration on immobilization efficiency. Various concentrations of S-S-Oligomer-FAM were immobilized onto 8 μg/μL silica nanoparticles.

The effect of reaction time on the immobilization efficiency was examined using 2 μM of the probe, S-S-Oligomer-FAM. The immobilization reaction times ranged from 15 minutes to 30 hours. As shown in Figure 4-6 (A), the immobilized probe concentration increased until approximately 18 hours when the rate of immobilization began to level off. Within 6 hours, 80% of the maximum of the attachment density was observed. In an attempt to obtain a more accurate range for immobilization time, 2 μM oligonucleotide probe was immobilized onto 8 μg/μL particles for 12 – 30 hours and analyzed using S-S-Oligomer-FAM and S-S-Oligomer hybridized with 2 μM target DNA. Results confirmed that approximately 18 hours resulted in optimal immobilization of the oligonucleotide probes as shown in Figure 4-6 (B) and (C). As compared to immobilization times for other solid supports using this method, the silica nanoparticles require a longer incubation due to the increased overall surface area.[115] The time required for oligonucleotide concentration may be reduced when a higher concentration, such as 10 μM, is used, but much of the DNA probe is wasted because it is not covalently attached to the nanoparticles.

Disulfide bond stability. With the optimized immobilization conditions, DNA-conjugated silica nanoparticles were successfully prepared using the disulfide-modified oligonucleotides. To evaluate the stability of the covalent attachment via disulfide bonds, samples of 8 μg/μL nanoparticles with dye-labeled probes were tested after being stored in a hybridization buffer containing a salt concentration of 37.5 mM $MgCl_2$ for 1–30 hours. The change in the fluorescence intensity of the nanoparticle solution was monitored over time by measuring the fluorescence of the solution before and after washing for each time interval. It was observed that less than 5% of the disulfide-bound

probes detached from the nanoparticles after one hour at room temperature, while less than 25% of the oligonucleotides were detached from the nanoparticles after 24 hours, as shown in Figure 4-7. The DNA nanoparticles have an optimal lifetime of approximately one day when stored in a buffer solution. The nanoparticle probes do exhibit reactivity with DNA/RNA targets for at least one week after synthesis if stored at 4°C under dry, relatively neutral pH conditions, but the hybridization efficiency is reduced (i.e. the amount of target DNA that can be detected by the DNA-conjugated silica nanoparticles is reduced).

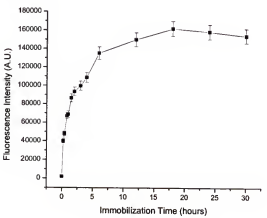

Figure 4-6. Effect of DNA immobilization reaction time on immobilization efficiency. Silica particles, 8 μg/μL, were immobilized with 2 μM oligonucleotides for up to 30 hours. 2 μM probe were reacted for 30 minutes to 30 hours to the nanoparticles.

Hybridization efficiency. To test whether the DNA probes on the nanoparticle surface are viable for hybridization with target DNA probes, the hybridization properties of the oligonucleotide-conjugated silica nanoparticles were tested. The DNA hybridization was monitored by mixing the nanoparticles and dye-labeled target DNA in an appropriate buffer. The procedure was described earlier in the Experimental Section. Fluorescence signal due to hybridization was observed over time.

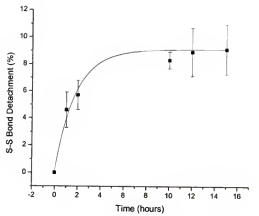

Figure 4-7. Disulfide stability of DNA-conjugated silica nanoparticles.

Hybridization reactions involving the DNA nanoparticles were assessed for the effects of salt concentration, temperature, and reaction time and are shown in Figure 4-8. To determine the optimal salt concentration, 8 μg/μL DNA-conjugated silica nanoparticles that were reacted with ~ 2 μM and ~ 5 μM probe DNA (actual probe DNA concentration was determined to be ~2 μM for both samples) were hybridized with 5 μM target in 20 mM Tris-HCl (pH 8.0) with various salt concentrations. A salt concentration of 37.5 mM $MgCl_2$ resulted in the highest hybridization signal and was used in all of the hybridization experiments. However, all of the salt concentrations tested (23 mM–1.5 M NaCl; 9–500 mM $MgCl_2$) produced comparable hybridization interactions. Thus, the presence of a minimal concentration of metals ions with an ionic strength (μ) of at least 0.23 is sufficient for hybridization.

The highest hybridization efficiency was observed when the reaction was carried out at room temperature. At other temperatures within 50 degrees below the melting temperature (~54°C), the hybridization signal was slightly lower. A 2.5:1 molar ratio of target to DNA-conjugated silica nanoparticles was used to determine the optimal hybridization time, and a time of 30 minutes produced the highest fluorescence signal.

When hybridized with two to six-fold excess of a complementary target sequence (5'-TTCTAAATCGCTATGGTCGC-3'), a single-base mismatch sequence (5'-TTCTAA ATCACTATGGTCGC-3'), or a random sequence (5'-ATCCTTATCAATATT-3'), the DNA-conjugated silica nanoparticles proved to be a sufficient substrate for hybridization interactions. Results showed that significant hybridization signal was detected for the perfect target, while no measurable signal was detected for the random sequence, as shown in Figure 4-9 (B). As expected, no significant difference was observed between the target sequence and the single-base mismatch sequence, as there is only a 1/20 or 5% difference in the two linear probes. Given these results, the DNA-conjugated silica nanoparticles are able to discriminate between its target and other oligonucleotide samples given reasonable concentration and sequence differences.

The oligonucleotide-conjugated nanoparticle probes were able to detect a complementary target concentration in the nanomolar range, as low as 5 nM based on initial target concentration in 62.5 μL hybridization buffer. As shown in Figure 4-9 (A), the highest target concentration detected, when using 2 μM, 8 μg/μL DNA nanoparticles, was approximately 1.25 μM target, based on initial target concentration in 62.5 μL hybridization buffer. In agreement with earlier work done using this immobilization method, no measurable non-specific attachment was observed.[115] Thus, the DNA-conjugated silica nanoparticles also provide reliable and accessible silica-surface-bound oligonucleotide probes for target hybridization when the probes are immobilized using the thiol/disulfide exchange reaction.

The pure silica nanoparticles were used to demonstrate that the nanoparticles were viable substrates for DNA immobilization. However, for more practical utility magnetic,

silica nanoparticles would enable both the separation and detection of DNA targets. Magnetic oligonucleotide-modified silica nanoparticles using the thiol/disulfide exchange conjugation method also showed promise as a substrate for the identification and detection of nucleic acid targets. The magnetic silica nanoparticles were synthesized using a previously described method[114] and were approximately 32 nm in diameter. The DNA immobilization procedure was similar to that described in the Experimental Section. Figure 4-10 (A) and (B) shows 4 and 8 μg/μL magnetic silica nanoparticles that were immobilized with initial DNA probe concentrations of 0.1 μM, 1 μM, and 5 μM. A direct comparison of hybridization efficiencies cannot be made between the magnetic silica nanoparticles and the pure-silica nanoparticles because the immobilization conditions used did not take into account the effects of the particles' magnetic properties on the immobilization process.

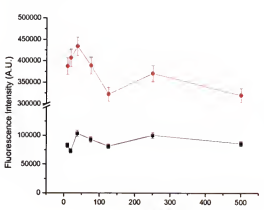

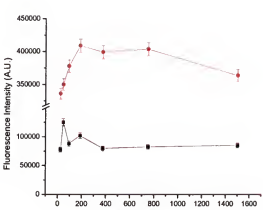

(A)

Figure 4-8. Effects of various experimental parameters on hybridization to DNA immobilized onto silica nanoparticles. (A) salt concentration, (B) temperature, and (C) hybridization reaction time when using 5 μM DNA target. (A) The red and black lines represent 8 μg/μL of silica nanoparticles that were reacted with ~ 2 μM probe and ~ 5 μM, respectively.

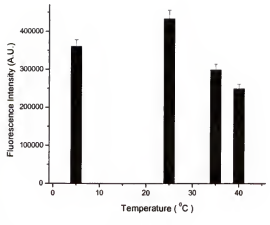

Figure 4-8. continued.

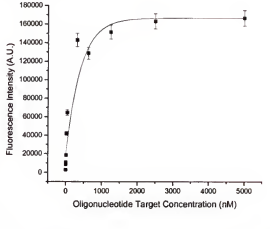

Figure 4-9. Hybridization on DNA-conjugated silica nanoparticles. (A) The target detection limit was determined by hybridizing target probe with 2 μM, 8 μg/μL particles. (B) The random sequence was TAMRA labeled at the 5'-end; when the optimal excitation wavelength of 514 nm was used, no significant hybridization signal was measured (data not shown).

Despite the less than ideal conditions, the viability of the DNA-conjugated magnetic silica nanoparticles as a substrate for hybridization reactions was demonstrated. As shown in Figure 4-10 (B), the fluorescence signal increased as the initial probe concentration immobilized onto the particles increased. In applications where magnetic localization is viable and with further particle development and optimization, magnetic silica nanoparticles using the thiol/disulfide exchange conjugation method can be used in

the identification and harvesting of DNA and RNA in cells or in other complex systems.[90]

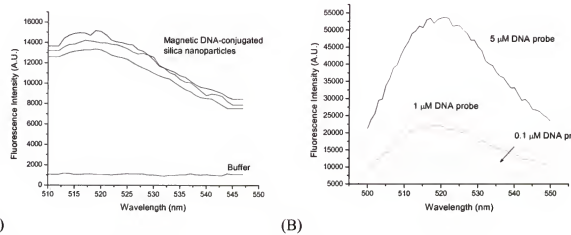

(A) (B)

Figure 4-10. Immobilization of DNA probe onto magnetic silica nanoparticles. (A) Magnetic silica nanoparticles, 8 μg/μL, were reacted with ~ 5 μM DNA probe. (B) Magnetic silica nanoparticles, 4 μg/μL, were reacted with ~ 0.1 μM, ~ 1 μM, and ~ 5 μM DNA probe.

Conclusions

The immobilization of oligonucleotides probes via disulfide bonds to silica nanoparticles and the subsequent DNA hybridization was successfully demonstrated. Using optimal hybridization conditions, the DNA-conjugated silica nanoparticle probes showed efficient hybridization with their nucleic acid targets down to the nanomolar range. The silica nanoparticles also provided a large surface area for DNA attachment and allowed the hybridization reaction to take place in a homogenous solution. This fundamental information on DNA-conjugated silica nanoparticle preparation and application conditions is highly useful for the development of ultrasmall DNA/mRNA nano-biosensors for trace analysis.

CHAPTER 5
DETECTION OF *Escherichia coli O157:H7* USING FLUORESCENT DYE-DOPED SILICA NANOPARTICLES

Introduction

Escherichia coli O157:H7 (*E. coli* O157:H7) is one of the most dangerous agents of food-borne diseases.[130] This toxin-producing bacteria, was first recognized as a human, enteric pathogen following two outbreaks of hemorrhagic colitis (characterized by severe abdominal pain and bloody diarrhea) in 1982.[131] Further studies identified this organism as a major cause of hemolytic uremic syndrome, or HUS (characterized by anemia and renal failure), and showed that the O157:H7 serotype has caused outbreaks of diarrhea-related illnesses since at least the 1950s.[132] The most common source of *E. coli* O157:H7 outbreaks has been associated with ground beef,[133] and the largest reported outbreak of *E. coli* O157:H7 infection occurred in 1992 and was linked with the consumption of undercooked ground beef at multiple outlets of a fast food chain in the northwestern part of the United States.[134] Other foods implicated in outbreaks of *E. coli* O157:H7 infection include vegetables, salad bar items, fruits, and salami.[133,134] Since *E. coli* O157:H7 is not heat resistant, proper cooking practices should eliminate the threat of this organism in foods such as ground beef. But for fruits, vegetables, and other food products usually uncooked, it poses a significant health threat. Given the low infectious dose of *E. coli* O157:H7 (~10–100 cells), the presence of even a single bacterial cell in food may pose a serious health risk.[130,135] Several of the reported outbreaks of *E. coli* O157:H7 have led to death, especially in cases involving children and the elderly.[136-140]

With the number of reported illnesses due to *E. coli* O157:H7 on the decline due to food safety efforts, rapid, sensitive, and simple detection techniques for food are needed to sustain and further reduce the number of infections and deaths associated with this pathogen and other foodborne infectious agents.

In addition to food safety, the ability to rapidly detect pathogenic bacteria is also vital for clinical diagnosis and therapies, potable water, and preventative security measures against the use of bioterrorism agents. Traditional detection methods provide both qualitative and quantitative information on the presence of pathogenic bacteria but are laborious and may take 1-5 days to complete. For the detection of trace amounts of bacteria, amplification or enrichment of the target bacteria in the sample is required.[130,142,143] Over the past decade, many important developments have improved these detection techniques. To address the need for pathogenic bacteria detection techniques that are rapid and simplistic without compromising specificity and sensitivity, these methods are currently used: modified and automated plating methods, cell counting methods, impedimetry, nucleic acid-based methods, and immunological methods, as shown in Table 5-1.[144]

Modifications and automation of conventional plating methods (which require the growth of bacteria in culture for 1-5 days) include faster and more convenient sample preparation methods, plating techniques, and counting and identification test kits.[144-146] These more efficient laboratory techniques can reduce the total analysis time by days, depending on the given method. Cell counting methods, including flow cytometry (approximately 10^2 - 10^3 bacterial cells/mL detected within a few minutes) and the direct epifluorescent filter technique (DEFT), are techniques used for rapid detection, especially

in fluids.[147,148] DEFT has been reported to detect *E. coli* O157:H7 counts of 10^6-10^8 cells/mL within 30 minutes. Automated systems based on impedimetry screen high numbers of samples based on total bacterial cell counts within 24 hours.[149] However, levels below 10^7 cells/mL cannot be detected. Some of the more recent efforts in rapid and sensitive pathogenic bacteria detection have focused on nucleic acid and immunological-based methods.

Table 5-1. Rapid methods for the detection of pathogenic bacteria. Adapted from de Boer, *International Journal of Food Microbiology*, 1999, 50, 127.[144]

Method	Detection limit (cfu/mL or cfu/g)	Time required for detection	Selectivity
Plating techniques	1	1- 5 days	Good
Bioluminescence	10^4	0.5 hours	None
Flow cytometry	$10^2 - 10^3$	0.5 hours	Good
Direct epifluorescent filter technique	$10^3 - 10^4$	0.5 hours	None
Impedimetry	1	6-24 hours	Moderate to good
Immunological methods	10^5	1-2 hours[a]	Moderate to good
Nucleic acid-based assays	10^3	6-12 hours[a]	Excellent

[a] Time following sample enrichment process.

Important developments in nucleic acid-based assays have been used for the genetic identification of pathogenic bacteria.[150,151] Genetic detection methods are based on the hybridization of target DNA or RNA with a specific DNA probe, usually containing 15 to 30 nucleotides. The hybridization assay is controlled by the nucleotide sequence of the probe. The nucleic acid-based assays normally consist of cell lysis, purification, and the denaturing of the double-stranded target by alkali or heat treatment, prior to hybridization with the respective probes. Following hybridization, separation of the hybrid complex from free, labeled probes is required, and detection, using

colorimetric or fluorescence techniques, is similar to that for antibody-antigen detection in immunological assays.[143] Nucleic acid methods usually include a target amplification step , and the most popular method of amplification is the polymerase chain reaction (PCR).[152] Starting from a single target DNA or RNA sequence, more than one billion product sequences can be synthesized. Using PCR, one *E. coli* O157:H7 cfu/mL can be detected within six hours but disadvantages include inhibition and contamination.

An array of immunological methods has made rapid detection and identification of *E. coli* O157:H7 possible. [153,154] Immunological methods rely on the binding of an antibody (Ab) to an antigen (Ag) on the surface of the bacteria. The development of monoclonal antibodies (mAbs) has greatly enhanced the success of immunoassays by providing a consistent and reliable source of characterized antibodies.[151] Commonly used immunoassays are divided into two categories: homogeneous and heterogeneous. In a homogeneous assay, bound and unbound labeled components, if any, are not separated, and the antigen–antibody complex formed is directly visible or measurable with relatively short incubation times. Examples of homogeneous assays are agglutination reactions, immunodiffusion, and turbidimetry.[155-157] In a heterogeneous assay, the activity of the label is unchanged upon the binding of the antibody and antigen; thus, separation of the bound and unbound components is required. In the commonly used heterogenous sandwich immunoassay, capture antibodies are first immobilized onto a solid support such as a microtiter plate.[158] Bacteria samples (containing target antigen) and reporter antibodies (antibodies conjugated with a labeled substrate) are then sequentially added, with appropriate incubation times, and a capture Ab-Ag-reporter Ab complex is formed. Then the plate is thoroughly washed to remove any unbound

reagents. The reporter antibodies are usually labeled with radioactive or fluorescent molecules, and the signal from the labeled reporter antibodies are used to determine the amount of target antigen (i.e., bacteria concentration) in the sample. In enzyme-linked immunosorbent assays (ELISA), reporter antibodies are conjugated to enzymes, which catalyze reactions that produce an amplified signal that can be detected by colorimetric or fluorescence techniques (detection limits ranging from 10^3 to 10^5 colony forming units (cfu)/ml achieved following sample enrichments of 16-24 hours).[159,160] Immunological methods, in general, can suffer from a lack of selectivity due to the cross-reactivity of many antibodies and be laborious and time-consuming as a result of complicated general assay procedures.[161]

Despite these advancements, methods still lack the sensitivity, selectivity, and simplicity for rapid or real time analysis.[155,156,162-169] Recently, many attempts have been made to improve the sensitivity of bacteria detection without the need for target amplification and enrichment.[170-172] However, rapid bacteria detection at the single cell level, in a given sample, has been quite challenging.

The two major challenges for the rapid detection of a single bacterial cell are the achievement of short to real-time detection and ultrasensitivity in bioanalysis. To reduce the time required for target detection, a minimal amount of sample manipulation is essential. The sensitivity of the detection method has to be high enough to eliminate the need for target amplification and enrichment steps and also allow for the accurate identification of a single bacterial cell in a short period of time. Recently, many novel techniques have been developed to amplify analytical signals from biorecognition events to improve the sensitivity of various bioassays for bacteria detection.[172-174]

Using fluorescent dye-doped silica nanoparticles conjugated with monoclonal antibodies, an immunoassay was developed for the detection of one bacterial cell per given sample in ~30 minutes (Reproduced in part with permission from X.J. Zhao, L.R. Hilliard, et al. *PNAS* **2004**, 101, 15027-15032. Copyright [2004] The National Academy of Sciences of the USA).[89] As highlighted in Chapter 1, fluorescent silica nanoparticles have been used to develop ultrasensitive methods for bioassays. Each nanoparticle encapsulates thousands of fluorescent dye molecules in a protective silica matrix, providing a highly amplified and reproducible signal for fluorescence-based bioanalysis. Compared with conventional immunoassays, where only one or a few dye molecules are linked to an antibody molecule and then used to signal an antibody–antigen binding event, the bioconjugated nanoparticles enable significant amplification of the analytical signal because of the many dye molecules inside each nanoparticle, which is attached to the antibody molecule. For a bacterial cell, there are many surface antigens available for specific recognition by using nanoparticle-antibody conjugates. Therefore, hundreds of thousands of nanoparticles can bind to each bacterial cell, producing a greatly amplified signal. To show the utility of this assay, 1-400 *E. coli* O157 bacterial cells were detected in spiked ground beef samples.

Experimental Section

Materials. Bovine serum albumin (BSA), 1-ethyl- 3-3(3-dimethylaminopropyl) carbodiimide hydrochloride (EDC), ikosaoxyethylene sorbitan monolaurate (tween 20), *Z*-morpholino-ethanesulfonic acid (MES), succinic anhydride, *N*-hydroxysuccinimide (NHS), tetraethylorthosilicate (TEOS), tris(2,2'- bipyridyl) dichlororuthenium(II) hexahydrate (RuBpy), and triton X-100were purchased from Sigma-Aldrich. Trimethoxysilylpropyldiethylenetriamine (DETA) was purchased from United Chemical

Technologies (UCT, Bristol, PA), and *N*-(trimethoxysilylpropyl)ethylenediamine was purchased from Gelest (Morrisville, PA). Ammonium hydroxide (28–30 wt %), *N*, *N*-dimethylformamide, and all other chemicals of analytical reagent grade were obtained from Fisher Scientific. Monoclonal antibody (mAb) against *E. coli* O157:H7 was purchased from Biodesign International (Kennebunkport, ME). *E. coli* O157:H7 and *E. coli* Dh5α were obtained from the American Type Culture Collection (ATCC) via Dr. Shouguang Jin in the Department of Molecular Genetics and Microbiology. Distilled, deionized water (EasyPure LF, Barnstead) was used in the preparation of all aqueous solutions.

Instrumentation. Spectrofluorometric analysis was done using a Tecan (Maennedorf, Switzerland) Spectrofluor Plus plate reader with Magellan™ software or a Jobin Yvon SPEX Fluorolog spectrofluorometer (TAU-3) with DataMax software. Dye-doped silica nanoparticle size and uniformity and binding properties were analyzed with a H-7000 transmission electron microscope (TEM) and a FE S-4000 scanning electron microscope (SEM, Hitachi, Tokyo). Fluorescence images were obtained with an inverted fluorescence microscope (IX70- S8F, Olympus, Melville, NY) assembled with a charge-coupled device (CCD) camera (Olympus, Melville, NY or Pixera, Los Gatos, CA) and xenon lamp (Olympus) for excitation. The CCD camera was controlled with Imageview and Studio software (Pixera).

Silica nanoparticle bioconjugation. Before immobilizing mAbs against *E. coli* O157 onto the nanoparticles, the surfaces of RuBpy-doped silica nanoparticles were functionalized. The silica nanoparticles, 32 mg, were reacted with 20 mL of 1% DETA in 1 mM acetic acid for 30 minutes at room temperature, with continuous stirring to

produce amine-functionalized nanoparticles. The nanoparticles were then thoroughly washed three times in distilled, deionized water. After washing with *N,N*-dimethylformamide, the nanoparticles were reacted with 10% succinic anhydride in *N,N*-dimethylformamide solution under N_2 gas for 6 hours with continuous stirring to add carboxyl groups to the silica nanoparticle surface for subsequent conjugation of antibody. After a thorough wash, the carboxylated nanoparticles were activated, using 5 mL of 100 mg/mL EDC and 5 mL of 100 mg/mL of NHS in MES buffer (pH 6.8), for 25 minutes at room temperature with continuous stirring. The activated nanoparticles were dispersed in 10 mL of 0.1 M PBS (pH 7.3). To covalently immobilize mAbs against *E. coli* O157 onto the nanoparticle surface, 5 mL of 0.1 mg/mL nanoparticles was reacted with 2 mL of 5 μg/mL antibody for *E. coli* O157 for 2–4 hours at room temperature with continuous stirring to form the resultant nanoparticle-antibody conjugates, followed by washing in 0.1 M PBS buffer (pH 7.3). To reduce the effects of nonspecific binding in the subsequent immunoassay, silica nanoparticles were reacted with 1% BSA and 40 mM glycine for 30 minutes at room temperature and washed in 0.1 M PBS (pH 7.3) before use.

Preparation of bacteria samples for solution-based detection. A 500 μL bacteria sample, which contained 1-1000 bacteria based on plate counting results, was dispersed into 1.0 mL of 0.1 mg/mL RuBpy-doped silica nanoparticle-antibody conjugates in 0.1 M PBS buffer (pH 7.3) and incubated for 10 minutes. To remove the free nanoparticle-antibody conjugates that did not bind to the bacteria for samples detected in solution, the sample was centrifuged at 20,817 x *g* for 30 seconds - 1 minute, and then the supernatant was removed. The sample was washed again to remove all

unbound nanoparticle-antibody conjugates and stored in 50 μL-1.5 mL of 0.1 M PBS buffer (pH 7.3). The nanoparticle-based immunoassay is illustrated in Figure 5-1.

A volume of 50 μL was transferred to quartz cuvettes for samples containing 1-1000 cfu/mL and detected using a SPEX Fluorolog spectrofluorometer with 450 nm excitation and 590 nm emission. For detection of single cells, samples containing 1-25 bacterial cells in 1.5 mL were divided into 100 aliquots and transferred to 96 or 384-well plates, and 85 μl of the 0.1 M PBS buffer (pH 7.3) was added to each aliquot to provide a detectable sample volume of 100 μl. The fluorescence intensity was detected using a Tecan Spectrofluor Plus fluorometer with 430-nm excitation and 595-nm emission. A negative control sample was obtained using the same experimental procedures but without the addition of bacteria.

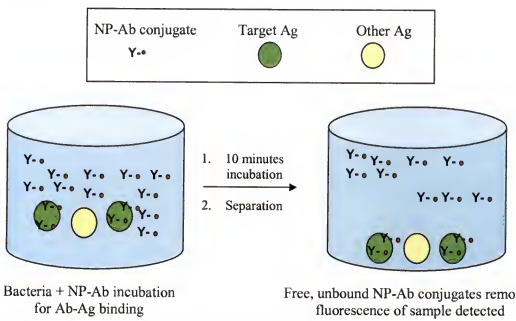

Figure 5-1. Schematic of fluorescent dye-doped silica nanoparticle-antibody conjugate (NP-Ab) based immunoassay for the rapid and accurate detection of pathogenic bacteria.

Detection of bacteria on filter membranes or glass slides. Bacteria samples were also counted on filter membranes and glass slides. Following incubation with the

nanoparticle-antibody conjugates as described above, the sample solutions were filtered through 6 mm polycarbonate membranes with a pore size of 0.2 μm. The free conjugates, those not bound to the target bacteria, were filtered through the membrane, while the nanoparticle-antibody conjugate-bacteria complexes remained on the membrane surface. After three washes with 0.1 M PBS buffer (pH 7.3), the membranes were sealed with two pieces of transparency film labeled with 25 squared grids. Fluorescence images were taken of each grid using a fluorescence microscope. For samples detected on glass slides, the samples were washed following incubation with the nanoparticles and then 20 μl of distilled, deionized water was added for transfer of the sample to the glass slides.

Preparation of ground beef samples. Fresh ground beef was purchased from a local grocery store and ground further in a blender into a paste-like consistency or frozen at -20°C until it was used. Several 25 g ground beef samples were divided into 25, 1 g samples and stored in sterile 15 mL conical tubes. E buffer (0.05% Tween 20 and 0.5% bovine serum albumin in 0.1 M PBS buffer, pH 7.3) in aliquots of 8 mL was added to each ground beef sample. Then, freshly cultured *E. coli* O157:H7 (~10^9 cfu/mL) was serially diluted 10-fold, in 1 ml aliquots, down to 1 cell/mL (as determined by plate counting) in a 0.1 M PBS buffer (pH 7.3). The 1 g ground beef samples were then spiked with 10-1000 cfu/mL of *E. coli* O157:H7. The entire slurry of ground beef, bacteria, and buffer was mixed by using a vortex for 1 minute, followed by centrifugation at 500 x *g* for 5 minutes. After homogenization, the sample consisted of a bottom layer of ground beef, a middle layer of buffer containing the *E. coli* O157:H7, and a top layer of fat. The middle layer was removed for testing; half of the sample was detected using the

nanoparticle-based immunoassay in a spectrofluorometer, and the other half was detected using the conventional plating method. For negative controls, sterile, 0.1 M PBS buffer (pH 7.3) was added to the ground beef samples. For positive controls, the ground beef mixture was replaced with various concentrations of 0.1 M PBS buffer (pH 7.3). Five parallel samples were prepared for each concentration.

Results and Discussion

Antibody conjugation to fluorescent dye-doped silica nanoparticles. RuBpy-doped silica nanoparticles[66] were synthesized using a water-in-oil microemulsion method, as described in Chapter 2. The optical properties of the particles were characterized before use to verify that the particles were highly fluorescent, photostable, and retained the RuBpy dye. The size of the nanoparticles used was uniform, with a diameter ranging from 60-70 nm for a given batch of particles. After surface modification, mAbs against the O-antigen of *E. coli* O157:H7 were covalently immobilized onto the nanoparticles for use in the immunoassay. Following antibody conjugation, the nanoparticles tended to settle in solution or form large aggregates that negatively affected the usage of the nanoparticle-antibody conjugates with *E. coli* O157:H7 samples. To reduce the aggregation and settling of the particles, the nanoparticle-antibody conjugates were briefly sonicated and vortexed and reacted with 1% bovine serum albumin (BSA) and 40 mM glycine. The BSA and primary amine-containing glycine interacted with any unreacted carboxyl groups on the nanoparticle surface and reduced the nonspecific binding of the conjugates with themselves or the bacteria samples, as shown by the reduction in the fluorescence background of Figure 5-2 (B) as compared to (A). When stored at 4°C, the nanoparticle-antibody conjugates were viable for antigen recognition for up to four weeks, whereas the nanoparticles were stable for several months. After

two weeks, the binding of the conjugates to the bacteria was not as efficient and sometimes resulted in inaccurate bacteria counts. Thus, nanoparticle-antibody conjugates were only used for up two weeks.

Fluorescence signal amplification and photostability of nanoparticle-antibody conjugates for bacteria detection. Due to the hundreds to thousands of dye molecules encapsulated within each nanoparticle, high signal amplification was achieved when the nanoparticle-antibody conjugates bound to antigens on the surface of the bacteria. To demonstrate the advantage of using fluorescent dye-doped silica nanoparticles, a high quantum yield organic dye, tetramethylrhodamine (TMR) was labeled with monoclonal antibodies against *E. coli* O157: H7 and used in an immunoassay similar to that described in the Experimental Section. Using a protein labeling kit from Molecular Probes[175 1-3. #64], 1-3 TMR molecules (~1.3 molecules for this study) were linked to one monoclonal antibody. Different concentrations of bacteria ranging from 1×10^5 to 1×10^7 cfu/mL were reacted with TMR-antibodies and RuBpy-doped nanoparticle-antibody conjugates at a ratio of 10^7:1 antibody:bacteria. When compared with the TMR tetramethylrhodamine (TMR)-labeled antibody, signal amplification by the nanoparticle-antibody conjugates was at least 500 times greater, as shown in Figure 5-3. The nanoparticle-based signal amplification provides the foundation for the rapid detection of a single bacterial cell in solution samples.

A photostability study was also conducted. Although, the quantum yield of RuBpy molecules is lower than that of TMR molecules, the cells that were labeled by RuBpy-doped silica nanoparticles were much brighter than those labeled with TMR, as shown in Figure 5-4. With constant irradiation using a xenon lamp, the fluorescence intensity of

the cells labeled with nanoparticles showed good photostability. After 6 minutes of continuous 450 nm excitation with a xenon lamp, the fluorescent intensity decreased by 35% but was still very bright, enabling the detection of bacterial cells over a long period of time.

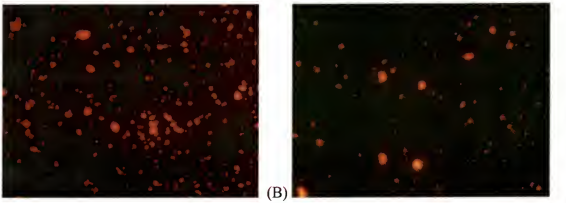

Figure 5-2. Effect of BSA blocking reaction on fluorescent dye-doped silica nanoparticle-antibody (NP-Ab) based immunoassay. *E. coli* O157:H7 (approximately 1000 cells) were labeled with fluorescent dye-doped silica nanoparticle-antibody conjugates. Images were taken of (A) conjugate-bacteria binding with untreated nanoparticles and (B) conjugate-bacteria binding with BSA treated nanoparticles. Magnification is 40x.

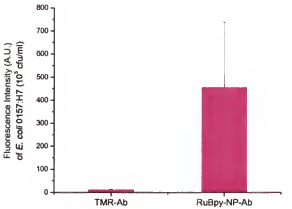

Figure 5-3. Comparison of TMR dye-labeled antibody (TMR-Ab) and RuBpy-doped silica nanoparticle antibody conjugates (RuBpy-NP-Ab) for the solution-based detection of *E. coli* O157:H7.

Selectivity of nanoparticle-antibody conjugate based immunoassay. In this study, the consistent and reliable source of characterized monoclonal antibodies[151]

against *E. coli* O157:H7 was used to obtain high selectivity. The nanoparticle-antibody conjugates bound to the surface of *E. coli* O157:H7 but not to *E. coli* Dh5α, which lacks the surface O157:H7 antigen. The SEM image of *E. coli* O157:H7 cells, in Figure 5-5 (A), after 30 minute incubation with the nanoparticles show that there were hundreds to thousands of nanoparticle-antibody conjugates bound to a single bacterial cell of *E. coli* O157:H7, providing significant fluorescent signal amplification.

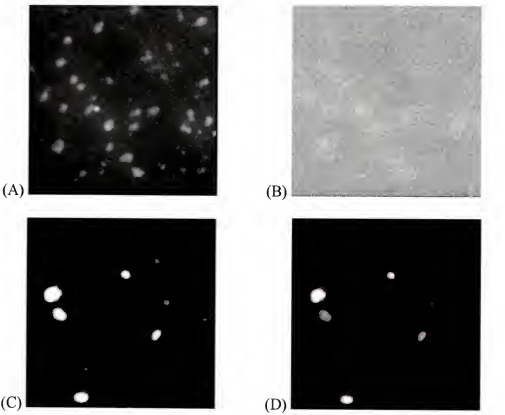

Figure 5-4. Photostability of TMR dye-labeled antibody and RuBpy dye-doped silica nanoparticle-antibody conjugates for bacterial cell detection. The images show (A) the initial fluorescence of TMR dye labeled bacterial cells and (B) the fluorescence after 6 minutes of continuous irradiation (xenon lamp) with 550 nm excitation and (C) the initial fluorescence of antibody conjugates labeled bacterial cells and (D) after 6 minutes of continuous irradiation (xenon lamp) with 450 nm excitation. Magnification is 40x.

Nanoparticle-antibody to bacteria antigen binding. To obtain accurate bacteria detection and cell counting, several experimental conditions were considered, including

the ratio of the monoclonal antibodies conjugated to the silica nanoparticles, the ratio of the nanoparticle-antibody conjugates to bacterial cells, and the incubation/reaction time of the bacteria with the conjugates. Each nanoparticle surface offered many binding sites for amine groups on the antibody; consequently, thousands of antibodies theoretically can be immobilized onto one nanoparticle surface. Given the cost of monoclonal antibodies, use of the smallest concentration of the antibody was reasonable as long as that concentration allowed the nanoparticle to effectively bind to the bacterial cell. Antibody was reacted with functionalized silica nanoparticles at concentrations 1-10 times the number of nanoparticles. Results showed that an approximate ratio of 5:1 antibody to nanoparticles was sufficient for effective binding to bacteria samples. At lower ratios, the nanoparticle to bacteria binding, within the desired 10 minute or less reaction time, was not reproducible.

Figure 5-5. SEM and fluorescence images of bacterial cells incubated with RuBpy-doped silica nanoparticle-antibody conjugates for *E. coli* O157:H7. (A) SEM image of *E. coli* O157:H7 cell labeled with nanoparticle-antibody conjugates; (B) SEM image of *E. coli* Dh5α cell (negative control) that were incubated nanoparticle-antibody conjugates; (C) Fluorescence image of an *E. coli* O157:H7 cell covered with dye-doped nanoparticle-antibody conjugates.

The ratio of the nanoparticle-antibody conjugates to bacteria cells affected the degree to which the bacteria samples were labeled with nanoparticles. If the concentration of conjugates was too dilute, the bacteria was not completely labeled as shown in Figure 5-6 (A), resulting in irregular fluorescence and making it difficult to

analyze the sample. When the ratio of the conjugates to the bacteria cells was greater than 10^5, the bacterial cells were completely covered with the nanoparticle-antibody conjugates, as shown in the SEM images in Figure 5-6 (B). For the bacteria samples detected and counted in this study, the number of bacteria used was 1000 or less and 0.1 mg of RuBpy-doped silica nanoparticle-antibody conjugates provided a ratio of $\geq 10^8$:1 nanoparticles to bacteria.

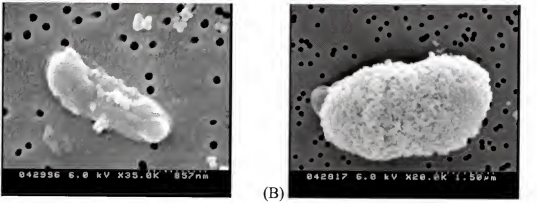

(A) (B)

Figure 5-6. SEM images of RuBpy-doped silica nanoparticle-antibody conjugates bound to *E. coli* O157:H7 cells. 10^6-10^7 cfu/ml samples were reacted for 1 hour with various concentrations of nanoparticle-antibody conjugates. (A) An *E. coli* O157:H7 cell from a sample that was incubated with a dilute concentration of nanoparticle-antibody conjugates. (B) An *E. coli* O157:H7 cell from a sample that was incubated with excess nanoparticle-antibody conjugates.

When the ratio of monoclonal antibodies to silica nanoparticles was at least 5 and the ratio of the nanoparticle-antibody conjugates to bacterial cells was about 10^8, 5-10 minutes of incubation was adequate for binding of the conjugates to the *E. coli* O157:H7 cells. This short reaction time enabled a total detection time of approximately 30 minutes, from the sampling to the counting of the number of bacterial cells for solution-based detection.

Fluorescence-based detection, imaging, and counting of *E. coli* O157:H7 on filter membranes or glass slides. The number of *E. coli* O157:H7 was detected and

counted using fluorescence images obtained either on the surface of filter membranes or on glass slides. The only advantage of using the glass slides for detection was that they were able to provide clearer optical images than the filter membrane. The polycarbonate filter membrane interfered with the optical images of the bacterial cells, but it did not affect the fluorescence images. The filtration-based detection, using the membranes, was based on the size difference between the bacteria and the nanoparticle-antibody conjugates. The pore size of the membrane was 0.2 μm in diameter, and *E. coli* O157:H7 was 1-5 μm, much larger than the pore size. Thus, the bacteria were not filtered through the membrane, while the conjugates not bound to the bacteria passed through the membrane pores due to their size (less than 70 nm in diameter). This result was confirmed by SEM imaging. To completely remove the free nanoparticle-antibody conjugates, the filter membranes were washed several times. The nanoparticle filtration efficiency was determined by monitoring the filtration of 0.1 mg/mL of silica nanoparticles. Before the filtration, the fluorescent intensity of the solution was detected. After filtration and each wash, the fluorescence intensities of the filtered solutions were detected. The results showed that 95% of the free nanoparticle-antibody conjugates were collected in the filtrate after 4 times washes in 0.1 M PBS. The small number of nanoparticle-antibody conjugates remaining on the membrane surface appeared in the fluorescence images as very small fluorescence spots. Due to the size difference between the bacteria and the conjugates, the fluorescence spots due to bacteria could be visually determined. It should be noted that the bacteria retained on the filter membrane did not affect the filtration of the unbound conjugates.

To evaluate the accuracy of using this method for bacteria detection and counting, the average numbers of *E. coli* O157: H7 cells, as determined by plate counting (a standard method in bacterial cell counting in microbiology and cell biology[176]) were compared with the average numbers of *E. coli* O157: H7, as detected by counting fluorescent spots on the filtered membranes. Each method was performed five times. As shown in Figure 5-7, 1 to 60 bacterial cells were counted, and the two results correlated well.

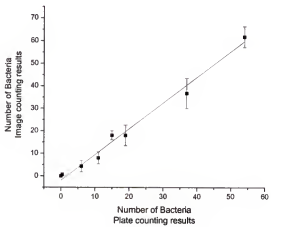

Figure 5-7. Comparison of *E. coli O157:H7* detection using the plate counting method and fluorescence imaging on filter membranes.

E. coli O157:H7 samples on the filter membranes were also analyzed in the spectrofluorometer using the solid-phase setup. The filter membranes were sandwiched between two glass slides, fixed in the sample holder in the spectrofluorometer, and a fluorescence intensity of an area of 6 mm^2 was detected. In addition, the bacteria samples retained on the membranes were detected in the solution by isolating the bacteria cells using 1% SDS in 0.1 M PBS (pH 7.3). Nonspecific binding to the nanoparticle-antibody conjugates was negligible in the control samples containing *E. coli* Dh5α as compared to

the *E. coli* O157:H7 samples but no quantitative information was obtained using either method.

Fluorescence-based detection and counting of *E. coli* O157:H7 in solution. Bacteria samples were analyzed quantitatively in solution using a spectrofluorometer or a plate reader, with centrifugation-based separation of the free from bacteria bound RuBpy-doped silica nanoparticle-antibody conjugates. The efficiency of the bacteria detection was dependent on the concentration of nanoparticle-antibody conjugates detected in solution. For detection with the spectrofluorometer, the nanoparticle labeled *E. coli* O157:H7 cells tended to settle to the bottom of the cuvette, and the detectable fluorescence signal decreased over time. To minimize this problem, the samples were treated with 0.2-1 μg/mL protease E, an enzyme that cleaves the nanoparticle-antibody conjugates from the bacteria, for 30 minutes at 37°C before detection of the fluorescence signal. The cleavage degree was dependent on the enzyme concentration used. When more than 0.5 μg/ml protease E was used, more accurate measurements of the fluorescent signals were obtained by allowing the nanoparticles to be freely dispersed in the solution for a longer period of time, as shown in Figure 5-8. As shown in Figure 5-9, no significant difference in fluorescence intensity was observed for 10-1000 E. coli O157:H7 cells.

To achieve rapid detection of *E. coli* O157:H7, a 96 or 384well-plate reading spectrofluorometer was used to detect the fluorescence signal of single bacterial cell samples in solution. This method required minimal sample preparation, as described in the Experimental Section. Consequently, the nanoparticle-based immunoassay was rapid, taking less than 30 minutes to complete sample preparation, instrumentation preparation,

and sample determination. To confirm the detection of a single bacterial cell, a sampling method was designed to ensure reproducible and accurate counting. The single bacterial cell counting method was based on a technique used in single-molecule studies[177], where the sample was diluted to a concentration in which there was only a 25% chance that a specific volume of the sample would have a bacterial cell cell. Based on OD_{600} data and further verification by plate counting, *E. coli* O157:H7 was accurately diluted into 10 cells per sample. Then, each sample was divided into 40 aliquots. Using the conventional plating method again, each aliquot was plated and grown on an agar plate for 16–18 hours at 37°C. Each plate had no bacteria or only 1 cfu, confirming that our sample preparation method enabled the isolation of single bacterial cells.

To obtain an accurate bacteria count, 21 samples were prepared with ~50 bacteria in each sample. Each sample was then divided into two parts. The first half of each sample was grown on agar plates to obtain an accurate number of bacterial cells. The result showed that the average bacterial count was 22 ± 4 (mean ± standard deviation), as shown in Figure 5-10. The second half of each sample was used for single bacterial cell determination using the plate reader. A bacterial cell was confirmed only when the fluorescence intensity was above the background plus three times the standard deviation of the controls. Control samples were obtained by using the same experimental procedures, but without the addition of bacteria. For the 21 tested samples, the average number of bacteria was 25 ± 5, as shown in Figure 5-10. The nanoparticle-antibody conjugate based detection results highly correlated with that of the plating method, confirming the validity of this method for single bacterial cell detection.

Given the demand for high throughput determination of multiple bacterial samples in toxicology screening, the detection of bioterrorism agents, and medical diagnosis, the nanoparticle-antibody conjugate based immunoassay can be adapted for multiple sample determination when many aliquots of samples are tested simultaneously. Using the plate reader, over 300 samples can be analyzed at one time with a single bacterial cell detection limit. To demonstrate the high throughput capability, multiple samples (3-9) were analyzed in a 384-well plate. Using the same procedures as described earlier, each aliquot of the sample, with a 25% probability of having a single bacterial cell, was dispensed into the plate, and the identification of a bacterial cell was based on the fluorescence intensities measured in each well. For a given plate, control samples without bacteria were added into 20 wells of the plate for the determination of background signal and standard deviation.

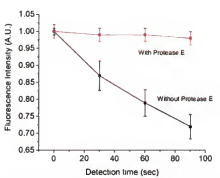

Figure 5-8. Effect of protease E on bacteria detection efficiency in solution over time using the RuBpy-doped silica nanoparticle-antibody conjugated based immunoassay.

***E. coli* O157:H7 detection in ground beef samples.** To test the utility of our bioassay for bacteria detection in real samples, the number of *E. coli* O157:H7 was determined in spiked ground beef samples. Following a reported sample preparation method[178], the recovery rate of the spiked bacteria from the ground beef increased from

50% to 90% as the number of spiked bacteria increased from 2 to 400. The recovered samples were equally divided into two portions as described in the Experimental Section. One portion was used for the cfu count on LB agar plates, whereas the other portion was subjected to fluorescence detection with the RuBpy-doped silica nanoparticle-antibody conjugates. It should be noted that the colony morphology of the *E. coli* O157:H7 on LB agar was easily distinguishable from other bacteria derived from the ground beef. As shown in Figure 5-11, the number of bacterial cells determined by the two methods were highly correlated. This result clearly demonstrates that the bacterial cell assay based on antibody-conjugated fluorescent dye-doped silica nanoparticles can be used to effectively detect a single bacterial cell in solution recovered from a ground beef sample within 20 minutes. Both positive and negative control experiments were conducted to confirm that the effects of potential interference, such as fat in the ground beef, were negligible.

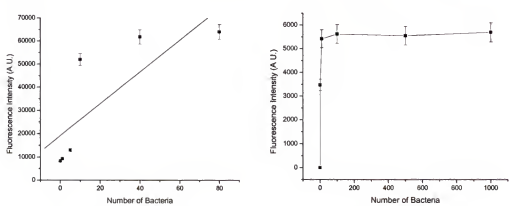

Figure 5-9. Solution-based detection *E. coli* O157:H7 cells using the RuBpy-doped silica nanoparticle-antibody conjugated based immunoassay.

Conclusions

In summary, a fast and ultrasensitive immunological method for bacterial detection that uses fluorescent dye-doped silica nanoparticle conjugates was developed. A single bacterial cell was accurately detected without any sample amplification or enrichment.

This bioassay is rapid (less than 30 minutes from bacterial cell binding to detection and analysis and could be further shortened), convenient, and highly selective. Furthermore, because multiple samples can be analyzed simultaneously, this assay is adaptable to high-throughput bioanalysis for multiple pathogens. In addition, the accurate and reliable detection of trace amounts of *E. coli* O157:H7 bacteria in spiked ground beef samples demonstrates the practical usefulness of this assay system. This study clearly exhibits the excellent properties of bioconjugated nanomaterials in applications in bioanalysis and biodetection. The results demonstrate the potential for a broad application of this type of bionanotechnology in practical biotechnological applications in various biodetection systems.

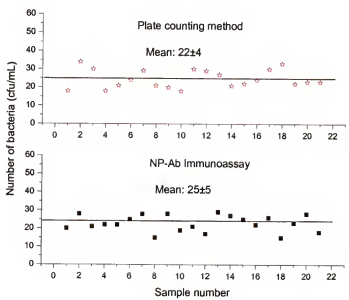

Figure 5-10. Detection of single bacterial cells using the plate counting and the nanoparticle-antibody conjugate based immunoassay methods. *E. coli* O157:H7 samples of 25 cfu/mL were counted via the plating method or divided into aliquots that contained only one bacteria cell and detected using the fluorescent dye-doped silica nanoparticle-antibody conjugate based immunoassay.

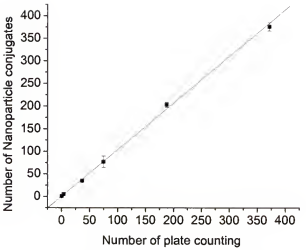

Figure 5-11. Detection of *E. coli* O157:H7 in spiked ground beef using the plate counting method and the RuBpy-doped silica nanoparticle-antibody conjugate based immunoassay.

CHAPTER 6
FLUORESCENT DYE-DOPED SILICA NANOPARTICLES FOR MULTIPLE PATHOGENIC BACTERIA DETECTION

Further Studies of Nanoparticle-Antibody Conjugate based Immunoassay for Multiple Bacteria Detection

Practical immunological methods for the detection of pathogenic bacteria in clinical, food, and environmental samples should be simple, fast, inexpensive, utilize a high-throughput format that enables the testing of many samples simultaneously, and ideally allows for the detection of a series of different pathogens in the same assay vial.[179] In Chapter 5, a fast and ultrasensitive immunoassay for bacteria detection that uses fluorescent dye-doped silica nanoparticle-antibody conjugates was described. In this chapter, the feasibility of simultaneous, multiple pathogen detection is explored.

Multiplexed analysis. Most diagnostic or monitoring assays are performed in a single test format using cell culture, molecular techniques (e.g., PCR), or immunoassay methods (e.g., enzyme-linked immunosorbent assay, ELISA) where a single biomarker can be detected from a complex sample such as serum.[180,181] It is often necessary or desirable to monitor multiple biomarkers simultaneously, yet few commercial assays and instruments capable of multiplexed detection are available in analytical laboratories.[182] Multiplexed analysis is the ability to perform multiple discrete assays in a single vial with the same sample at the same time. Compared to single-target detection methods, multiplexed assays reduce the time and cost per analysis, allow for simpler assay protocols, decrease the sample volumes required, and, most importantly, make comparison of samples feasible and measurements reproducible and reliable.[183]

Multiplexed assays have become important complements to advances in genomics and proteomics, allowing a large number of nucleic acids and proteins to be rapidly screened. Oligonucleotide microarrays[184-186] and protein arrays[187-194] can handle a high degree of multiplexed detection using spatially resolved measurements, but the experimental equipment and detection systems are not convenient to use on a routine basis.

Multiplexed microsphere-based flow cytometry assays[195,196] offer several advantages, such as flexibility in target selection, fast binding kinetics, and well controlled binding conditions. The first use of flow cytometry for analysis of microsphere-based immunoassays was published in 1977.[197,198 575-595 #92] Because a flow cytometer has the ability to discriminate different particles on the basis of size or color, the possibility of multiplexed analysis of different analytes with different microsphere populations was explored. Two distinct sizes of microspheres were used for simultaneous detection of two different antibodies by flow cytometry, and subsequently expanded to the use of four different sizes of microspheres to detect four different specificities of anti-HIV antibodies.[199,200] Size discrimination of microspheres allows simultaneous detection of small numbers of analytes, but the inability to distinguish aggregates of smaller microspheres from larger microspheres severely limits the extent of multiplexing that can be achieved.

In contrast, differential dyeing of identically sized microspheres with two different dyes, emitting in two different wavelengths, allows aggregates to be distinguished and permits discrimination of at least 64 different sets of microspheres.[20] Both organic fluorophores and quantum dots have been embedded into polymer microspheres or beads for high-capacity spectral coding.[15,195,201] With the unique advantage of size-tunable

emission and broad excitation properties as described in Chapter 1, quantum dots have the potential to be ideal luminescent nanoparticles for the multiplexing of biological samples, but they need to be further developed with regard to biocompatibility.[15]

Using the simple basic principle of dye-doped nanoparticle-antibody conjugate to bacteria surface antigen binding, multiple types of bacteria can be rapidly detected with ultrasensitivity and high specificity at the same time in various detection schemes. A simple flow channel based detection system or flow cytometer, developed in the Tan laboratory to detect silica nanoparticle-antibody conjugates bound to single bacterial cells, has been characterized and is currently being optimized for multiple bacteria detection (Reproduced in part with permission from X.J. Zhao, L.R. Hilliard, et al. *PNAS* **2004**, 101, 15027-15032. Copyright [2004] The National Academy of Sciences of the USA).[89]

Materials. *Escherichia coli* O157:H7 and *Escherichia coli* Dh5α, and *E. coli, Salmonella typhimurium*, and *Staphylococcus aureus* were obtained from American Type Culture Collection (ATCC) via Dr. Shouguang Jin in the Department of Molecular Genetics and Microbiology Department and Dr. Samuel Farrah in the Department of Microbiology and Cell Science, respectively. Monoclonal antibodies (mAb) against *E. coli* O157:H7, *E. coli* Dh5α, *Salmonella typhimurium*, and *Staphylococcus aureus,* and polyclonal antibody for *E. coli* and mouse IgG were purchased from Biodesign International (Kennebunkport, ME). *Bacillus cereus*, *Bacillus thuringiensis* spores and the corresponding polyclonal antibodies were obtained from Dr. Ben Koopman in the Department of Environmental Engineering. All other reagents were purchased from

Gelest, Fisher-Scientific, and Sigma-Aldrich, as listed in Chapter 5. Distilled, deionized water (EasyPure LF, Barnstead) was used in the preparation of all aqueous solutions.

Instrumentation. The laboratory-made flow cytometer used an Ar^+ laser (model series 532, Omnichrome, Chino, CA) as the excitation light source. The sample flow channel was a glass capillary (i.d. 50 μm) purchased from Polymicro Technologies (Phoenix). The photomultiplier tube signal was sent to a computer interfaced with a data acquisition card (NI DAQPad-6020E, National Instruments, Austin, TX) for data collection. The acquisition board was controlled with the National Instruments LABVIEW program. A schematic diagram of the laboratory-made flow cytometer is shown in Figure 6-1.

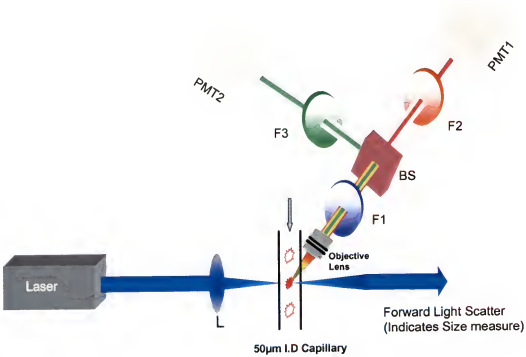

Figure 6-1. Schematic diagram of laboratory-made flow-channel system or flow cytometer. PMT-1 and PMT-2 are the photomultiplier tubes. F1-F3 are long pass filters at 495 nm, 570 nm, and 650 nm, respectively. Samples were pumped through the capillary using a syringe and a mechanical syringe pump system.

The optical detection system in the flow cytometer is a homemade set-up designed by Dr. Shelly John in the Department of Physics, comprising a micrometer-sized capillary channel to flow the sample at a steady flow rate. An Ar^+ Laser (Omnichrome), at 488 nm, is tightly focused to the central region of the channel to probe the nanoparticle bound bacteria species. The ultrasensitive optical detection scheme was designed to detect the fluorescence signal as each bacterial cell passed through the probing volume. Fluorescence events produced at the probing region were collected using a microscope objective (40x), followed by an optical beam splitter and filter system. Subsequently, the fluorescence signals due to a single bacterial cell were detected with two highly sensitive photomultiplier tubes (Hammamatsu, Middlesex, NJ), which have a built-in amplifier. The bursts of fluorescence from each bacterial species were recorded through a data-acquisition system (NI DAQPad- 6020E) interfaced to a computer and analyzed with custom-built software (LabVIEW, Austin, TX).

Silica nanoparticle bioconjugation. During nanoparticle synthesis, the silica nanoparticles were post-coated and functionalized with carboxyl groups as outlined in Chapter 3, using a carboxylated silane, N-(trimethoxysilylpropyl)-ethylenediamine.

Preparation of bacteria samples for solution-based detection using the flow cytometer. Other bacterial samples, such as *E. coli* O157, *Salmonella*, *and Bacillus* spores, were prepared using a similar procedure, as described in Chapter 5. Specific antibodies were used for the recognition of the individual bacterial samples. However, in an attempt to lower the detection time, the bacterial samples are not washed following reaction with the nanoparticle-antibody conjugates. A schematic diagram of the altered detection method is shown in Figure 6.2

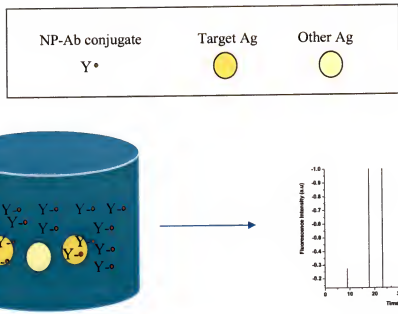

Bacteria/Spore + NP-Ab conjugate incubation for Ab-Ag binding

Free, unbound NP-Ab conjugates differentiated from NP-Ab-Bacteria/Spores

Figure 6-2. Schematic of fluorescent dye-doped silica nanoparticle-antibody conjugate (NP-Ab) based immunoassay using the flow cytometer, which allows for the rapid and accurate detection of pathogenic bacteria. When using the flow channel detection system, separation of the free, from bound nanoparticle-antibody conjugates is not required.

Results and Discussion

Experimental design requirements for the simultaneous detection of multiple bacteria. In order for the fluorescent dye–doped silica nanoparticle-antibody conjugated based immunoassay to be effectively used for the simultaneous detection of multiple pathogenic bacteria, a number of requirements must be met. First, antibodies must be selected that bind specifically to only one type of bacteria or, at the very least, do not cross react with any of the other bacteria species to be detected in the assay. Each of the selected antibodies then needs to be conjugated to silica nanoparticles that are doped with fluorescent dyes that emit at different wavelengths. The emission spectra of the different

dye-doped silica nanoparticles conjugated to the different antibodies have to not overlap with each other, allowing each type of bacteria to be clearly labeled and detected.

As novel types of fluorescent silica nanoparticles are being developed, RuBpy-doped silica nanoparticles are being used to further study and optimize experimental conditions for the nanoparticle-based immunoassay and the specificity of the antibodies selected for the detection of *E. coli*, *S. typhimurium*, *S. aureus,* and other bacterial cells or spores.

Determination of fluoresence signal for bacteria detection. Given the variances in the high fluorescence background from the nanoparticles in the flow cytometer, the determination of fluorescence signal versus noise was reexamined. RuBpy-nanoparticle-antibody conjugates, 0.1 and 0.5 mL, were used to detect 25 *E. coli* cells using the plate reader. The results are shown in Table 6-1 and the detection procedure is described in the Experimental Section in Chapter 5. Based on these experiments, the most accurate count is achieved when we use 0.1 mg NPs and average signal plus the standard deviation or 0.5 mg and background signal plus 3 times the standard deviation.

Table 6-1. Detemination of fluorescence signal from bacterial samples containing 25 *E. coli* cells.

	0.1 mg NPs		0.5 mg NPs	
	Sample 1 Threshold Count	Average Count	Sample 1 Threshold Count	Average Count
Signal + 1 SD	21	29	34	49
Signal + 2 SD	6	8	30	34
Signal + 3 SD	4	5	17	20
	Sample 2 Threshold Count	Average Count	Sample 2 Threshold Count	Average Count
Signal + 1 SD	28	34	45	67
Signal + 2 SD	8	10	27	33
Signal + 3 SD	2	3	17	22

Detection of *S. typhimurium*. RuBpy- NP-anti-mouse IgG conjugates (0.1-1 mL) were used to detect 30-100 cells of *S. typhimurium* that were reacted with 10 μg of unlabeled antibody for *Salmonella* for 10 minutes, washed and then reacted with the RuBpy nanoparticle-conjugates for 10 minutes. Using 0.1 mL nanoparticle-antibody conjugates, some but not all of the cells were labeled based on SEM imaging of the sample, as shown in Figure 6-3. However, when using 1 mL nanoparticle-antibody conjugates, the sample was overloaded with nanoparticles and bacterial cells and aggregates of nanoparticles could not be distinguished. Based on previous nanoparticle-antibody-bacterial antigen binding studies, as described in Chapter 5, 0.1 mg of nanoparticles should be sufficient for the complete coverage of the bacteria surface. Consequently, more antibody-antigen binding studies will be conducted to determine whether more antibodies are needed for efficient nanoparticle conjugation or if a longer nanoparticle-antibody conjugation reaction time with the bacterial samples is needed.

Detection of *B. thuringensis*. RuBpy- NP-anti-mouse IgG conjugates (1 mL) have been were to detect *B. thuringensis* spores. Preliminary results show that the nanoparticle-antibody conjugates show moderate to good binding affinity toward the spores.

Selectivity RuBpy-anti mouse IgG silica NPs. Nanoparticle-antibody-bacteria binding experiments have been repeated to verify selectivity of the RuBpy doped silica nanoparticle-antibody conjugates for *E. coli*, *S. typhimurium*, and *S. aureus* but the results are inconclusive. Fluorescence imaging was used to test the nanoparticle-antibody conjugates when other bacteria samples, not the target, are present in solution. In Figure 6-5, ~10^5 cells of *E. coli*, *S. typhimurium*, and *S. aureus* were reacted with 0.1 mg

nanoparticle-conjugates for *S. typhimurium*. Results showed highly fluorescent spots in all samples. However, SEM images of similar experiments show no binding of the nanoparticles to non-target samples.

Detection of *S. Typhimurium* using 0.1 mL NPs

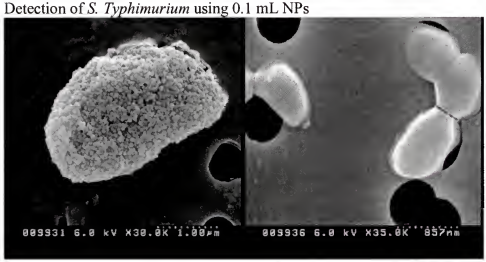

Detection of *S. Typhimurium* using 1 mL NPs

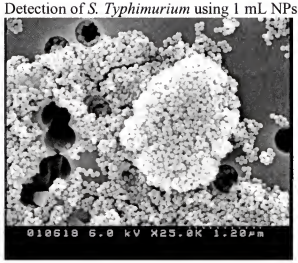

Figure 6-3. Detection of *S. typhimurium* using RuBpy-doped silica nanoparticle-antibody conjugates.

Bacteria detection using a simple optical flow cytometer. Fluorescent dye-doped silica nanoparticle-antibody conjugates bound to bacteria were detected using a laboratory-made flow cytometer, which can precisely detect a single bacterial cell when the cell flows through the detection zone. Laser excitation and an optical design for the

collection of the fluorescence emission in the orthogonal direction of the forward scattered light beam made the cytometric analysis more efficient and accurate. In the current scheme, a micrometer-sized capillary flow cell and the narrow focusing of the excitation light beam reduces the probing volume of the sample to a few picoliters. Moreover, this design decreases the chance of detection of two or multiple events simultaneously. The total time for the sample detection and analysis with this present system is 60 seconds to 15 minutes, depending upon the sample volume.

Detection of *B. thuringensis* using 1 mL NPs

Figure 6-4. Detection of *B. thuringensis* using RuBpy-doped silica nanoparticle-antibody conjugates.

Various scan rates were used to optimize the signal to noise ratio (S/N) to eliminate the need for separation of the free nanoparticle-antibody conjugates from the nanoparticle-antibody-conjugate labeled bacteria. The scan rate should be low enough to detect signal from the bacteria in solution but high enough to minimize the nanoparticle background signal. When the scan rate was too low, the high background signal made it difficult to determine the fluorescence signal due to the bacteria in the sample, as shown in Figure 6-6.

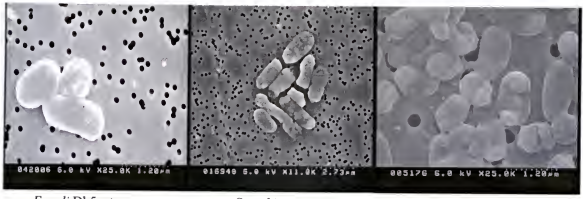

E. coli Dh5α + NP-Ab for *E. coli* O157

S. typhimurium + NP-Ab for *E. coli*

S. typhimurium + NP-Ab for mouse IgG

(A)

Salmonella

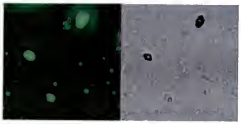

Salmonella + NP-Ab for *E. coli*

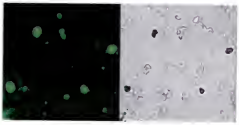

Salmonella + NP-Ab for *Salmonella*

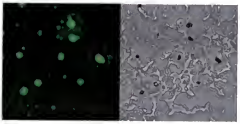

Salmonella + NP-Ab for *Staphylococcus aureus*

(B)

Figure 6-5. Nanoparticle-antibody conjugate selectivity. (A) The SEM images show that the nanoparticle-antibody conjugates are highly selective for the bacteria of interest, but (B) fluorescence imaging shows nonspecific binding.

Bacteria samples were accurately detected when a scan rate of 2000 Hz was used, shown in Figure 6-7. Each spike, which was higher than the background plus three times the standard deviation, represented one bacterial cell. The height of the spikes was not uniform, which might be caused partly by the rod-shaped bacterial rotation as the signal beams are collected by the detector.

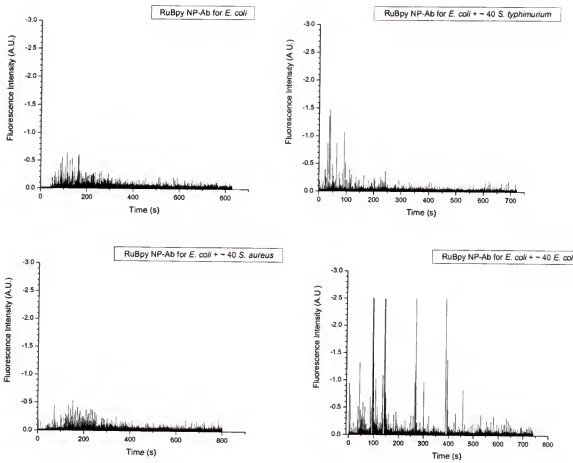

Figure 6-6. Detection of different types of bacteria using a lab-made flow cytometer following incubation with nanoparticle-antibody conjugates. The flow rate was 0.5 mL/hour and the scan rate was 250 Hz.

Qualitative and quantitive information on samples comparable to current methods can be obtained using the flow cytometer. Bacterial samples containing 10^5 cells/mL and higher can be qualitatively detected, as shown in Figure 6-8. However, the flow based system is best suited for the analysis of trace bacterial analytes.

Multiple pathogen bacteria detection. Using the dual detectors on the lab-made flow cytometer and dual/multiple-luminophore doped silica nanoparticles currently being developed in the Tan lab, the rapid, simultaneous, multiple pathogen detection and counting in water samples can be achieved using the flow channel detection system with

one bacterial cell sensitivity. The nanoparticle-antibody conjugates with antibodies specific to the target pathogens can quantitate the pathogens present in aqueous samples. This method is currently being used for the simultaneous quantification of model pathogens, *E. coli*, *S. typhimurium*, and *S. aureus*.

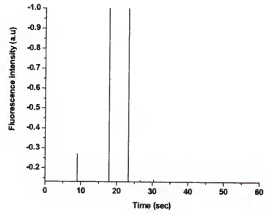

(A)

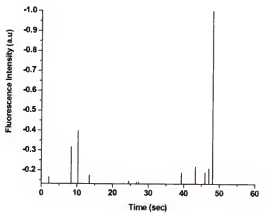

(B)

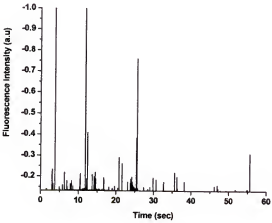

(C)

Figure 6-7. Detection of different concentrations of *E. coli* O157:H7 using a lab-made flow cytometer following incubation with nanoparticle-antibody conjugates. (A) 100 cfu/mL , Flow rate: 1 mL/hour, (B) 500 cfu/mL, Flow rate: 1 mL/hour, and (C) 500 cfu/mL, Flow rate: 2 mL/hour.

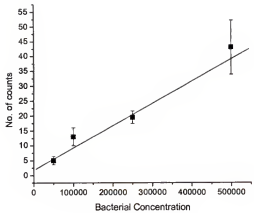

Figure 6-8. Calibration curve of bacteria detection using the lab-made flow cytometer.

Near-Infrared (NIR) Fluorescent Dye-doped Silica Nanoparticles for Multiple Bacteria Detection

Near-Infrared (NIR) chromophores have been used successfully[202-205] in replacing their shorter wavelength counterparts in several analytical applications. The advantage of NIR fluorescence spectroscopy is especially obvious in bioanalytical chemistry where the inherently low background fluorescence of the long wavelength spectral region reduces the need for sample preparation, but other areas of analytical chemistry also benefit. Typically, NIR techniques utilize the 680-1000 nm spectral region for excitation of the NIR label. NIR dyes have become more and more important in analytical chemistry and several laboratories use these dyes with great success. NIR applications are becoming increasingly more mainstream as commercialization advances.

Results and Discussion

The synthesis of various types of lanthanide complex-doped silica nanoparticles or lanthanide oxides has been investigated for their potential use in multiple bacteria detection. The objective of this study is to produce water soluble, highly luminescent, lanthanide-doped silica nanoparticles. Europium and yttrium oxides have been synthesized and with further development can be doped inside of silica nanoparticles.

Four types of nanoparticles were synthesized: 1. Eu_2O_3, 2. Y_2O_3, 3. Y_2O_3:Eu^{3+} (1:3 molar ratio), and 4. Eu_2O_3 with an Y_2O_3 shell using a bicontinuous microemulsion method.[206] Two microemulsions were used to prepare the nanoparticles. Microemulsion I was slowly added into microemulsion II under stirring, and continuously mixed for ~ 8 hours. The resulting precipitates were washed with ethanol and water. Following synthesis, the particles were analyzed for size and fluorescence properties and examples of the particle sizes and fluorescence properties are shown in Figure 6-9.

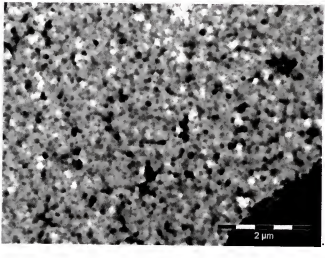

Figure 6-9. Nanoparticle size and fluorescence spectrum of europium oxide.

1,1',3,3,3',3'-Hexamethylindo tricarbocyanine iodide (HITC)-doped silica nanoparticles were synthesized using an altered version of the Stöber method described in the Experimental Section of Chapter 2. The hydrophobic silane, phenyltriethoxysilane (PTES), was reacted with HITC, prior to be added to the reaction mixture for Stöber synthesis in order to aid in the trapping of the HITC. This method was previously used to trap rhodamine 6G (R6G) dye inside silica nanoparticles.[67] The reaction time for the PTES solution was varied from 30 minutes - 8 hours at 0°C with continuous sonication. Aliquots of 500 µL PTES solution were used in each synthesis batch. The size of the

HITC doped silica nanoparticle produced range from 145 – 733 nm in diameter. The fluorescence spectrum of HITC and its structure are shown in Figure 6-10. The fluorescence intensity and nanoparticle size as a function of PTES silane precursor/HITC reaction time are shown in Figure 6-11. The fluorescence intensity of HITC-doped silica nanoparticles synthesized with various concentrations of PTES silane precursor/HITC are shown in Figure 6-12. These results show that with further development, this Stöber based method may be used to trap hydrophobic near-IR dyes into silica nanoparticles.

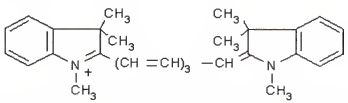

1,1',3,3,3',3'-Hexamethylindotricarbocyanine iodide (HITC)

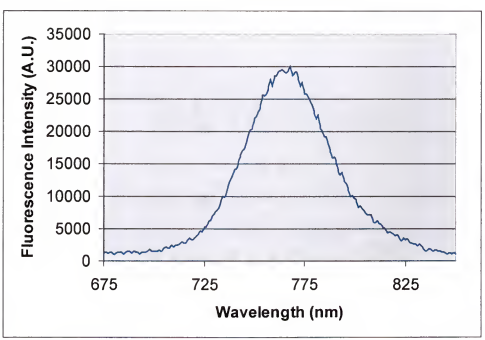

Figure 6-10. Structure and fluorescence spectrum of 1,1',3,3,3',3'-hexamethylindotricarbocyanine iodide (HITC). The excitation/emission wavelengths for HITC are 590 nm and 740 nm, respectively.

30 minutes

Average size = 315 ± 33 nm

1 hour

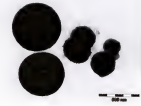

Average size = 400 ± 182 nm

1 hour 30 minutes

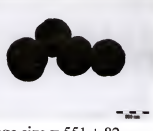

Average size = 551 ± 82 nm

2 hours

Average size = 258 ± 150 nm

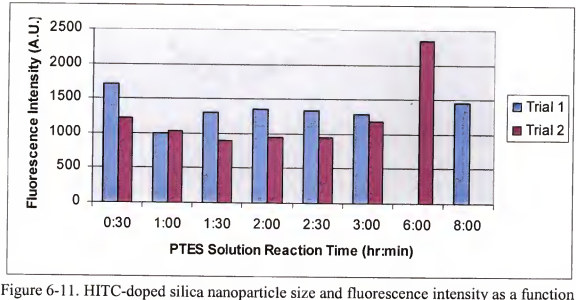

Figure 6-11. HITC-doped silica nanoparticle size and fluorescence intensity as a function of PTES silane precursor/HITC reaction time prior to Stöber based synthesis.

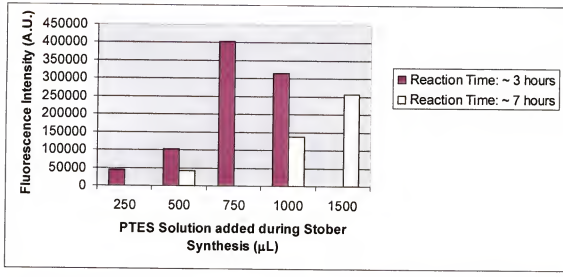

Figure 6-12. HITC-doped silica nanoparticle fluorescence intensity as a function of PTES silane precursor/HITC concentration added, after reaction times of 3 and 7 hours, in Stöber based synthesis.

Conclusions

The different antibodies selected for conjugation to the silica nanoparticles show moderate to good selectivity. The preliminary results presented show that the nanoparticle-based immunoassay has the potential to be used for rapid and ultrasensitive detection of multiple target cells with high selectivity. In addition, the development of novel types of fluorescent silica nanoparticles geared toward the near infrared region will expand the options of detection schemes for bacteria detection.

CHAPTER 7
SUMMARY AND FUTURE DIRECTIONS

Summary

Recently, nanomaterials have demonstrated their unique advantages when combined with biomolecules for bioanalysis and biotechnology applications. The demand for highly sensitive nonisotopic bioanalysis systems for biotechnology applications, such as in clinical diagnostics, food quality control, and drug delivery, has driven the development of nanomaterials geared more toward biological applications. The dye-doped silica nanoparticles described in this dissertation emit a strong fluorescent signal, enabling ultrasensitive target detection and monitoring of rare events that would be otherwise undetectable with existing labeling technologies. Furthermore, the nanoscale size of the particles minimizes physical interference with the biological recognition events and the nature of silica particles enables easy modification of the particle surface for conjugation with various biomolecules for a wide range of applications. The potential to dope the silica particles with any of the existing fluorophores provides a diversity of nanoparticles for various applications. With further development and advancement bioconjugated, fluorescent dye-doped silica nanoparticles will emerge as a revolutionary tool for ultrasensitive detection of infectious agents and disease markers. The fluorescent dye-doped silica nanoparticles will also be highly useful for bioimaging of cells and cellular components, neurochemical monitoring, and mRNA/DNA detection techniques.

The optimization of fluorescent silica nanoparticle synthesis, modification, and bioconjugation has been presented in this dissertation. The three major advantages of dye-doped silica nanoparticles —high fluorescent intensity, excellent photostability, and good biocompatibility— were investigated in order to obtain a better understanding of how these properties can be enhanced and controlled. In addition, novel bioanalytical applications using the fluorescent dye-doped nanoparticles were demonstrated.

The formation of tris (2,2'-bipyridyl) dichlororuthenium (II) (Rubpy) dye-doped silica nanoparticles by ammonia-catalyzed hydrolysis of tetraethyl orthosilicate (TEOS) in water-in-oil microemulsion (W/O) was studied. The particle size and size distribution of RuBpy dye-doped silica nanoparticles were examined as a function of reactant concentrations (TEOS and ammonium hydroxide), nature of surfactant molecules, and molar ratios of water to surfactant and cosurfactant to surfactant. The particle size was dependent upon the type of microemulsion system chosen and was found to decrease with an increase in concentration of ammonium hydroxide and increase in water to surfactant molar ratio and cosurfactant to surfactant molar ratio. This optimization study of the preparation of dye-doped silica nanoparticles provides a fundamental knowledge of the synthesis and optical properties of Rubpy dye-doped silica nanoparticles. Using this information, these nanoparticles can be easily manipulated, with regard to particle size and size distribution, and bioconjugated as needed for bioanalysis and bioseparation applications. In addition, the development of new types of organic dye-doped silica nanoparticles was explored using the Stöber and reverse microemulsion synthesis methods.

A study of the design and development of surface modification schemes for fluorescent dye-doped silica nanoparticles was also presented. The nanoparticle surface design involved an optimum balance of the use of inert and active surface functional groups to achieve minimal nanoparticle aggregation and reduce nanoparticle non-specific binding. Silica nanoparticles, doped with the fluorescent dye tris (2,2'-bipyridyl) dichlororuthenium (II) hexahydrate (RuBpy), were prepared in a water-in-oil microemulsion and subsequently surface modified via co-hydrolysis with tetraethylorthosilicate (TEOS) and various organosilane reagents. Nanoparticles with different functional groups, including carboxyl, amine, amine/phosphonate, polyethylene glycol, octadecyl, and carboxylate/octadecyl groups were produced. Aggregation studies, using SEM, dynamic light scattering, and zeta potential analysis, indicate that severe aggregation among amine-modified silica nanoparticles can be reduced by adding inert functional groups, such as methylphosphonate, to the surface. Using these surface modification schemes, fluorescent dye-doped silica nanoparticles can be more readily conjugated with biomolecules and used as highly fluorescent, sensitive, and reproducible labels in bioanalytical applications.

The utility of the functionalized silica nanoparticles was demonstrated via the development of oligonucleotide-functionalized nanoparticles. Disulfide-coupling chemistry was used for the immobilization of oligonucleotides onto silica nanoparticles and the properties of the resulting DNA nanoparticles were investigated. Factors influencing the immobilization and hybridization processes were examined and optimized. The oligonucleotide-modified silica nanoparticles provide an efficient

substrate for hybridization and can be used in the development of DNA biosensors and biochips.

An ultrasensitive immunoassay using fluorescent dye-doped silica nanoparticles as highly fluorescent and photostable probes was also developed. Trace amounts of bacterial cells can be counted easily and accurately without sample amplification or enrichment. Compared to dye molecule labeled bacterial cells, the nanoparticle-antibody conjugate labeled bacteria not only show significant signal amplification in bacterial antibody-antigen recognition, but also provide highly photostable fluorescent signals regardless of the detection time. The detection limit is as low as 1 bacterial cell per sample. To show the usefulness of this assay, 1–400 *E. coli* O157 bacterial cells were accurately detected in spiked ground beef samples. This assay is rapid, technically simple, and specific for *E. coli* O157:H7. Using antibodies specific for various bacterial pathogens, this assay can potentially be adapted for the detection of a wide variety of bacterial pathogens to make the early detection of multiple bacteria simpler and more accurate.

Future Directions

Many theoretical and technical problems still have to be solved—from understanding the nanofabrication of smaller sized particles that span the visible to near-infrared region of the electromagnetic spectrum, to the better control of the bioconjugation and application of biologically active molecules— for fluorescent dye-doped silica nanoparticles to reach their full potential as labels or probes for biological applications.

Dye-doped silica nanoparticle synthesis. The synthesis parameters that affect the size and optical properties of RuBpy dye-doped silica nanoparticles have been extensively studied. However, these parameters, such as temperature, silica precursor

concentration, and surfactant systems, need to be further explored for the doping of silica nanoparticles with organic or lanthanide complex dyes. A more complete and systematic study of the synthesis parameters will reduce the trial-and-error aspect of dye-doped silica nanoparticle synthesis and enable the development of many different dye-doped silica nanoparticles.

To further extend the spectral range of dye-doped silica nanoparticles, the doping of lanthanide complexes will enable silica nanoparticle labels in the near infrared region. In addition, these particles can be used for time-resolved fluorescence measurements.

Nanoparticle surface modification and bioconjugation. In order for the dye-doped silica nanoparticles to be used in a given biological application, the particles must be efficiently conjugated to the biomolecule of interest and not interfere with the biological event being detected. Thus, the controlled addition of surface functional groups and subsequent bioconjugation must be tailored for the given biological application. In future studies, the effect of the concentration of the given functional group on the efficiency of nanoparticle conjugation to a biomolecule, such as antibodies, can be studied.

DNA-conjugated nanoparticles. For bioanalytical applications, the effect of nanoparticle size on the efficiency of the biological process can be studied. With the DNA-conjugated nanoparticles, the efficiency of immobilization and hybridization might be affected by the size of the nanoparticles. Results obtained from such evaluation would greatly improve the efficiently and reproducibility of DNA assays using dye-doped silica nanoparticles.

The use of extended spacer arms or linkers (longer than a C_6 chain) can also be investigated to further increase the efficiency of DNA hybridization on silica nanoparticles by increasing the degrees of freedom of the oligonucleotide and availability of the bases.

Bacteria detection using dye-doped silica nanoparticles. More work needs to be done to optimize the nanoparticle-based immunoassay for bacteria detection. To evaluate the relative efficiency of the immunoassay, the activity of the antibodies, and the stability and fluorescence properties of the nanoparticles needs to be demonstrated. The activity of the reporter antibodies can be compared to that of free antibodies to ensure that the immobilization process does not inhibit antigen binding.

Nonspecific binding to the antibody-nanoparticle conjugates was negligible in the control samples, E. coli Dh5α, as compared to the E. coli O157:H7 samples. Other studies have shown that this Mab is non-reactive with the following serotypes: O111, O125, O20, O55, and K12.[153] Cross-reactions and thus, false-positive results may be observed with *S. dysenteriae*, *E. hermanii*, and *S. urbana*.[150] To further verify the specificity of the reporter antibodies, 20-50 strains of bacteria can be tested to determine the host range and specificity of the immunoassay.

In addition, the results obtained using the nanoparticle-based immunoassay can be compared with those from a standard, FDA-approved detection method such as the VIDAS bioMérieux automated system for immunoassays based on ELISA (VIDAS 2001).[144] Results of these experiments will be indicative of the efficiency of the reporter antibodies as biomarkers for antibody-antigen interactions.

LIST OF REFERENCES

1. Kneuer, C.; Sameti, M.; Bakowsky, U.; Schiestel, T.; Schirra, H.; Schmidt, H.; Lehr, C. M. *Bioconjugate Chemistry* **2000**, *11*, 926-932.

2. Kneuer, C.; Sameti, M.; Haltner, E. G.; Schiestel, T.; Schirra, H.; Schmidt, H.; Lehr, C. M. *International Journal of Pharmaceutics* **2000**, *196*, 257-261.

3. Mao, H. Q.; Roy, K.; Troung-Le, V. L.; Janes, K. A.; Lin, K. Y.; Wang, Y.; August, J. T.; Leong, K. W. *Journal of Controlled Release* **2001**, *70*, 399-421.

4. Benns, J. M.; Kim, S. W. *Journal of Drug Targeting* **2000**, *8*, 1-12.

5. Truong-Le, V. L.; Walsh, S. M.; Schweibert, E.; Mao, H. Q.; Guggino, W. B.; August, J. T.; Leong, K. W. *Archives of Biochemistry and Biophysics* **1999**, *361*, 47-56.

6. Soppimath, K. S.; Aminabhavi, T. M.; Kulkarni, A. R.; Rudzinski, W. E. *Journal of Controlled Release* **2001**, *70*, 1-20.

7. Sershen, S. R.; Westcott, S. L.; Halas, N. J.; West, J. L. *Journal of Biomedical Materials Research* **2000**, *51*, 293-298.

8. Kubitschko, S.; Spinke, J.; Bruckner, T.; Pohl, S.; Oranth, N. *Analytical Biochemistry* **1997**, *253*, 112-122.

9. Lyon, L. A.; Musick, M. D.; Smith, P. C.; Reiss, B. D.; Pena, D. J.; Natan, M. J. *Sensors and Actuators B-Chemical* **1999**, *54*, 118-124.

10. Schaertl, S.; Meyer-Almes, F. J.; Lopez-Calle, E.; Siemers, A.; Kramer, J. *Journal of Biomolecular Screening* **2000**, *5*, 227-237.

11. Dabbousi, B. O.; RodriguezViejo, J.; Mikulec, F. V.; Heine, J. R.; Mattoussi, H.; Ober, R.; Jensen, K. F.; Bawendi, M. G. *Journal of Physical Chemistry B* **1997**, *101*, 9463-9475.

12. Alivisatos, A. P. *Journal of Physical Chemistry* **1996**, *100*, 13226-13239.

13. Chan, W. C. W.; Nie, S. M. *Science* **1998**, *281*, 2016-2018.

14. Emory, S. R.; Nie, S. *Journal of Physical Chemistry B* **1998**, *102*, 493-497.

15. Han, M. Y.; Gao, X. H.; Su, J. Z.; Nie, S. *Nature Biotechnology* **2001**, *19*, 631-635.

16. Bruchez, M.; Moronne, M.; Gin, P.; Weiss, S.; Alivisatos, A. P. *Science* **1998**, *281*, 2013-2016.

17. Dahan, M.; Laurence, T.; Pinaud, F.; Chemla, D. S.; Alivisatos, A. P.; Sauer, M.; Weiss, S. *Optics Letters* **2001**, *26*, 825-827.

18. Hranisavljevic, J.; Dimitrijevic, N. M.; Wurtz, G. A.; Wiederrecht, G. P. *Journal of the American Chemical Society* **2002**, *124*, 4536-4537.

19. Cao, Y. W.; Jin, R.; Mirkin, C. A. *Journal of the American Chemical Society* **2001**, *123*, 7961-7962.

20. Fulton, R. J.; McDade, R. L.; Smith, P. L.; Kienker, L. J.; Kettman, J. R. *Clinical Chemistry* **1997**, *43*, 1749-1756.

21. Santra, S.; Zhang, P.; Wang, K. M.; Tapec, R.; Tan, W. H. *Analytical Chemistry* **2001**, *73*, 4988-4993.

22. Godovsky, D. Y. *Advances in Polymer Science* **2000**, *153*, 163-205.

23. Michalet, X.; Pinaud, F. F.; Bentolila, L. A.; Tsay, J. M.; Doose, S.; Li, J. J.; Sundaresan, G.; Wu, A. M.; Gambhir, S. S.; Weiss, S. *Science* **2005**, *307*, 538-544.

24. Gerion, D.; Pinaud, F.; Williams, S. C.; Parak, W. J.; Zanchet, D.; Weiss, S.; Alivisatos, A. P. *Journal of Physical Chemistry B* **2001**, *105*, 8861-8871.

25. Schroedter, A.; Weller, H. *Angewandte Chemie-International Edition* **2002**, *41*, 3218-3221.

26. Maxwell, D. J.; Taylor, J. R.; Nie, S. M. *Journal of the American Chemical Society* **2002**, *124*, 9606-9612.

27. Krug, J. T.; Wang, G. D.; Emory, S. R.; Nie, S. M. *Journal of the American Chemical Society* **1999**, *121*, 9208-9214.

28. Niemeyer, C. M. *Angewandte Chemie-International Edition* **2001**, *40*, 4128-4158.

29. Sastry, M.; Lala, N.; Patil, V.; Chavan, S. P.; Chittiboyina, A. G. *Langmuir* **1998**, *14*, 4138-4142.

30. Zanchet, D.; Micheel, C. M.; Parak, W. J.; Gerion, D.; Alivisatos, A. P. *Nano Letters* **2001**, *1*, 32-35.

31. Weizmann, Y.; Patolsky, F.; Willner, I. *Analyst* **2001**, *126*, 1502-1504.

32. Souza, G. R.; Miller, J. H. *Journal of the American Chemical Society* **2001**, *123*, 6734-6735.

33. Reichert, J.; Csaki, A.; Kohler, J. M.; Fritzsche, W. *Analytical Chemistry* **2000**, *72*, 6025-6029.

34. Dubertret, B.; Calame, M.; Libchaber, A. J. *Nature Biotechnology* **2001**, *19*, 365-370.

35. Siiman, O.; Gordon, K.; Burshteyn, A.; Maples, J. A.; Whitesell, J. K. *Cytometry* **2000**, *41*, 298-307.

36. Gole, A.; Dash, C.; Soman, C.; Sainkar, S. R.; Rao, M.; Sastry, M. *Bioconjugate Chemistry* **2001**, *12*, 684-690.

37. Storhoff, J. J.; Elghanian, R.; Mucic, R. C.; Mirkin, C. A.; Letsinger, R. L. *Journal of the American Chemical Society* **1998**, *120*, 1959-1964.

38. Cao, Y. W. C.; Jin, R. C.; Mirkin, C. A. *Science* **2002**, *297*, 1536-1540.

39. Park, S. J.; Taton, T. A.; Mirkin, C. A. *Science* **2002**, *295*, 1503-1506.

40. Reynolds, R. A.; Mirkin, C. A.; Letsinger, R. L. *Pure and Applied Chemistry* **2000**, *72*, 229-235.

41. Storhoff, J. J.; Mirkin, C. A. *Chemical Reviews* **1999**, *99*, 1849-1862.

42. Cai, H.; Xu, C.; He, P.; Fang, Y. *Journal of Electroanalytical Chemistry* **2001**, *510*, 78-85.

43. Mirkin, C. A.; Letsinger, R. L.; Mucic, R. C.; Storhoff, J. J. *Nature* **1996**, *382*, 607-609.

44. Demers, L. M.; Mirkin, C. A.; Mucic, R. C.; Reynolds, R. A., III; Letsinger, R. L.; Elghanian, R.; Viswanadham, G. *Analytical Chemistry* **2000**, *72*, 5535-5541.

45. Watson, K. J.; Zhu, J.; Nguyen, S. T.; Mirkin, C. A. *Pure and Applied Chemistry* **2000**, *72*, 67-72.

46. Letsinger, R. L.; Mirkin, C. A.; Elghanian, R.; Mucic, R. C.; Storhoff, J. J. *Phosphorus Sulfur and Silicon and the Related Elements* **1999**, *146*, 359-362.

47. Elghanian, R.; Storhoff, J. J.; Mucic, R. C.; Letsinger, R. L.; Mirkin, C. A. *Science* **1997**, *277*, 1078-1081.

48. Taton, T. A.; Mirkin, C. A.; Letsinger, R. L. *Science* **2000**, *289*, 1757-1760.

49. Reynolds, R. A., III; Mirkin, C. A.; Letsinger, R. L. *Journal of the American Chemical Society* **2000**, *122*, 3795-3796.

50. Zhou, C.; Zhao, Y.; Jao, T.-C.; Winnik, M. A.; Wu, C. *Journal of Physical Chemistry B* **2002**, *106*, 1889-1897.

51. Kwon, S. S.; Nam, Y. S.; Lee, J. S.; Ku, B. S.; Han, S. H.; Lee, J. Y.; Chang, I. S. *Colloids and Surfaces, A: Physicochemical and Engineering Aspects* **2002**, *210*, 95-104.

52. Ito, S.; Yoshikawa, H.; Masuhara, H. *Applied Physics Letters* **2001**, *78*, 2566-2568.

53. Quintanar-Guerrero, D.; Allemann, E.; Doelker, E.; Fessi, H. *Colloid and Polymer Science* **1997**, *275*, 640-647.

54. Taylor, J. R.; Fang, M. M.; Nie, S. M. *Analytical Chemistry* **2000**, *72*, 1979-1986.

55. Jain, T. K.; Roy, I.; De, T. K.; Maitra, A. *Journal of the American Chemical Society* **1998**, *120*, 11092-11095.

56. Lopez-Quintela, M. A. *Current Opinion in Colloid & Interface Science* **2003**, *8*, 137-144.

57. Bagwe, R. P.; Khilar, K. C. *Langmuir* **2000**, *16*, 905-910.

58. Bagwe, R. P.; Mishra, B. K.; Khliar, K. C. *Journal of Dispersion Science and Technology* **1999**, *20*, 1569-1579.

59. Bagwe, R. P.; Khilar, K. C. *Langmuir* **1997**, *13*, 6432-6438.

60. Zhang, P.; Gao, L. *Journal of Materials Chemistry* **2003**, *13*, 2007-2010.

61. Ueba, H. *Journal of Chemical Physics* **1980**, *73*, 725-732.

62. Vanhelden, A. K.; Vrij, A. *Journal of Colloid and Interface Science* **1980**, *78*, 312-329.

63. Wang, D. S.; Chew, H.; Kerker, M. *Applied Optics* **1980**, *19*, 2256-2257.

64. Wang, D. S.; Kerker, M.; Chew, H. W. *Applied Optics* **1980**, *19*, 2315-2328.

65. Weitz, D. A.; Gramila, T. J.; Genack, A. Z.; Gersten, J. I. *Physical Review Letters* **1980**, *45*, 355-358.

66. Santra, S.; Wang, K. M.; Tapec, R.; Tan, W. H. *Journal of Biomedical Optics* **2001**, *6*, 160-166.

67. Tapec, R.; Zhao, X. J. J.; Tan, W. H. *Journal of Nanoscience and Nanotechnology* **2002**, *2*, 405-409.

68. Chen, C.-C.; Yet, C.-P.; Wang, H.-N.; Chao, C.-Y. *Langmuir* **1999**, *15*, 6845-6850.

69. Zhao, X. J.; Bagwe, R. P.; Tan, W. H. *Advanced Materials* **2004**, *16*, 173-+.

70. Bohren, C. F.; Huffman, D. R. *Absorption and Scattering of Light by Small Particles*; Wiley: New York, 1983.

71. Correa-Duarte, M. A.; Giersig, M.; Liz-Marzan, L. M. *Chemical Physics Letters* **1998**, *286*, 497-501.

72. Mulvaney, P.; Giersig, M.; Ung, T.; Liz-Marzan, L. M. *Advanced Materials* **1997**, *9*, 570-575.

73. Stathatos, E.; Lianos, P.; Del Monte, F.; Levy, D.; Tsiourvas, D. *Langmuir* **1997**, *13*, 4295-4300.

74. Shiojiri, S.; Hirai, T.; Komasawa, I. *Chemical Communications* **1998**, 1439-1440.

75. Shah, D. O. *Micelles, Microemulsions, and Monolayers: Science and Technology* **1998**, 1-52.

76. Qhobosheane, M.; Santra, S.; Zhang, P.; Tan, W. H. *Analyst* **2001**, *126*, 1274-1278.

77. Shibata, S.; Taniguchi, T.; Yano, T.; Yamane, M. *Journal of Sol-Gel Science and Technology* **1997**, *10*, 263-268.

78. Babes, L.; Denizot, B.; Tanguy, G.; Le Jeune, J. J.; Jallet, P. *Journal of Colloid and Interface Science* **1999**, *212*, 474-482.

79. Tchikov, V.; Schutze, S.; Kronke, M. *Journal of Magnetism and Magnetic Materials* **1999**, *194*, 242-247.

80. Santra, S.; Liesenfeld, B.; Dutta, D.; Chatel, D.; Batich, C. D.; Tan, W.; Moudgil, B. M.; Mericle, R. A. *Journal of Nanoscience and Nanotechnology* **2005**, *5*, 899-904.

81. Santra, S.; Yang, H.; Dutta, D.; Stanley, J. T.; Holloway, P. H.; Tan, W.; Moudgil, B. M.; Mericle, R. A. *Chemical Communications* **2004**, 2810-2811.

82. Turney, K.; Drake, T. J.; Smith, J. E.; Tan, W.; Harrison, W. W. *Rapid Communications in Mass Spectrometry* **2004**, *18*, 2367-2374.

83. He, X.; Duan, J.; Wang, K.; Tan, W.; Lin, X.; He, C. *Journal of Nanoscience and Nanotechnology* **2004**, *4*, 585-589.

84. Zhao, X.; Tapec-Dytioco, R.; Tan, W. *Journal of the American Chemical Society* **2003**, *125*, 11474-11475.

85. He, X.; Wang, K.; Li, D.; Tan, W.; He, C.; Huang, S.; Liu, B.; Lin, X.; Chen, X. *Journal of Dispersion Science and Technology* **2003**, *24*, 633-640.

86. Zhao, X.; Hilliard, L. R.; Wang, K.; Tan, W. *Encyclopedia of Nanoscience and Nanotechnology* **2004**, *1*, 255-268.

87. Bagwe, R. P.; Yang, C. Y.; Hilliard, L. R.; Tan, W. H. *Langmuir* **2004**, *20*, 8336-8342.

88. Hilliard, L. R.; Zhao, X.; Tan, W. *Analytica Chimica Acta* **2002**, *470*, 51-56.

89. Zhao, X.; Hilliard, L. R.; Mechery, S. J.; Wang, Y.; Bagwe, R. P.; Jin, S.; Tan, W. *Proceedings of the National Academy of Sciences of the United States of America* **2004**, *101*, 15027-15032.

90. Zhao, X. J.; Tapec-Dytioco, R.; Wang, K. M.; Tan, W. H. *Analytical Chemistry* **2003**, *75*, 3476-3483.

91. Vos, W. L.; Sprik, R.; vanBlaaderen, A.; Imhof, A.; Lagendijk, A.; Wegdam, G. H. *Physical Review B* **1996**, *53*, 16231-16235.

92. Bentivegna, F.; Canva, M.; Georges, P.; Brun, A.; Chaput, F.; Malier, L.; Boilot, J. P. *Applied Physics Letters* **1993**, *62*, 1721-1723.

93. van Blaaderen, A.; Vrij, A. *Journal of Colloid and Interface Science* **1993**, *156*, 1-18.

94. van Blaaderen, A.; Vrij, A. *Langmuir* **1992**, *8*, 2921-2931.

95. Stöber, W.; Fink, A.; Bohn, E. *Journal of Colloid and Interface Science* **1968**, *26*, 62-69.

96. Zhao, X. J.; Bagwe, R. P.; Tan, W. H. *Advanced Materials* **2004**, *16*, 173-176.

97. Fletcher, P. D. I.; Howe, A. M.; Robinson, B. H. *Journal of the Chemical Society-Faraday Transactions I* **1987**, *83*, 985-1006.

98. Chang, C. L.; Fogler, H. S. *Langmuir* **1997**, *13*, 3295-3307.

99. Marchand, K. E.; Tarret, M.; Lechaire, J. P.; Normand, L.; Kasztelan, S.; Cseri, T. *Colloids and Surfaces a-Physicochemical and Engineering Aspects* **2003**, *214*, 239-248.

100. Arriagada, F. J.; Osseo-Asare, K. *Journal of Colloid and Interface Science* **1999**, *211*, 210-220.

101. Arriagada, F. J.; Osseo-Asare, K. *Colloids and Surfaces a-Physicochemical and Engineering Aspects* **1999**, *154*, 311-326.

102. Arriagada, F. J.; Osseoasare, K. *Journal of Dispersion Science and Technology* **1994**, *15*, 59-71.

103. Nagy, J. B. *Colloids and Surfaces* **1989**, *35*, 201-220.

104. Hermanson, G. T. *Bioconjugate Techniques*; Academic Press: San Diego, 1996.

105. Drake, T. J.; Zhao, X. J.; Tan, W. *Nanobiotechnology* **2004**, 444-457.

106. Bagwe, R. P.; Zhao, X. J.; Tan, W. H. *Journal of Dispersion Science and Technology* **2003**, *24*, 453-464.

107. Deng, G.; Markowitz, M. A.; Kust, P. R.; Gaber, B. P. *Materials Science & Engineering C-Biomimetic and Supramolecular Systems* **2000**, *11*, 165-172.

108. Udenfrie.S; Stein, S.; Bohlen, P.; Dairman, W. *Science* **1972**, *178*, 871-&.

109. Southern, E. M. *Journal of Molecular Biology* **1975**, *98*, 503-517.

110. Gilham, P. T. *Journal of the American Chemical Society* **1964**, *86*, 4982-4985.

111. Poonian, M. S.; Schlabac, A. J.; Weissbac, A. *Biochemistry* **1971**, *10*, 424-427.

112. Kremsky, J. N.; Wooters, J. L.; Dougherty, J. P.; Meyers, R. E.; Collins, M.; Brown, E. L. *Nucleic Acids Research* **1987**, *15*, 2891-2909.

113. Bunemann, H.; Westhoff, P.; Herrmann, R. G. *Nucleic Acids Research* **1982**, *10*, 7163-7180.

114. Santra, S.; Tapec, R.; Theodoropoulou, N.; Dobson, J.; Hebard, A.; Tan, W. *Langmuir* **2001**, *17*, 2900-2906.

115. Rogers, Y. H.; Jiang-Baucom, P.; Huang, Z. J.; Bogdanov, V.; Anderson, S.; Boyce-Jacino, M. T. *Analytical Biochemistry* **1999**, *266*, 23-30.

116. Henke, L.; Piunno, P. A. E.; McClure, A. C.; Krull, U. J. *Analytica Chimica Acta* **1997**, *344*, 201-213.

117. Joos, B.; Kuster, H.; Cone, R. *Analytical Biochemistry* **1997**, *247*, 96-101.

118. Chrisey, L. A.; Lee, G. U.; Oferrall, C. E. *Nucleic Acids Research* **1996**, *24*, 3031-3039.

119. Beattie, W. G.; Meng, L.; Turner, S. L.; Varma, R. S.; Dao, D. D.; Beattie, K. L. *Molecular Biotechnology* **1995**, *4*, 213-225.

120. Guo, Z.; Guilfoyle, R. A.; Thiel, A. J.; Wang, R. F.; Smith, L. M. *Nucleic Acids Research* **1994**, *22*, 5456-5465.

121. Lamture, J. B.; Beattie, K. L.; Burke, B. E.; Eggers, M. D.; Ehrlich, D. J.; Fowler, R.; Hollis, M. A.; Kosicki, B. B.; Reich, R. K.; Smith, S. R.; Varma, R. S.; Hogan, M. E. *Nucleic Acids Research* **1994**, *22*, 2121-2125.

122. Lund, V.; Schmid, R.; Rickwood, D.; Hornes, E. *Nucleic Acids Research* **1988**, *16*, 10861-10880.

123. Chu, B. C. F.; Orgel, L. E. *Nucleic Acids Research* **1988**, *16*, 3671-3691.

124. Zuckermann, R.; Corey, D.; Schultz, P. *Nucleic Acids Research* **1987**, *15*, 5305-5321.

125. Day, P. J. R.; Flora, P. S.; Fox, J. E.; Walker, M. R. *Biochemical Journal* **1991**, *278*, 735-740.

126. Bischoff, R.; Coull, J. M.; Regnier, F. E. *Analytical Biochemistry* **1987**, *164*, 336-344.

127. Soukka, T.; Harma, H.; Paukkunen, J.; Lovgren, T. *Analytical Chemistry* **2001**, *73*, 2254-2260.

128. Bunemann, H. *Nucleic Acids Research* **1982**, *10*, 7181-7196.

129. Zhang, Y.; Coyne, M. Y.; Will, S. G.; Levenson, C. H.; Kawasaki, E. S. *Nucleic Acids Research* **1991**, *19*, 3929-3933.

130. Phillips, C. A. *Journal of the Science of Food and Agriculture* **1999**, *79*, 1367-1381.

131. Riley, L. W.; Remis, R. S.; Helgerson, S. D.; McGee, H. B.; Wells, J. G.; Davis, B. R.; Hebert, R. J.; Olcott, E. S.; Johnson, L. M.; Hargrett, N. T.; Blake, P. A.; Cohen, M. L. *New England Journal of Medicine* **1983**, *308*, 681-685.

132. Johnson, R. P.; Clarke, R. C.; Wilson, J. B.; Read, S. C.; Rahn, K.; Renwick, S. A.; Sandhu, K. A.; Alves, D.; Karmali, M. A.; Lior, H.; McEwen, S. A.; Spika, J. S.; Gyles, C. L. *Journal of Food Protection* **1996**, *59*, 1112-1122.

133. Griffin, P. M.; Tauxe, R. V. *Epidemiologic Reviews* **1991**, *13*, 60-98.

134. Del Rosario, B. A.; Beuchat, L. R. *Journal of Food Protection* **1995**, *58*, 105-107.

135. Nataro, J. P.; Kaper, J. B. *Clinical Microbiology Reviews* **1998**, *11*, 142-201.

136. Hopkins, R. S.; Jajosky, R. A.; Hall, P. A.; Adams, D. A.; Connor, F. J.; Sharp, P.; Anderson, W. J.; Fagan, R. F.; Aponte, J. J.; Jones, G. F.; Nitschke, D. A.; Worsham, C. A.; Adekoya, N.; Chang, M.-h. *MMWR, Morbidity and Mortality Weekly Report* **2005**, *52*, 1-85.

137. Groseclose, S. L.; Brathwaite, W. S.; Hall, P. A.; Adams, D. A.; Connor, F. J.; Sharp, P.; Anderson, W. J.; Fagan, R. F.; Aponte, J. J.; Jones, G. F.; Nitschke, D. A.; Worsham, C. A.; Adekoya, N.; Chang, M.-H.; Doyle, T.; Dhara, R.; Jajosky, R. A. *MMWR, Morbidity and Mortality Weekly Report* **2004**, *51*, 1–84.

138. Varma, J. K.; Greene, K. D.; Reller, M. E.; Delong, S. M.; Trottier, J.; Nowicki, S. F.; Diorio, M.; Koch, E. M.; Bannerman, T. L.; York, S. T.; Lambert-Fair, M.-A.; Wells, J. G.; Mead, P. S. *JAMA, the Journal of the American Medical Association* **2003**, *290*, 2709-2712.

139. Bruce, M. G.; Curtis, M. B.; Payne, M. M.; Gautom, R. K.; Thompson, E. C.; Bennett, A. L.; Kobayashi, J. M. *Archives of Pediatrics & Adolescent Medicine* **2003**, *157*, 1016-1021.

140. Mohle-Boetani, J. C.; Farrar, J. A.; Werner, S. B.; Minassian, D.; Bryant, R.; Abbott, S.; Slutsker, L.; Vugia, D. J. *Annals of internal medicine* **2001**, *135*, 239-247.

141. Vugia, D.; Cronquist, A.; Hadler, J.; Tobin-D'Angelo, M.; Blythe, D.; Smith, K.; Thornton, K.; Morse, D.; Cieslak, P.; Jones, T.; Varghese, R.; Guzewich, J.; Angulo, F.; Griffin, P.; Tauxe, R.; Dunn, J. *MMWR, Morbidity and Mortality Weekly Report* **2005**, *54*, 352-356.

142. Deisingh, A. K.; Thompson, M. *Journal of Applied Microbiology* **2004**, *96*, 419-429.

143. Iqbal, S. S.; Mayo, M. W.; Bruno, J. G.; Bronk, B. V.; Batt, C. A.; Chambers, J. P. *Biosensors & Bioelectronics* **2000**, *15*, 549-578.

144. de Boer, E.; Beumer, R. R. *International Journal of Food Microbiology* **1999**, *50*, 119-130.

145. de Boer, E. *International Journal of Food Microbiology* **1998**, *45*, 43-53.

146. Williams, D. W.; Lewis, M. A. O. *Oral Diseases* **2000**, *6*, 3-11.

147. Marie, D.; Brussaard, C. P. D.; Thyrhaug, R.; Bratbak, G.; Vaulot, D. *Applied and Environmental Microbiology* **1999**, *65*, 45-52.

148. Boisen, F.; Skovgaard, N.; Ewald, S.; Olsson, G.; Wirtanen, G. *Journal of Aoac International* **1992**, *75*, 465-473.

149. Gibson, D. M.; Coombs, P.; Pimbley, D. W. *Journal of Aoac International* **1992**, *75*, 293-302.

150. Abel, A. P.; Weller, M. G.; Duveneck, G. L.; Ehrat, M.; Widmer, H. M. *Analytical Chemistry* **1996**, *68*, 2905-2912.

151. Doyle, M. P.; Beuchat, L. R.; Montville, T. J., Eds. *Food Microbiology: Fundamentals and Frontiers*; ASM Press: Washington, D. C., 1997, 710-727.

152. Scheu, P. M.; Berghof, K.; Stahl, U. *Food Microbiology* **1998**, *15*, 13-31.

153. Gehring, A. G.; Patterson, D. L.; Tu, S. I. *Analytical Biochemistry* **1998**, *258*, 293-298.

154. Paffard, S. M.; Miles, R. J.; Clark, C. R.; Price, R. G. *Journal of Immunological Methods* **1996**, *192*, 133-136.

155. Edwards, R., Ed. *Immunoassays: Essential Data*; John Wiley & Sons: New York, 1996, 84-87.

156. Delves, P. J., Ed. *Antibody Applications: Essential Techniques*; Wiley: New York, 1995, 43–51.

157. Maclin, E.; Rohlfing, D.; Ansour, M. *Clinical Chemistry* **1973**, *19*, 832-837.

158. Cao, L. K.; Anderson, G. P.; Ligler, F. S.; Ezzell, J. *Journal of Clinical Microbiology* **1995**, *33*, 336-341.

159. Brett, M. M. *Journal of Applied Microbiology* **1998**, *84*, 110S-118S.

160. BioMérieux Industry. *Tomorrow's Solution Today: VIDAS Next Day*; BioMérieux Industry, Inc., 2004, http://industry.biomerieux-usa.com-news-pressreleases-vidas_nextday.pdf, November 2005.

161. Adams, M. R.; Hope, C. F. A., Eds. *Progress in Industrial Microbiology, Vol. 26: Rapid Methods in Food Microbiology*; Elsevier: Amsterdam, 1989, 121-167.

162. Alexandre, M.; Prado, V. *Expert Review of Molecular Diagnostics* **2003**, *3*, 105-115.

163. Bettelheim, K. A.; Beutin, L. *Journal of Applied Microbiology* **2003**, *95*, 205-217.

164. Ibekwe, A. M.; Grieve, C. M. *Journal of Applied Microbiology* **2003**, *94*, 421-431.

165. Kourkine, I. V.; Ristic-Petrovic, M.; Davis, E.; Ruffolo, C. G.; Kapsalis, A.; Barron, A. E. *Electrophoresis* **2003**, *24*, 655-661.

166. Feldsine, P. T.; Kerr, D. E.; Leung, S. C.; Lienau, A. H.; Miller, S. M.; Mui, L. A.; Anderson, G.; Beasley, M.; Dillon, J.; Dombroski, P.; Forgey, R.; Hernandez, C.; Hopkins, S.; Johnson, K.; Meier, J.; Nguyen, T.; Ortega, R.; Reynolds, J.; Smith, J.; Solis, D.; Summers, C.; Terry, J.; Tuncan, E.; Vrana, D.; Warren, W.; Wood, S. *Journal of AOAC International* **2002**, *85*, 1037-1044.

167. Tu, S.-I.; Golden, M.; Andreotti, P.; Irwin, P. *Journal of Rapid Methods and Automation in Microbiology* **2002**, *10*, 37-48.

168. Yu, L. S. L.; Reed, S. A.; Golden, M. H. *Journal of microbiological methods* **2002**, *49*, 63-68.

169. Henry, Y. M.; Natrajan, N.; Lauer, W. F. *Journal of AOAC International* **2001**, *84*, 752-760.

170. Song, J. M.; Vo-Dinh, T. *Analytica Chimica Acta* **2004**, *507*, 115-121.

171. Muhammad-Tahir, Z.; Alocilja, E. C. *IEEE Sensors Journal* **2003**, *3*, 345-351.

172. Ho, J.-a. A.; Hsu, H.-W. *Analytical Chemistry* **2003**, *75*, 4330-4334.

173. Kim, M.; Oh, S.; Durst, R. A. *Journal of Microbiology and Biotechnology* **2003**, *13*, 509-516.

174. Wu, C.-F.; Valdes, J. J.; Bentley, W. E.; Sekowski, J. W. *Biosensors & Bioelectronics* **2003**, *19*, 1-8.

175. Molecular Probes. *FluoReporter® Tetramethylrhodamine Protein Labeling Kit (F-6163)*, Molecular Probes Inc., 2001, 1-3.

176. Boyd, R. F. *General Microbiology*, 2nd ed.; Times Mirror/Mosby: St. Louis, 1988, 401–404.

177. Nie, S.; Zare, R. N. *Annual Review of Biophysics and Biomolecular Structure* **1997**, *26*, 567-596.

178. Weimer, B. C.; Walsh, M. K.; Beer, C.; Koka, R.; Wang, X. *Applied and Environmental Microbiology* **2001**, *67*, 1300-1307.

179. Vet, J. A. M.; Majithia, A. R.; Marras, S. A. E.; Tyagi, S.; Dube, S.; Poiesz, B. J.; Kramer, F. R. *Proceedings of the National Academy of Sciences of the United States of America* **1999**, *96*, 6394-6399.

180. Schaller, G.; Evers, K.; Papadopoulos, S.; Ebert, A.; Buhler, H. *Annals of Oncology* **2001**, *12*, 97-100.

181. Rao, R. S.; Visuri, S. R.; McBride, M. T.; Albala, J. S.; Matthews, D. L.; Coleman, M. A. *Journal of Proteome Research* **2004**, *3*, 736-742.

182. Vignali, D. A. A. *Journal of Immunological Methods* **2000**, *243*, 243-255.

183. Wang, L.; Yang, C. Y.; Tan, W. H. *Nano Letters* **2005**, *5*, 37-43.

184. Beaucage, S. L. *Current Medicinal Chemistry* **2001**, *8*, 1213-1244.

185. Stimpson, D. I.; Knepper, S. M.; Shida, M.; Obata, K.; Tajima, H. *Biotechnology and Bioengineering* **2004**, *87*, 99-103.

186. Vora, G. J.; Meador, C. E.; Stenger, D. A.; Andreadis, J. D. *Applied and Environmental Microbiology* **2004**, *70*, 3047-3054.

187. Li, Y. W.; Reichert, W. M. *Langmuir* **2003**, *19*, 1557-1566.

188. Peluso, P.; Wilson, D. S.; Do, D.; Tran, H.; Venkatasubbaiah, M.; Quincy, D.; Heidecker, B.; Poindexter, K.; Tolani, N.; Phelan, M.; Witte, K.; Jung, L. S.; Wagner, P.; Nock, S. *Analytical Biochemistry* **2003**, *312*, 113-124.

189. Qiu, J.; Madoz-Gurpide, J.; Misek, D. E.; Kuick, R.; Brenner, D. E.; Michailidis, G.; Haab, B. B.; Omenn, G. S.; Hanash, S. *Journal of Proteome Research* **2004**, *3*, 261-267.

190. Levit-Binnun, N.; Lindner, A. B.; Zik, O.; Eshhar, Z.; Moses, E. *Analytical Chemistry* **2003**, *75*, 1436-1441.

191. Askari, M. D. F.; Miller, G. H.; Vo-Dinh, T. *Cancer Detection and Prevention* **2002**, *26*, 331-342.

192. Coleman, M. A.; Miller, K. A.; Beernink, P. T.; Yoshikawa, D. M.; Albala, J. S. *Proteomics* **2003**, *3*, 2101-2107.

193. McBride, M. T.; Gammon, S.; Pitesky, M.; O'Brien, T. W.; Smith, T.; Aldrich, J.; Langlois, R. G.; Colston, B.; Venkateswaran, K. S. *Analytical Chemistry* **2003**, *75*, 1924-1930.

194. Dasso, J.; Lee, J.; Bach, H.; Mage, R. G. *Journal of Immunological Methods* **2002**, *263*, 23-33.

195. Spiro, A.; Lowe, M.; Brown, D. *Applied and Environmental Microbiology* **2000**, *66*, 4258-4265.

196. Brodsky, A. S.; Silver, P. A. *Molecular & Cellular Proteomics* **2002**, *1*, 922-929.

197. Horan, P. K.; Wheeless, L. L. *Science* **1977**, *198*, 149-157.

198. McHugh, T. M. In *Methods in Cell Biology*; Academic Press: San Diego, 1994, Volume 42, 575-595; Vol. 42.

199. McHugh, T. M.; Miner, R. C.; Logan, L. H.; Stites, D. P. *Journal of Clinical Microbiology* **1988**, *26*, 1957-1961.

200. Scillian, J.; McHugh, T.; Busch, M.; Tam, M.; Fulwyler, M.; Chien, D.; Vyas, G. *Blood* **1989**, *73*, 2041-2048.

201. Xu, H. X.; Sha, M. Y.; Wong, E. Y.; Uphoff, J.; Xu, Y. H.; Treadway, J. A.; Truong, A.; O'Brien, E.; Asquith, S.; Stubbins, M.; Spurr, N. K.; Lai, E. H.; Mahoney, W. *Nucleic Acids Research* **2003**, *31*.

202. Semiatin, I. K. *R&D Magazine* **2005**, *47*, 24-25.

203. Wang, L. Q.; Peng, X. J.; Lu, E. H.; Cui, J. N.; Gao, X. Q. *Chinese Chemical Letters* **2005**, *16*, 461-464.

204. Wang, L. Q.; Peng, X. J.; Zhang, R.; Cui, J. N.; Xu, G. Q.; Wang, F. G. *Dyes and Pigments* **2002**, *54*, 107-111.

205. Narayanan, N.; Patonay, G. *Journal of Organic Chemistry* **1995**, *60*, 2391-2395.

206. Li, F.; Vipulanandan, C. *IEEE Transactions on Applied Superconductivity* **2003**, *13*, 3196 - 3198.

BIOGRAPHICAL SKETCH

Lisa R. Hilliard was born on August 8, 1977. She grew up in Orangeburg, SC, where she attended Felton Laboratory School and Orangeburg Wilkinson High School, for her primary and secondary education. In 1995, Lisa graduated from the South Carolina Governor's School for Science and Mathematics (Hartsville, SC). She attended Furman University and received a Bachelor of Science in chemistry and Bachelor of Arts in political science in 1999. Lisa then pursued graduate studies in bioanalytical chemistry at the University of Florida, under the direction of Professor Weihong Tan, and obtained a Doctor of Philosophy in December 2005.

I certify that I have read this study and that in my opinion it conforms to acceptable standards of scholarly presentation and is fully adequate, in scope and quality, as a dissertation for the degree of Doctor of Philosophy.

Weihong Tan, Chairman
Professor of Chemistry

I certify that I have read this study and that in my opinion it conforms to acceptable standards of scholarly presentation and is fully adequate, in scope and quality, as a dissertation for the degree of Doctor of Philosophy.

James D. Winefordner
Graduate Research Professor of Chemistry

I certify that I have read this study and that in my opinion it conforms to acceptable standards of scholarly presentation and is fully adequate, in scope and quality, as a dissertation for the degree of Doctor of Philosophy.

Willard W. Harrison
Professor of Chemistry

I certify that I have read this study and that in my opinion it conforms to acceptable standards of scholarly presentation and is fully adequate, in scope and quality, as a dissertation for the degree of Doctor of Philosophy.

Jon D. Stewart
Associate Professor of Chemistry

I certify that I have read this study and that in my opinion it conforms to acceptable standards of scholarly presentation and is fully adequate, in scope and quality, as a dissertation for the degree of Doctor of Philosophy.

Ben L. Koopman
Professor of Environmental Engineering Sciences

This dissertation was submitted to the Graduate Faculty of the Department of Chemistry in the College of Liberal Arts and Sciences and to the Graduate School and was accepted as partial fulfillment of the requirements for the degree of Doctor of Philosophy.

December 2005

_____

Dean, Graduate School